1-1-1976

The effects of compatibility on the physical and mechanical properties of the blend: Poly (styrene-co-para-chlorostyrene)/Poly (2,6-dimethyl-1,4-phenylene oxide) (PPO).

Joel Robert Fried
University of Massachusetts Amherst

THE EFFECTS OF COMPATIBILITY ON THE PHYSICAL AND MECHANICAL PROPERTIES OF THE BLEND: POLY(STYRENE-CO-PARA-CHLOROSTYRENE)/ POLY(2,6-DIMETHYL-1,4-PHENYLENE OXIDE) (PPO)

A Dissertation Presented

by

JOEL ROBERT FRIED

Submitted to the Graduate School of the
University of Massachusetts in partial fulfillment
of the requirements for the degree of

DOCTOR OF PHILOSOPHY

September 1976

Department of Polymer Science and Engineering

THE EFFECTS OF COMPATIBILITY ON THE PHYSICAL AND MECHANICAL PROPERTIES OF THE BLEND: POLY(STYRENE-CO-PARA-CHLOROSTYRENE)/ POLY(2,6-DIMETHYL-1,4-PHENYLENE OXIDE) (PPO)

A Dissertation Presented

by

JOEL ROBERT FRIED

Approved as to style and content by:

William J. MacKnight, Chairman of Committee

Frank E. Karasz, Member

Richard Farris, Member

Roger S. Porter, Department Head
Polymer Science and Engineering

ACKNOWLEDGEMENTS

The theme for this dissertation was suggested by Professors MacKnight and Karasz. I am grateful for their guidance and helpful comments and suggestions during the course of its execution and for the opportunity to proceed in directions dictated by my own interests and professional objectives. I also wish to thank Professor Farris for his help with the mechanical data and especially for agreeing to collaborate as a member in my thesis committee after the untimely death of Professor Fraser Price whose personal warmth we will all greatly miss.

I would also like to thank Dr. James Tkacik for his initial work on the poly(styrene-co-para-chlorostyrene)/PPO system, Mr. Tom Kirschner for his help with the GPC results, and particularly Mr. Lothar Kleiner whose preliminary efforts in the characterization of the mechanical properties of PS/PPO greatly facilitated the mechanical analysis of the blends used in this study. Finally I wish to extend my appreciation to the Polymer Science and Engineering Department for financial support and for the opportunity to study and expand the breadth of my academic training.

ABSTRACT

THE EFFECTS OF COMPATIBILITY ON THE PHYSICAL AND MECHANICAL PROPERTIES OF THE BLEND: POLY(STYRENE-CO-PARA-CHLOROSTYRENE)/ POLY(2,6-DIMETHYL-1,4-PHENYLENE OXIDE) (PPO)

(September 1976)

Joel Robert Fried, B.S., B.S.Ch.E., M.E.,
Rensselaer Polytechnic Institute, M.S., Ph.D.
University of Massachusetts

Directed by: Professor William J. MacKnight

Blends of styrene/para-chlorostyrene copolymers and poly(2,6-dimethyl-1,4-phenylene oxide) (PPO) have been investigated by differential scanning calorimetry (DSC), by density measurements, and by tensile property studies. Whether or not these copolymers were compatible with PPO, i.e. mutually miscible, depended critically upon copolymer composition. In addition, the mechanical properties of these blends were strongly influenced by the degree to which these two components were compatible.

It has been shown that at or below 67.1 mole % para-chlorostyrene (pClS), these copolymers were compatible with PPO. This was demonstrated by the clarity and good

mechanical properties of films compression molded from these blends and by the presence of a single, although broadened glass transition intermediate in temperature between those of the unblended copolymer and PPO components. In addition, densities of these films were nearly 1% larger than predictions on the basis of additivity would suggest. Similar increases in density, or negative excess volumes of mixing, have been observed for other compatible blends. These observations have been interpreted on the basis of favorable intermolecular interactions suggestive of negative or near zero interaction parameters.

Blends of PPO and copolymers with 75.4 mole % pClS and higher pClS compositions were incompatible. In addition, blends of PPO and poly(ortho-chlorostyrene) were also incompatible. Films made from all of these blends appeared opaque and exhibited two comparatively sharp glass transitions corresponding almost exactly in temperature with those of the two blend components. In addition, densities were additive and plots of tensile strength and elongation at break exhibited broad minima at low and intermediate volume fractions of PPO.

Blends of PPO and copolymers with 67.8 and 68.6 mole % pClS exhibited properties that were intermediate between those of the compatible low pClS copolymer blends and those of the incompatible high pClS copolymer blends. Films appeared hazy to clear and for most blend compositions, two

broadened glass transitions were evident but were displaced in temperature from those of the blend components. The raising of the glass transition temperature (T_g) of the copolymer-phase and the lowering of the PPO-phase T_g indicated that partial miscibility of these copolymers and PPO was occuring within separate copolymer-rich and PPO-rich phases. In addition, quantitative measurement of the amounts of the two components contributing to each glass transition suggested that some copolymer and PPO may be present in large interphase layers between domains. Small density increases were also observed for these blends as would be expected for partial compatibility; while tensile strength and elongation at break exhibited a nearly sigmoidal dependence upon blend composition. At low weight fractions of PPO, these properties exhibited a shallow minimum but at intermediate and at high PPO compositions, values more characteristic of the compatible blends were attained. The apparent increase in blend compatibility with increasing PPO content has been explained in terms of the entropy effects arising from the lower molecular weight of the PPO component.

What the above results have indicated is that polymer compatibility is an extremely subtle and sensitive phenomenon which is strongly dependent upon minor alterations in the chemical structure of either of the blend components. Simple theoretical approaches such as solubility parameter theory were inadequate to explain narrow and/or multiple

compatibility-incompatibility transitions. In addition, classical free volume theories of the glass transition were unable to predict the correct relation of the T_g of compatible blends upon blend composition. What are needed are new and more sophisticated approaches which take into account volume changes in mixing and the interactive energies of segmental polymer contacts.

In memory of my parents without whose constant love, devotion, and encouragement, my life would have reached a substantially lower plateau. And in appreciation of my loving wife, Ava, without whose patience and understanding, this work would have not been completed.

TABLE OF CONTENTS

TABLE OF CONTENTS (cont.)

TABLE OF CONTENTS (cont.)

LIST OF TABLES

LIST OF FIGURES

LIST OF FIGURES (cont.)

LIST OF FIGURES (cont.)

LIST OF FIGURES (cont.)

LIST OF FIGURES (cont.)

CHAPTER I

POLY(2,6-DIMETHYL-1,4-PHENYLENE OXIDE) (PPO) AND BLENDS WITH POLYSTYRENE: A REVIEW

Introduction

Linear, high molecular weight polymers with good mechanical properties can be synthesized by the oxidative coupling of 2,6-disubstituted phenols in the presence of a cuprous salt-amine catalyst. The most important of these is poly(2,6-dimethyl-1,4-phenylene oxide) or PPO, first commercially produced by the oxidative coupling of 2,6-xylenol in 1964.[1] An interesting history of PPO and related polymers is given in a recent review article by Hay.[2]

Oxidative coupling is believed to proceed through a step-growth polymerization of phenoxy radicals. A generalized reaction scheme is shown in Figure 1 while more detailed descriptions of the mechanism of oxidative coupling are given in several sources.[2-4] Competitive with the polymerization reaction is direct carbon-carbon coupling to give diphenoquinone, which in only trace amounts imparts a characteristic yellow color to PPO. The substituents on the phenol precursor are used to block the reactive ortho-sites which would otherwise lead to extensive branching. Both aromatic and aliphatic substituted phenols can be

polymerized with high yield. Some of these are noted in Figure 1. Halogen substituted phenols also can be polymerized to high molecular weight, but the resulting polymers are highly branched and have no useful properties. Large or bulky substituents, e.g. isopropyl or tert-butyl groups, are not used because they favor the competitive dimerization to diphenoquinone.

The molecular dimensions of PPO in solution have been determined from intrinsic viscosity data.[5,6] Due to the crystallization of PPO at theta conditions, unperturbed dimensions were estimated by the methods of Stockmayer and Fixman[9] or Kurata and Stockmayer[10] for PPO in non-ideal solvents.* It was shown that the unperturbed dimensions of PPO by assuming free rotation of bonds and a reasonable value for the C-O-C bond angle, often reported as 118-120°.[11,12] Recently, the free rotation of the phenyl group in the PPO backbone has been postulated on the basis of conformational calculations by Tonelli[13] and by Laupêtre and Monnerie.[14]

The physical properties of PPO are summarized by Hay.[2] PPO has good hydrolytic and dimensional stability, high heat

---

*PPO, like Bisphenol A polycarbonate and several other polymers, does not readily crystallize from the melt but can crystallize from dilute solution[7] or by exposure to the vapors of some solvents.[8]

Figure 1. Oxidative coupling polymerization of 2,6-disubstituted phenols. Substituent groups (R,R') are those which favor polymerization, rather than dimerization to diphenoquinone.

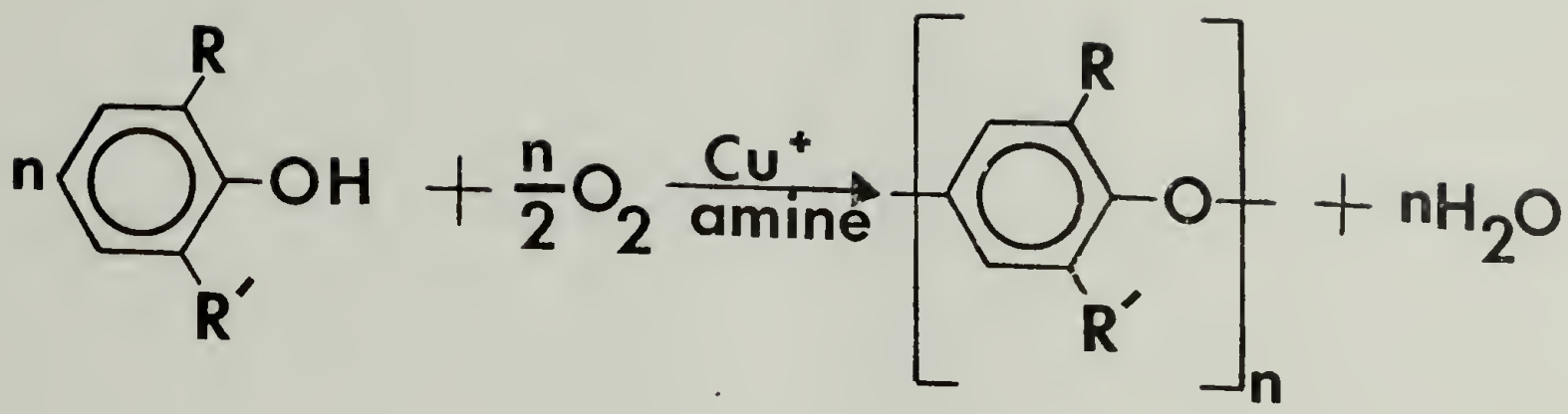

R	R´
CH_3	CH_3
CH_3	CH_2CH_3
CH_3	$CH(CH_3)_2$
CH_3	
CH_3	OCH_3
	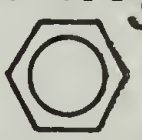
CH_2CH_3	CH_2CH_3

distortion temperature (355°F at 66 psi), and considerable impact strength (1.2 ft-lb/in. notch at 73°F). These are properties of a good engineering material. In addition, thermal gravimetric analysis (TGA) has indicated that PPO undergoes no apparent degradation under 400°C;[15] however, other information suggests that oxidation and thermal cross-linking may occur at temperatures appreciably below 400°C. First, autoxidation of the methyl groups is known to occur at temperatures approaching the glass transition temperature (T_g) of PPO (ca. 208°C).[2] Furthermore, melt processing at about 280°C can result in an increase in all molecular weight averages as determined by solution viscosity and gel permeation chromatography (GPC) in addition to a broadening in the molecular weight distribution. The finding that the high molecular weight tail is extended more than the low molecular weight end suggests that branching or cross-linking has occurred.[16] Due to autoxidation and cross-linking and because of high melt viscosity, PPO is fabricated into film and fiber on a commercial scale only from solution.[17]

To find a resin which could be melt processed but which still retained many of the desirable properties of PPO, an alternative approach was sought. It was discovered that unlike most other high molecular weight polymers, PPO could be solubilized by another high molecular weight polymer, polystyrene (PS).[17] Of hundreds of other polymer

blends which have been investigated over the years, only a handful are judged mutually miscible, i.e. compatible, by the criteria of film clarity and a single composition-dependent glass transition temperature. Most of the known compatible blends are included in reviews by Bohn,[18] by Peterson et al.,[19] and more recently by Krause;[20] some of these, however, are compatible only over a limited composition range. PPO and PS are apparently compatible in all proportions and films made from their blends are clear. Film refractive index has been reported to increase linearly with increasing PPO content.[21] In addition, T_g and all physical properties are intermediate between those of pure PS and PPO. Properties of PS/PPO blends are given in a patent by Cizek.[17] The PS/PPO blends have lower processing temperatures and as a bonus substantially lower cost in comparison with unblended PPO.

Even among members of its own family group, the compatibility of PPO with PS appears unique. For example, Shultz and Gendron have shown by differential scanning calorimetry (DSC) and by thermal optical analysis (TOA) that although poly(2-methyl-6-phenyl-1,4-phenylene oxide) (PMPPO)[22] and PPO are themselves compatible,[23-25] PMPPO and PS are not.[24,25] In addition, poly(2,6-diphenyl-1,4-phenylene oxide)[26] is incompatible with PS.[27]

The first commercial PPO/PS blends were marketed by General Electric as the Noryl series of engineering resins

in 1966.[2] Bair[28] has deduced from a quantitative thermal analysis of these resins that Noryl is actually a blend of high impact PS (5% polybutadiene content) and PPO with about 1% low density polyethylene which is probably added as a processing lubricant. Properties of Noryl resins are given by Kramer.[29]

Over the last decade, substantial effort has been expended by industry and academic research groups to explore the nature of the PS/PPO system and to extrapolate these findings toward a fundamental understanding of the phenomenon of polymer compatibility. As a consequence, there presently exists a large body of information concerning the viscoelastic, thermodynamic, rheological, physical, and mechanical properties of PPO and the PS/PPO blends. In the sections that follow, this body of information is reviewed with the goal of presenting the current state of understanding of the causes of compatibility and its effects upon the properties of these blends.

Thermodynamics of PS/PPO Blending

The thermodynamic requirement for compatibility is often given to be a negative Gibbs free energy mixing (ΔG_m), although recent treatment of polymer compatibility by Koningsveld[30] has indicated that even in the region of negative ΔG_m, partial miscibility or phase separation may occur in some systems for which the plot of ΔG_m versus

blend composition exhibits local maxima and minima. Early approaches[31,32] used to obtain an expression for ΔG_m of mixtures of two high molecular weight polymers were a natural extension of the Huggins[33] and Flory[34,35] lattice model which has been successful in predicting the thermodynamics of polymers dissolved in low molecular weight solvents. The expression for ΔG_m is given in the familiar form cited by Krause[20]

$$\Delta G_m = \frac{RTV}{V_r} \left[\frac{v_A}{x_A} \ln v_A + \frac{v_B}{x_B} \ln v_B + \chi_{AB} v_A v_B \right] \qquad (1)$$

where

V, total volume of mixture

V_r, reference volume equal to molar volume of the smallest polymer repeat unit

R, ideal gas law constant, 1.987 cal $^{o}C^{-1}$ $mole^{-1}$

v, volume fraction of polymer A or B in mixture

x, degree of polymerization of A or B in terms of V_r

χ, interaction parameter

The first two (entropic) terms within the brackets of eq.(1) are negative but are small due to the denominator, x, which for the case of high molecular weight polymers is large. In fact, the entire entropy contribution, $T\Delta S$, where $\Delta G=\Delta H-T\Delta S$, is typically less than 0.005 cal gm^{-1}.[36] In order for ΔG_m

to be negative, the third (enthalpic) term, $\chi_{AB}v_Av_B$, must be small or negative. The value of this term, and therefore ΔG_m, is determined by the interation parameter, χ_{AB}, which is related to the enthalpy of interaction between molecules of the two polymers. When there is specific interactions such as hydrogen bonding between molecules, χ_{AB} is negative and mixing is favored. If one molecule perceives the same interactive environment in the blend as in its pure state, χ_{AB} is zero and again mixing is favored. In most cases, polymers of one type prefer their own molecular environment, i.e. positive χ_{AB}, and therefore phase separation will occur at equilibrium conditions.

Shultz and McCullough[37] have measured the melting point depression of PPO in a binary PPO-toluene mixture and in a ternary PS-PPO-toluene system. From the melting point data and use of the melting point depression equation of Flory,[38] they deduced that the interaction parameter for PS/PPO was approximately zero. This is in agreement with some indications from NMR analysis that there may be only weak interactions, possibly dipolar in nature, between PS and PPO.[39]

An alternate to interaction parameters which are difficult to determine is the use of the Hildebrand-Scatchard solubility parameters (δ) to predict compatibility.[40,41] Polymers whose solubility parameters are close in value are expected to be compatible. Krause[20] has estimated that for

polymers of 100,000 molecular weight, the critical difference between solubility parameters is about 0.11, above which incompatibility is expected. Alternately, χ_{AB} may be related to the solubility parameters of the two polymers by the relation[20]

$$\chi_{AB} = \frac{V_r}{RT} (\delta_A - \delta_B)^2 \quad . \qquad (2)$$

A limitation to solubility parameter theory is that specific interactions are not included, i.e. negative interaction parameters are excluded by the form of eq. (2). A possible improvement would be the use of three-dimensional solubility parameters which weigh the contributions of dipole-dipole, hydrogen bonding, and other specific interactions,[42] but these are difficult to evaluate with precision. The other limitation to solubility parameter theory is that consistent values for δ are hard to find since different experimental determinations of δ often give substantially different results. Krause[20] has suggested that values of δ calculated from the empirical structural and group parameters of Small[43] or more recently of Hoy[44] are more useful for predicting compatibility.

Bernier and Kambour[45] have calculated δ for PPO from Small's parameter to be 8.9 $(\text{cal cc}^{-1})^{1/2}$. For PS, δ has been calculated[20] from the parameters of Small or Hoy to be 9.0 $(\text{cal cc}^{-1})^{1/2}$. Using these values of δ for PPO and PS

and a value of 100 cc mole^{-1} for V_r as suggested by Krause,[46] the interaction parameter for PS/PPO at 25°C is calculated from eq. (2) to be 0.0017. This value agrees with the near zero figure reported by Shultz and McCullough.

Recently, Lacombe and Sanchez[47] have developed a unified molecular theory of liquid and gaseous mixtures based on a lattice model which allows for empty lattice sites, i.e. free volume, not accomodated by the classical Flory-Huggins approach. This new theory satisfactorily predicts lower critical solution temperatures (LCST) for phase separation in polymer solutions and mixtures of high polymers.[48] In addition, volume changes due to mixing can be calculated, whereas they can not in Flory-Huggins theory. This more realistic approach utilizes dimensionless parameters and in this regard resembles the theory of corresponding states developed by Prigogine[49] and applied to polymer mixtures by Flory.[50,51] According to the Lacombe and Sanchez theory, compatibility is predicted for two polymers that have nearly equal characteristic temperatures (T*) where T* is a dimensionless interaction energy related parameter. For PS, T* is given as 735 which is in the range estimated for PPO (700-800).

Glass Transitions and Secondary Relaxations

The dependence of the glass transition temperature (T_g) of PS/PPO blends upon composition has been studied by

differential scanning calorimetry (DSC),[8,24,25,28,52-59] thermomechanical (TMS) analysis,[54] differential thermal analysis (DTA),[21] thermo-optical analysis (TOA),[23-25,55,56] dynamic mechanical techniques,[52,53,56-58,60] and dielectric measurements.[53,57,58] In each study, the T_g of the blend was intermediate between those of PS and PPO, but in several cases different techniques gave dissimilar T_g-composition relationships.[53,57] The results of these studies and their implications for the intimacy of PS/PPO mixing are discussed below.

Calorimetric and Related Studies. T_g's of unblended PS and PPO as determined by DSC, TOA, DTA, dilatometry, and adiabatic calorimetry are listed in Table I in order of increasing heating rate. The low value of 89°C determined by adiabatic calorimetry for the T_g of PS and given as the first entry in Table I was attributed in part to about 0.8% volatile material present in the PS sample used by that study and, in part, to the low heating rate of $\sim 0.1\,^{\circ}C\ min^{-1}$.[63]

Table I. Glass Transition Temperatures of PS and PPO

T_g (°C) PS	T_g (°C) PPO	Technique	Heating Rate °C min^{-1}	Reference
89	-	Adiabatic calorimetry	0.083	61
-	207	Adiabatic calorimetry	0.083	62,63
100	-	Dilatometry	1	64
101	219	DSC	10	54

Table I. (cont.)

T_g (°C) PS	T_g (°C) PPO	Technique	Heating Rate °C min^{-1}	Reference
108	225	DSC	10	52
113	222	TOA	10	55
-	230	DSC	16	65
-	234	DTA	20	65
106	220	DSC	40	28
-	225	DSC	40	65

The high T_g's of 230°C by DSC and 234°C by DTA were reported by Nicolais and Landel[65] as the temperatures at the onset of the high temperature "T_g" peak of an uncharacterized PPO sample. They reported that if this powder was annealed at 300°C in the DSC, T_g dropped sharply with time to the more frequently quoted value of 210°C. The same high T_g values and the subsequent drop in T_g following heating were also observed for PPO powder mixed with glass beads. In fact, T_g for this filled system was even 4°C higher than for unfilled PPO. The possibility that the high temperature peak was a crystalline melting peak was rejected by the authors who claimed no evidence for crystallinity from X-ray diffraction. This is surprising because there is substantial support from other sources that PPO obtained as a powder by precipitation from solution is semi-crystalline and does not obey a simple two-phase crystalline-amorphous model.[8,62,63,66] This latter fact means that even for low degrees of crystallinity, the discontinuity in the heat

capacity (C_p) versus temperature plot may not be detected at T_g. It should be noted that the high temperature peak of Nicolais and Landel does correspond exactly in temperature with the crystalline melting peak observed by Karasz and O'Reilly[66] for PPO powder by DSC once allowances are made for a few degrees variation attributable to the different heating rates used in the two studies (16^{o} min^{-1} in the former and 40^{o} min^{-1} in the latter).

The T_g's of PS/PPO blends as measured by DSC,[8,24,25,28,52-59] by TOA,[23-25,55,56] by DTA,[21] or by thermomechanical (TMS)[54] techniques follow the same dependence upon composition. In each case, the curve relating blend T_g to composition falls below the tie-line connecting the T_g's of pure PS and PPO, i.e. a concave relation. Jacques, Jopfenberg, and Stannett[59] have shown that only the position of the curve is changed when T_g is defined alternately as the temperature at the onset, at the midpoint, or at the maximum of the transition.

Prest and Porter[54] have shown that the experimental data for blend T_g can be fitted closely by the relation derived by Kelley and Bueche[67] for polymer–diluent systems. The assumptions used here were iso-free volume at T_g and the equality of blend free volume to the volume fraction sum of the free volumes of the components. That the free volume concept of the glass transition appears to apply here may be fortuitous. In fact, application of free

volume theory to the prediction of blend T_g from the recent PS/PPO density results of Jacques and Hopfenberg[21] and of Hopfenberg, Stannett, and Folk[68] does not agree with experiment. Densities of PS/PPO blends were found to be up to 1% larger than those calculated from weighted additivity of the specific volumes of unblended PS and PPO. These findings suggest a negative excess volume of mixing from which free volume theory predicts that blend T_g's should fall above, rather than below, the tie-line connecting the T_g's of PS and PPO.[68] It is known that free volume theory incorrectly predicts T_g effects in systems in which specific interactions are present, e.g. nylon-water. The apparent negative excess volume of mixing suggests that some specific interactions, however small, may occur in the PS/PPO system as well. The success of the Kelley-Bueche treatment on the other hand is interesting and warrants further study.

In Figure 2, T_g blend is plotted versus weight fraction PPO (W_{PPO}) for the DSC and TMS data of Prest and Porter.[54] The two T_g-composition curves which are offered for comparison with the above data points are drawn from T_g's calculated from equations given by Shultz and Gendron[55] for their DSC and TOA results. They are:

$$\frac{1}{T_g(\text{TOA})} = \frac{1-W_{PPO}}{386.2} + \frac{W_{PPO}}{495.2} \qquad (3)$$

and

Figure 2. Glass transition temperatures (T_g) of PS/PPO blends versus weight fraction PPO (W_{PPO}) as measured by DSC, TMS, and TOA techniques. Circles (●) and squares (■) represent DSC and TMS data, respectively, for a heating rate of 10^{o} min^{-1} from the results of Prest and Porter, ref. (54). Solid and broken curves were drawn from equations given by Shultz and Gendron, ref. (55), for their DSC (20^{o} min^{-1}) and TOA (10^{o} min^{-1}) data, respectively.

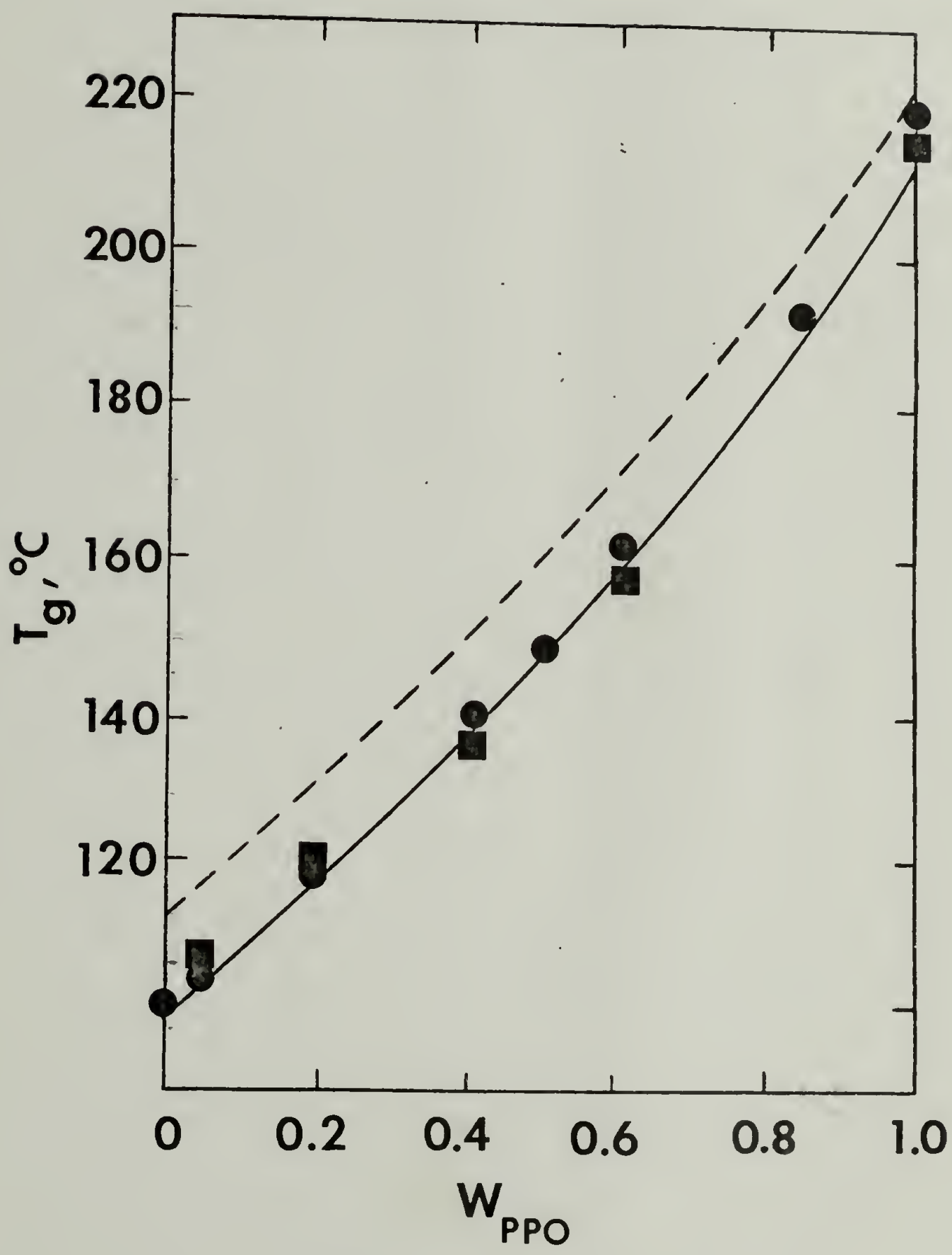
220
200
180
160
140
120
$T_{g'}$, °C
0
0.2
0.4
0.6
0.8
1.0
W_{PPO}

$$\frac{1}{T_g(DSC)} = \frac{1-W_{PPO}}{372.2} + \frac{W_{PPO}}{485.2} \qquad (4)$$

where T_g (TOA) and T_g (DSC) are in ^{o}K. The upper curve in Figure 2 corresponds to the T_g(TOA) values calculated from eq.(3) while the lower curve corresponds to the T_g(DSC) values calculated in eq. (4). At each composition, T_g(TOA) is about 13^{o} higher than T_g(DSC), but both follow the same concave relation to composition as does TMS and DTA determined T_g's.

Dynamic Mechanical Studies. Although the relaxational processes of PPO have been investigated by spin probe (ESR)[69] and by NMR[70] techniques, the most extensive studies have been made by dynamic mechanical methods.[71-74] Although all sources agree as to the presence of a well-defined α relaxation associated with the thermal excitation of cooperative motions in the chain above T_g (480^{o}K),[71] there remains considerable controversy as to the number, the location, and the assignment of specific molecular motions to as few as one or as many as four secondary relaxations. There is considerable evidence to suggest that some of these relaxations may be extremely sensitive to trapped impurities such as diphenoquinone or copper salts[74] and to the presence of water.[72-74] It is therefore reasonable to expect that much of this controversy may be due to differences in the manufacture, methods of purification, thermal history, and the drying procedures applied to each of the PPO samples used

by various authors. The effects of different sample preparations and annealing conditions have been studied by Eisenberg and Cayrol.[73] The controversial nature of the mechanical spectrum of pure PPO makes difficult an unambiguous interpretation of the dynamic mechanical results for PS/PPO blends. Some of the conclusions reached by different authors are reviewed briefly below.

Stoelting, Karasz, and MacKnight[52] have studied blends of PS and PPO by DSC and dynamic mechanical (Vibron) measurements of films that were compression molded from a physical mixture of the two powders. Their results for unblended PPO agrees with those of Heijboer[72] who found a small low temperature (-115°C) γ peak and a broad, poorly defined peak near 5°C in addition to the main α glass transition above 200°C. The previous assignment of the γ peak to the presence of water was questioned because this peak persisted when the compression molded films of PPO were annealed at elevated temperatures in vacuum. No β peak was observed at 40°C and 110 Hz. as would have been expected from the results of de Petris et al.[71] This β peak has been attributed to hindered torsional oscillations of the phenylene units in the backbone around the C-O-C axis.[71,73] For pure PS, three peaks designated as α (106°C), β (52°C), and γ (-140°C) were observed by Stoelting et al. in agreement with results found elsewhere.[75]

Stoelting et al.[52] investigated three blend compositions (W_{PPO}=0.25, 0.50, and 0.75) for which films had been molded at different temperatures (290° and 330°C) and times (2 to 10 minutes), slow cooled, and annealed at 180°C for 0 or 12 hrs. The dynamic mechanical spectra showed a small γ maximum in the dynamic loss tensile modulus (E") at 110 Hz. One γ maximum was observed for the PS/PPO blends and was located between the corresponding γ maxima for pure PS (-121°C) and pure PPO (-104°C). In addition, the α relaxations of the blends appeared at temperatures intermediate between those of PS (114°C) and PPO (224°C) but were broad and had a distinct shoulder which suggested two overlapping peaks. This latter result was interpreted as evidence for the presence of two mixed PS/PPO phases, one PS-rich in composition and the other PPO-rich. The temperature corresponding to the maximum of each of these two overlapping peaks is plotted versus W_{PPO} in Figure 3. The low temperature of PS-rich peak maxima follow a concave relation similar to the DSC, TMS, and TOA results cited previously. By contrast, the high temperature or PPO-rich maxima follow a convex relation which curiously would have been expected from free volume interpretation of the PS/PPO density data discussed in the previous section. The two phases were not evident in their DSC results which showed only a single step in C_p. This difference between DSC and dynamic mechanical sensitivites may be explained by the proposition

Figure 3. Glass transition temperatures (T_g) of PS/PPO blends versus weight fraction PPO (W_{PPO}) as measured by dynamic mechanical and dielectric techniques. Filled (●) and Open (○) circles represent temperatures at the maxima of the low-temperature and high-temperature shoulders, respectively, observed in the dynamic mechanical α peak by Stoelting et al., ref. (52). Filled squares (■) represent temperatures at the maximum of the dynamic mechanical tan δ from the data of Shultz and Beach, ref. (56). Open squares (□) represent temperatures at the maximum of the dielectric loss (ε") from the data of MacKnight et al., ref. (53).

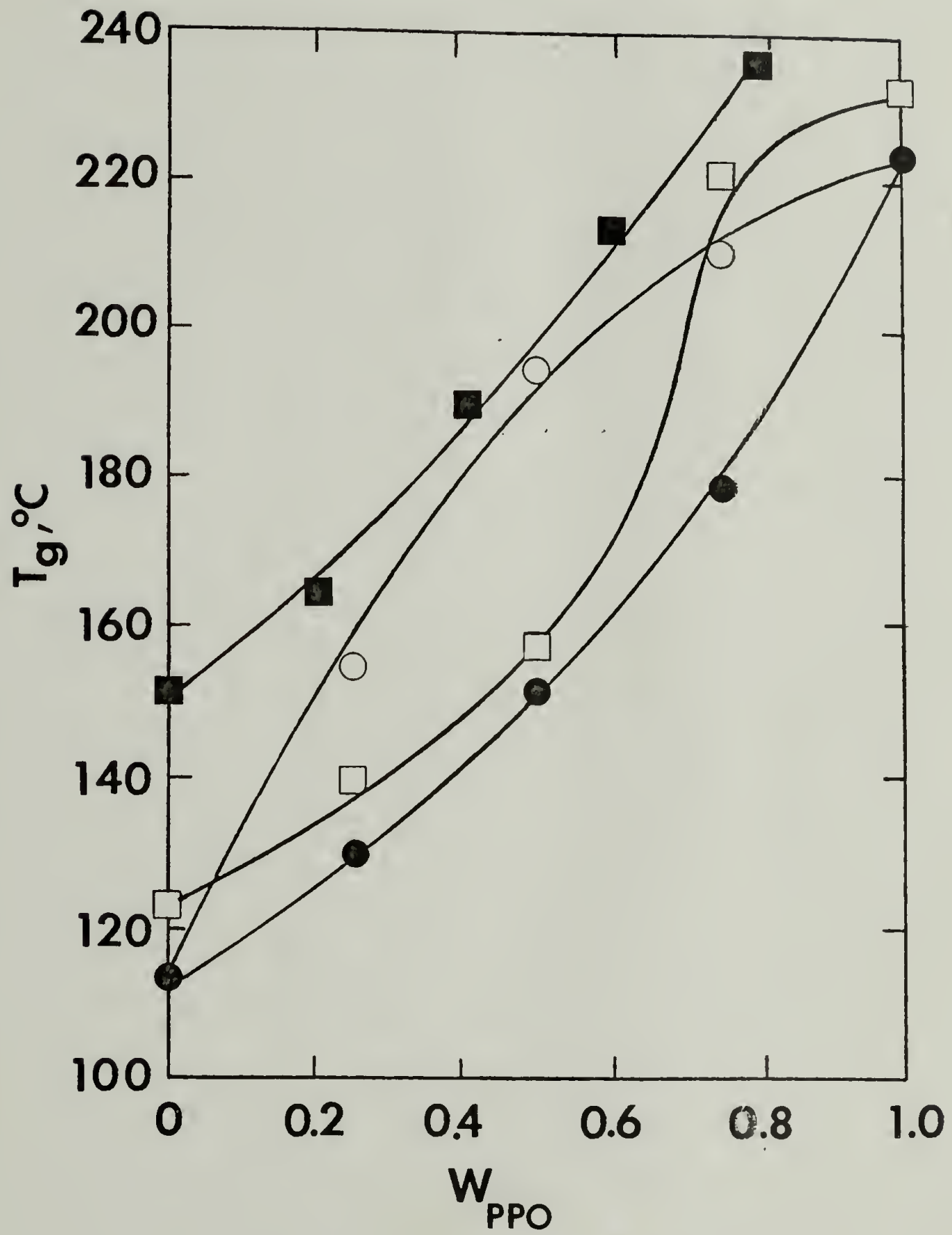
240
220
200
180
160
140
120
100
T_g, °C
0
0.2
0.4
0.6
0.8
1.0
W_{PPO}

that different techniques of T_g measurements may be responsive to motions of chain atoms occuring over very different domain sizes. Apparently, the molecular processes responsible for the discontinuity in C_p by DSC may involve longer range motions than the segmental microbrownian motions of perhaps 30 to 40 main chain carbon atoms responsible for the dynamic mechanical loss peaks.

The compositions of the PS-rich and PPO-rich phases were calculated by Stoelting, Karasz, and MacKnight from the peak temperatures by the simple relationship

$$T_g = (1-W_{PPO})T_{g_{PS}} + W_{PPO}T_{g_{PPO}} \qquad (5)$$

which is the equation of the tie-line joining the T_g's of PS and PPO. The apparent blend compositions calculated from the substitution of DSC T_g into eq. (5) and solving for W_{PPO} were roughly comparable to those identically calculated for the dynamic mechanical PS-rich peaks. As previously shown, both the plots of DSC T_g and T_g corresponding to the PS-rich maxima versus overall blend composition follow similar concave relations.

Following these early studies, Shultz and Beach[56] and more recently Yee[60] have conducted dynamic mechanical studies (Vibron) on PS/PPO blends that were made by different blending procedures. Shultz and Beach coprecipitated their blends from 10% toluene solution into a large excess (20:1) of a

nonsolvent, methanol. The dried precipitates (80°C for 16 hrs. in vacuum) were then compression molded into thin films at temperatures ranging from 180°C for PS to 270°C for PPO. Yee used blends that were made by coextruding PS pellets and PPO powder in a masterbatch of 50/50 composition. The extrudate was then chopped and again coextruded, but this time weighed amounts of either PS pellets or PPO power were added to give overall compositions of 10, 30, 50, 70, and 90% PPO in the final extrudate. This final extrudate was chopped and then compression molded into films at the same temperatures employed by Shultz and Beach.

Shultz and Beach have reported that each PS/PPO blend (20, 40, 60, and 80% PPO) exhibited a single dynamic storage tensile modulus (E') decrease region at T_g and a single, well defined loss tangent (tan δ = E"/E') with no apparent shoulder. The temperatures at maximum tan δ for each blend showed a smooth, nearly linear dependence upon blend composition as indicated in Figure 3.

Yee using the same frequency of 110 Hz. observed a broad β peak (tan δ) for PPO at about 100°C and a broad shoulder in the α transition for PS which was also discernable in blends containing 10 and 30% PPO. For those blends containing 50, 70, and 90% PPO, there was a suppression of the broad β peak of pure PPO except for a small, unassigned peak centered around 80 to 90°C. The suggestion was made that this latter small peak may be the peak responsible for

the shoulder in the α transition of pure PS and therefore may exist in the blends as a result of trace amounts of PS not perfectly mixed in the blend. The suppression of the β peak was interpreted as an indication of strong intermolecular interactions between PS and PPO which could cause a negative excess volume of mixing. As previously mentioned, the density results of Jacques and Hopfenberg[21] and Hopfenberg, Stannett, and Folk[68] support the tenet of a negative excess volume of mixing.

Wellinghoff and Baer[76] have studied the dynamic mechanical spectrum of blends of PPO and isotactic polystyrene (iPS) by torsion pendulum measurements at 1 Hz. When quenched to the amorphous state, iPS has nearly identical thermal and mechanical properties to atactic PS.[8,61] In agreement with the results of Yee, they found a suppression of the broad β peak of PPO in blends of 15% iPS. Interestingly, this suppression occurs at the same amount of antiplasticizer which must be added to polycarbonate or to poly(vinyl chloride) in order to eliminate the β relaxations in these materials. Further indication that PPO and iPS or aPS mix at the segmental level comes from their analysis of the Fourier-Transform infrared (FTIR) spectra of iPS/PPO. They noted an increase in band intensity and a frequency shift to higher wave numbers for the C-H out-of-plane bending mode for PPO when a solvent such as

ethyl benzene was added. A similar change in band intensity and an even larger increase in intensity was observed in the spectrum of iPS/PPO.

The single, well defined tan δ peaks found by Shultz and Beach, the β suppression observed by Yee and by Wellinghoff and Baer, and the shift in the C-H bending mode are strong evidence that PPO and PS approach segmental compatibility. These conclusions are at odds with the mixed-phase findings of Stoelting, Karasz, and MacKnight.[52] The fact that PS and PPO may be thermodynamically compatible, which can be stated conclusively only when the heat of mixing (ΔH_m) is actually measured for this system, does not mean that the kinetics of the mixing process need not be considered. It is clear that the interdiffusion of large polymer molecules at temperatures not far above the melt temperature of one of the components, as is the case for physically mixed powders of PS and PPO at 275°C, is a tediously slow process. This may be an explanation for the small, mixed-composition domains evident from the dynamic mechanical results of Stoelting et al.[52] In this case, DSC may not be able to resolve two phases whose T_g's are so close. The mixing processes of Shultz and Beach and of Yee allow greater opportunity for an equilibrium state to be reached by effectively reducing viscosity by coprecipitation from dilute solution in the former case and by

permitting greater residence time for diffusion coupled with mechanical mixing in the case of the latter.

Dielectric Studies. The dielectric properties of PPO have been investigated by Karasz, MacKnight, and Stoelting.[77] As in the dynamic mechanical spectrum, PPO is characterized by a dielectric α peak representing the glass transition and a low temperature γ peak presumably attributable to a localized vibrational or librational mode of a dipolar moiety. The temperatures at the maxima of the α and γ dielectric peaks are comparable to those observed in the dynamic mechanical spectrum[52] when compared at equivalent frequencies. PPO is only a weakly polar molecule with the only dipolar contribution arising from the cosine projection of the two ortho methyl-phenylene dipoles along the 0--0 axis. For this reason, the intensities of both the α and γ peaks are weak and unlike the dynamic mechanical case both peaks are nearly equal in intensity. Activation energies have been given as 150 kcal $mole^{-1}$ for the α relaxation and 8.7 kcal $mole^{-1}$ for the γ relaxation.

The dielectric properties of the PS/PPO blends have been described by MacKnight, Stoelting, and Karasz.[53] These blends were prepared in the same manner as in their dynamic mechanical studies[52] with similar thermal treatment. Unlike the dynamic mechanical results, each blend composition showed a single, although broad α relaxation with no evidence for a PS-rich or a PPO-rich phase. The

temperatures corresponding to the maxima of the dielectric α peaks for PS/PPO are plotted versus W_{PPO} in Figure 3. There is a pronounced increase in T_g above 50% PPO to give a nearly sigmoid relation. The authors noted that if only the stronger of the overlapping peaks in the dynamic mechanical data are considered, then a similar sigmoid curve is obtained. Shultz and Beach[56] in studying blends of PPO with random copolymers of styrene and para-chlorostyrene which are at the verge of incompatibility have found a similar sigmoid relation by TOA. This comparison is interesting because one might expect similar mixed composition domains in the copolymer/PPO blends which are near thermodynamic incompatibility as in the thermodynamically compatible PS/PPO blends which are partially phase separated due to the kinetics of the mixing process.

Mechanical and Rheological Properties

The mechanical properties of PPO have been summarized by Hay[2] and are given for completeness in Table II.

Table II. The Mechanical Properties of PPO

Tensile strength, psi	
at 73°F	9,600
at 200°F	6,500
Elongation at break, percent	
at 73°F	20-30
at 200°F	30-40
Tensile modulus, psi	
at 73°F	355,000
at 200°F	230,000

Table II. (cont.)

Flexural strength, psi	
at 0°F	15,900
at 73°F	13,500
at 200°F	7,300
Flexural modulus, psi	
at 0°F	380,000
at 73°F	360,000
at 200°F	260,000
Shear strength, psi	10,500
Deformation under load, percent	
at 122°F, 2,000 psi	0.3
Creep, 300 hr., 73°F, 2,000 psi, percent	0.75
Izod impact strength, notched (1/4 x 1/2 in. bar)	
at -40°F, ft-lb/in. notch	1.4
at 73°F, ft-lb/in. notch	1.8
at 200°F, ft-lb/in. notch	4.2

Heijboer[72] has shown that PPO has good impact strength at temperatures as low as -80°C even though PPO unlike polycarbonate (PC) has no pronounced damping maximum at corresponding temperatures. Wambach, Trachte, and Dibenedetto[78] have studied the fracture properties of PPO and PPO filled with glass beads while Nicolais and Dibenedetto[79] have defined failure criteria for PPO which can be used to predict creep behavior, for example, from constant rate of loading experiments.

Recently, the mechanical properties of PS/PPO blends have received special attention.[60,76] This interest is partly due to the observation that PS/PPO undergoes a transition from a ductile to brittle mode of failure as PPO content is decreased. At temperatures below T_g, pure PPO like other polymers with flexible oxygen linkages and

main chain phenyl units (e.g. PC and PET) yields and cold draws under tensile deformation. This is in contrast to PS and other vinyl polymers with bulky side chains which fail in the brittle mode with extensive crazing at temperatures as low as -90°C.[76] On the other hand, PPO crazes only at higher temperatures approaching T_g or in the presence of crazing agents such as ethanol.[45,80] Wellinghoff and Baer[76] have observed that for thick films, the ductile to brittle transition occured at about 70 to 80% PPO and was unaffected by the tacticity of the PS component. It is interesting to note that at approximately the same blend compositions, the β peak of PPO was suppressed.[60,76] This suggests that strong intermolecular attractions and the accompanying decrease in volume and/or the absence of a significant main chain relaxation at low temperatures suppresses ductility.

The composition marking the ductile-brittle transition depends upon strain rate and to a certain extent upon the thickness of the sample. Yee[60] has shown that ductility extends to blends of lower PPO content as strain rate is reduced. Wellinghoff and Baer[76] have noticed that thin films are more ductile than thick ones. This was attributed to looser packing for films of high surface-to-volume ratio which probably enables delocalized shear yielding to occur at lower stress levels and thereby prevents craze nucleation and growth.

Cizek[17] has shown that the flexural strength, compressive strength, Rockwell hardness, tensile strength, and flexural modulus for PS/PPO blends are synergistic to those properties measured for pure PS and PPO. This means that plots of these properties versus W_{PPO} show a maximum at some composition range. This maximum is often very broad and difficult to locate with any accuracy. The favorable increase in some mechanical property, such as tensile strength, must be weighed against a slight decrease in impact strength and the loss of ductility over most blend compositions. To improve impact performance, high impact PS is used in the commercial resins.

Tensile strength for PS/PPO blends at high W_{PPO} is about 10 to 20% higher than for unblended PPO (9,600 psi at 73°F). This effect is particularly pronounced for blends of PPO and low molecular weight PS for which tensile strength is very small.[81] The tensile strength of such blends is dramatically increased with increasing PPO content until a maximum is reached at about 75% PPO. This maximum corresponded almost exactly in magnitude with that found for blends of PPO and high molecular weight PS with nearly an order-of-magnitude higher tensile strength.

Yee[60] has measured tensile strengths of injection molded samples of PS/PPO over four decades of strain rate ($\dot{\varepsilon}$). Two maxima in the plot of blend tensile strength versus composition were observed for $\dot{\varepsilon}$ between 10^{-2} sec^{-1}

and 10^2 sec^{-1}. These maxima diminished in intensity with decreasing $\dot{\varepsilon}$. One of these maxima was situated in the composition range in which failure is ductile and one in the range in which failure is brittle. The ductile region maximum was found to shift to higher W_{PPO} with increasing $\dot{\varepsilon}$ while the brittle region maximum remained nearly stationary in the region between 15 and 20% PPO.

The plot of yield strength of pure PPO versus log $\dot{\varepsilon}$ has been found to be nearly linear.[60,78] For PS/PPO blends, Yee[60] has reported a decrease in yield strength at 50% PPO for high $\dot{\varepsilon}$; this was interpreted as evidence for a ductile-to-brittle transition. For all blends, the slope of the yield strength versus log $\dot{\varepsilon}$ was found to increase with decreasing PPO content. Using a reference the Rhee-Eyring[82] model for stress activated flow, Yee has related this increase in slope to a decrease in flow volume. This decrease is consistent with the other evidence for a negative excess volume of mixing previously reviewed.

Additional support for mixing at the segmental level comes from the rheological studies of Prest and Porter.[54] They have determined the viscoelastic (VE) properties of PS/PPO blends by thermomechanical analysis (TMS) and rheology (Weissenberg cone-and-plate). The blends used in this study were freeze-dried from dilute solutions of monodisperse, anionic PS ($\bar{M}_n$=97,200) and polydisperse PPO ($\bar{M}_w$= 69,000). These blends exhibited a compositionally dependent

time-temperature shift factor and a VE response independent of applied strain over the measured range of strain amplitudes, 5-9%, in contrast to the nonlinear response of two-phase systems such as filled polymer melts. In addition, when the blends were compared at equal free volumes, the monomeric friction factor (ξ_o) was observed to be independent of composition. This suggests that segment-segment interactions in the blend are the same as in unblended PS and PPO. From the plot of probe penetration (TMS) versus temperature as well as from the plot of dynamic loss shear modulus (G") versus reduced frequency from the cone-and-plate results, Prest and Porter showed that the height of the rubbery plateau increased with increasing PPO content. This is indicative of a decrease in the effective molecular weight between entanglements (M_e). PPO is highly entangled in its unblended state and has a M_e of only about 25% of that of PS. The observed decrease in M_e or alternately the increase in the average number of entanglements per molecule in the blend indicates that mixing is intimate. This also accounts for the increase in blend viscosity as the concentration of PPO is raised even though the overall molecular weight of the blend is decreasing for the particular molecular weights used in their study.

Solvent-Induced Crystallization and Craze Formation

Craze Formation. The stress crazing of PPO in the presence of organic agents has been investigated by Bernier and Kambour.[45] PPO was found to craze when stressed in the presence of liquids of even negligible solubility in PPO. The influence of these crazing agents on PPO apparently was to reduce the surface energy of the holes in the craze structure and thereby to make their formation easier. When liquids whose solubility parameters are close to that of PPO (δ=8.9) were used as crazing agents, an additional effect of limited plasticization was observed. Such plasticization allows liquidlike flow of the glass in the stress direction upon application of sufficient stress and a reduction in the critical strain for craze formation. Those liquids that were closest to the solubility parameter of PPO in value did not allow stable crazes to be formed. These were classified as cracking agents because cracks were produced and proceeded rapidly through the sample without intermediate craze formation. The development of spiral cracks in biaxially stressed films of PPO in a solvent environment has been reported by MacNulty.[83]

The morphological features of PPO crazes have been described by Kambour and Holik[80] who were able to examine the craze structure directly by transmission electron microscopy of PPO sections reinforced by a sulfur impregnant. The undamaged craze structure of PPO crazed in

ethanol resembled an open-celled foam composed of holes and polymer elements uniformly averaging ∿200A in diameter. In addition, some orientation was observed in the original tensile stress direction.

Jacques, Hopfenberg, Stannett, and Folk[21,59,68,84] have extensively investigated the sorption kinetics and equilibria in addition to crazing of PS, PPO, and their blends. The sorption of n-hexane or n-heptane at higher temperatures was found to be predominantly by stress-induced relaxations at the sharp boundary between the swollen outer region and the inner unaffected zone (Case II transport). This boundary moved at constant velocity and therefore the gain in weight due to solvent absorption was linear with time in contrast to diffusion of simple gases, non-solvents, or partial solvents at very low activities and temperatures where weight gain is proportional to the square root of time (Fickian transport). At 30°C and a penetrant activity (P/P_o) of 0.775, the absorption rate of n-hexane was found to increase monotonically with PPO content over about four orders of magnitude while the equilibrium solvent content increased by a factor of only two going from 100% PS to 100% PPO in blend composition. There was a slight change in the time dependence of absorption from predominantly relaxation controlled processes at the extremes of the composition range, i.e. pure components, to more Fickian transport at 50% PPO content. When immersed

in liquid (P/P_o=1.0) n-hexane at 35° to 55°C, all films appeared white or opaque with randomly distributed non-interconnecting holes 1 to 3μ in size. There was, in addition, a pronounced minimum in the rate of absorption at 50% PPO content.

In a later study, Jacques and Hopfenberg[21] measured the sorption kinetics and equilibria of PS/PPO films over a wider temperature range and at penetrant activities between the previous bounds of 0.775 and 1.0. The minimum in the equilibrium sorption and in the sorption rate previously observed only for films immersed in liquid n-hexane was found for films exposed to vapor at penetrant activities above 0.775. This minimum was shown to be not a special property of the PS/PPO system but was associated with differences in the effective T_g for different blend compositions at equal penetrant activities and temperatures. When sufficient solvent was absorbed to lower the effective T_g below the test temperature, a marked change in the sorption equilibrium and kinetics was observed. For pure PS, for example, a sharp upturn in the equilibrium sorption occured at sufficiently high penetrant activities to lower T_g below the test temperature in addition to an apparent decrease in the activation energy for absorption. The dependence of effective T_g ($T_{g_{12}}$) upon volume fraction of the penetrant (ϕ_2) could be approximated by the simple relationship:

$$T_{g_{12}} = (1-\phi_2)T_{g_1} \qquad (6)$$

where T_{g_1} represents the T_g of the dry polymer. Below $T_{g_{12}}$, the equilibrium sorption of the blends increased with increasing PPO content, while above $T_{g_{12}}$ the equilibrium sorption decreased. The observed minimum in the sorption equilibrium and kinetics was the result of the crossing of the sorption isotherms at temperatures and penetrant activities at which the PS-rich films equilibrated with n-hexane were rubbery and the PPO-rich films were still glassy. When all the blend compositions were at temperatures below their $T_{g_{12}}$ for a given penetrant activity and temperation, e.g. P/P_o = 0.775, or when all are above $T_{g_{12}}$, the equilibrium solubility was monotonic with blend composition.

No crazing at any blend composition was observed below a penetrant activity of 0.925.[84] At or above 0.925, PS and PS-rich films extensively crazed and had an overall microvoid fraction which was determined from density measurements to be about 15%. At corresponding conditions, PPO and PPO-rich films had a smaller microvoid fraction of 2%. The whitening of these films was proposed to be a consequence of solvent-induced crystallization of the PPO component. Due to the absence of externally applied stresses, any craze formation was a result of stresses generated at the boundary between the outer swollen gel and the inner glassy core when the

effective T_g was reduced to near or below the temperature of the experiment.[21]

The effect of annealing at 20° above T_g upon sorption equilibria and kinetics was investigated by Hopfenberg, Stannett, and Folk.[68] This type of thermal pretreatment had only a slight effect upon pure PS but sharply increased the density and decreased the rate of sorption in PPO and PPO-rich films although the sorption equilibria of all blend compositions were unaffected. This decrease in the sorption rate of the PPO and the PPO-rich films was followed by a rapid acceleration near the end of the sorption (Super Case II transport) as a result of overlapping of Fickian waves which precede the advancing front of the penetrant at long times. The different effects of annealing upon PPO and PS were explained by the difference in T_g between the two in relation to the low drying temperatures, 50° to 55°C, used to prepare the films. Due to its substantially lower T_g, PS was effectively annealed during drying and therefore further thermal treatment had no additional effect upon packing volume. It is important to note that although the density of PPO had increased from about 1.063 gm cc^{-1} to 1.073 gm cc^{-1} during annealing, the shape of the curve of blend density versus composition and the maximum in the difference between measured and additive densities remained unchanged. This indicates that the origin of the observed excess volume of mixing inferred from density measurements

is a real effect of favorable molecular interactions between PS and PPO and is not due to artifacts in blend preparation.

Crystallization. The whitening of PPO and PPO-rich films upon exposure to solvents has been attributed previously to crystallization of the PPO component. Like polycarbonate, PPO does not crystallize from the melt, but single crystals of PPO can be grown in dilute solution.[7,85] In addition, moderate amounts of crystallinity can be induced in PPO by exposure to certain solvents such as 2-butanone (MEK) followed by thermal treatment.[8,86]

As received commercial powder samples of PPO have a weight fraction crystalline content of about 20-40% as a result of the solution precipitation technique used to obtain PPO powder; however, all crystallinity is lost when the powder is melted. The extent and nature of crystallinity in PPO powder has been studied by Karasz et al.[62,63,66] by means of DSC and adiabatic calorimetry. They found a broad crystalline melting peak indicative of imperfect crystalline order. The temperature (T_m) corresponding to the maximum in peak height was 540°K (267°C) by DSC (40° min^{-1})[66] and 510°K (237°C) by adiabatic calorimetry (∿5° hr^{-1})[62,63] In addition, there were indications of further recrystallization (∿5%) below T_g at about 430°K (157°C). This suggests that relatively minor reorganization is required to promote PPO crystallization which is reflected

in the very low entropy of fusion (ΔS_f) estimated as 9.5±1.8 joule $^{o}K^{-1}$ per mole of repeat unit (120 gm/mole).[63] A low ΔS_f is also the reason for the high value of T_g/T_m (0.92) which has been shown to be consistent with current glass transition theory and which suggests an universal value of 7±2 joule $^{o}K^{-1}$ $mole^{-1}$ for the configuration entropy of polymers at T_g.

Barrales-Rienda and Fatou[7] have postulated that crystallization of PPO from dilute solution occurs by a regular ordering of PPO molecules with the aid of a complex between PPO and the solvent (α-pinene). A complex of this type has been reported by Factor et al.[87] for PPO precipitated from methylene chloride solution or equilibrated in methylene chloride vapor. They suggested that the solvent molecules may occupy voids in a crystalline lattice composed of helical PPO molecules.

More recently, Wenig et al.[86] have investigated the crystalline structure of PPO which had been exposed to MEK vapor at 75°C for 72 hrs. and vacuum dried at 110°C for 24 hrs. These conditions previously were shown to induce maximum crystallinity in PPO.[8] By DSC and wide-angle X-ray (WAXS) measurements, they have estimated that solvent crystallized PPO had about 30% crystalline content. The crystalline structure was not spherulitic as it is for iPS, for example, but was modeled to consist of a superstructure of unoriented rodlike entities which contain clusters of

randomly oriented fibrous bundles. Small-angle X-ray (SAXS) indicated that very thin lamellae about 38Å in thickness make up these bundles.

Neira[8] has shown by DSC measurements of crystallinity that PPO can be crystallized from PS/PPO blends by exposing films to acetone vapor (50°C for 24 hrs.) and then heating them in vacuum at temperatures between 110° and 170°C. In these studies, acetone was used in place of MEK because of the appreciable solubility of PS in the latter. It was felt that the solvent acted to reduce the T_g of the blend through plasticization and thereby to widen the T_g-T_m interval. The conclusion of these studies was that PPO could crystallize from the blend but only within an intermediate composition range, $0.20<W_{PPO}<0.50$. In addition, T_m was depressed from its equilibrium value (T_m^o) for pure PPO. If the magnitude of this depression ($1/T_m - 1/T_m^o$) is substituted into the expression obtained by Flory[38] for polymer-diluent systems, the effective molar volume of the diluent, PS, can be calculated and was found to be substantially smaller than that of an entire molecule of PS. This result may be taken as evidence for mixing at the segmental level between PPO and PS. The T_g of the amorphous phase was also lowered a few degrees. This suggests that as PPO crystallizes from the blend, the remaining amorphous phase becomes richer in the lower T_g component, PS.

Similar results were found by Niera[8] for thermally annealed (at 170°C) blends of PPO and isotactic PS (iPS) in which only iPS can crystallize. Neira observed a depression in T_m from 231°C for pure iPS to 217°C for iPS/PPO at 50% PPO. In addition, there was an elevation in blend T_g due to the amorphous phase becoming richer in PPO, especially for high iPS content (90 and 75% iPS). More recently, Wenig et al.[88] have employed SAXS to study iPS crystallinity in these blends. They found that these blends contained about 30% crystalline content up to about 50% PPO content above which all traces of crystallinity disappeared. This system could be modeled by a linear paracrystalline lattice for which the thickness distribution functions for both the crystal lamellae and amorphous layers were symmetrical Gaussian functions. With increasing PPO content, the mean lamellar thickness decreased while the spherulite radii increased and became no longer volume filling at 30% PPO. They felt that this decrease in lamellae thickness was in part responsible for the observed T_m depression.

Neira further showed that it was possible to crystallize both the PPO and the iPS components if films of their blends were first exposed to MEK vapor (75°C for 72 hrs.) prior to vacuum drying (at 110°C for 24 hrs.); however, this simultaneous crystallization of PPO and iPS was restricted to blend compositions in the range from 20 to 50% PPO. Hammel et al.[89] have used WAXS and the paracrystal-

line model of Wenig et al.[88] to study crystallinity in iPS/PPO films treated in the above manner. They also investigated crystallinity in thermally treated iPS/PPO films (crystalline iPS component) and solvent and thermally treated PS/PPO films (crystalline PPO component). They found that for the iPS/PPO blends, the sizes of the iPS crystals were independent of W_{PPO} in contrast to the observed decrease in iPS lamellar thickness with increasing PPO content. In addition, the iPS crystal sizes were found to be larger for the thermally treated iPS/PPO blends in which only iPS crystallized than for the solvent and thermally treated iPS/PPO blends in which both PPO and iPS crystallized.

Whether or not solvent-induced crystallization of PPO is facilitated by a solvent-PPO complex and/or by easing of kinetic restrictions through plasticization may still be argued. The conclusions reached from the single crystal studies were that the choice of solvent and possible structural factors such as PPO branching during film preparation or polymerization could affect the crystalline structure. Hammel et al.[89] have observed on the other hand that the X-ray pattern for PPO crystallized in an acetone or MEK environment was very similar to the pattern found by Barrales-Rienda and Fatou[7] for dry mats of single crystals grown from α-pinene solution. More important are the conclusions concerning the level of compatibility between PS

and PPO that can be inferred from the crystallization results of PPO crystallized from PS/PPO blends. The depression of T_m and the limited blend composition range over which crystallization can occur suggest intimate if not segmental PS-PPO interactions.

REFERENCES

1. A. S. Hay, U. S. Patent 3,306,875 (assigned to General Electric), February 28, 1967.
2. A. S. Hay, Polym. Eng. Sci., 16, 1 (1976).
3. E. L. McCaffery, "Laboratory Preparation for Macromolecular Chemistry," McGraw-Hill, New York, 1970, pp. 271-278.
4. G. Odian, "Principles of Polymerization," McGraw-Hill, New York, 1970, pp. 135-137.
5. J. M. Barrales-Rienda and D. C. Pepper, J. Polym. Sci., B, 4, 939 (1966).
6. P. J. Akers, G. Allen, and M. J. Bishell, Polymer, 9, 575, (1968).
7. J. M. Barrales-Rienda and J. M. G. Fatou, Kolloid-Z.Z. Polym., 244, 317 (1971).
8. R. A. Niera Lemos, Ph.D. Dissertation, University of Massachusetts, 1974.
9. W. H. Stockmayer and M. Fixman, J. Polym. Sci., 1, 137 (1963).
10. M. Kurata and W. H. Stockmayer, Fortschr. Hochpolym.-Forsch, 3, 196 (1963).
11. A. Opshoor, Polymer, 9, 599 (1968).
12. A. R. Shultz, J. Polym. Sci., A-2, 8, 833 (1970).
13. A. E. Tonelli, Macromolecules, 6, 503 (1973).
14. F. Lauprêtre and L. Monnerie, Eur. Polym. J., 10, 21

REFERENCES (cont.)

(1974); Eur. Polym. J., 11, 845 (1975).

15. A. Factor, J. Polym. Sci., A-1, 7, 363 (1969).

16. D. M. White and A. R. Shultz, private communication.

17. E. P. Cizek, U. S. Patent 3,383,435 (assigned to General Electric), August 11, 1967.

18. L. Bohn, Rubber Chem. Technol., 41, 495 (1968).

19. R. J. Petersen, R. D. Corneliussen, L. T. Rozelle, Polym. Prepr., 10, 385 (1969).

20. S. Krause, J. Macromol. Sci.-Revs. Macromol. Chem., C7, 251 (1972).

21. C. H. M. Jacques and H. B. Hopfenberg, Polym. Eng. Sci., 14, 441 (1974).

22. D. M. White and H. J. Klopfer, J. Polym. Sci., A-1, 10, 1565 (1972).

23. A. R. Shultz and B. M. Gendron, J. Polym. Sci., c, 43, 89 (1973).

24. A. R. Shultz and B. M. Gendron, Report 73CRD024, General Electric, Schenectady, January, 1973; J. Macromol. Sci.-Chem., A8, 175 (1974).

25. A. R. Shultz and B. M. Gendron, Polym. Prepr., 14(1), 571 (1973).

26. A. R. Shultz, A. L. Bridgeman, E. M. Hadsell, and C. R. McCullough, J. Polym. Sci., A-2, 10, 273 (1972).

27. A. S. Hay, private communication.

REFERENCES (cont.)

28. H. E. Bair, Polym. Eng. Sci., 10, 247 (1970).

29. M. Kramer, J. Appl. Polym. Sci., Appl. Polym. Sym. 15, 227 (1970).

30. R. Koningsveld, L. A. Kleintjens, and H. M. Schoffeleers, Pure Appl. Chem., 39, 1 (1974).

31. R. L. Scott, J. Chem. Phys., 17, 279 (1949).

32. H. Tompa, Trans. Faraday Soc., 45, 1142 (1949).

33. M. L. Huggins, J. Chem. Phys., 9, 440 (1941).

34. P. J. Flory, J. Chem. Phys., 12, 425 (1944).

35. P. J. Flory, "Principles of Polymer Chemistry,"Cornell University Press, Ithaca, 1953.

36. G. Gee, Quart. Revs., 1, 26 (1947).

37. A. R. Shultz and C. R. McCullough, J. Polym. Sci., A-2, 10, 307 (1972),

38. P. J. Flory, J. Chem. Phys., 17, 223 (1949).

39. E. P. Otocka, Bell Telephone Laboratories memorandum for record (1968).

40. G. Scatchard, Chem. Revs., 8, 321 (1931).

41. J. H. Hildebrand and R. L. Scott, "Solubility of Non Electrolytes," Reinhold, New York, 1950.

42. C. M. Hansen, J. Paint Technol., 39, 104 (1967).

43. P. A. Small, J. Appl. Chem., 3, 71 (1953).

44. K. L. Hoy, J. Paint Technol., 42, 76 (1970).

REFERENCES (cont.)

45. G. A. Bernier and R. P. Kambour, Macromolecules, 1, 393 (1968).

46. S. Krause, A. L. Smith, and M. G. Duden, J. Chem. Phys., 43, 2144 (1965).

47. R. H. Lacombe and I. C. Sanchez, J. Chem. Phys., submitted for publication.

48. T. K. Kwei, T. Nishi, and R. F. Roberts, Macromolecules, 7, 667 (1974).

49. I. Prigogine, "The Molecular Theory of Solutions," North-Holland Publishing, Amsterdam, 1957.

50. P. J. Flory, J. Amer. Chem. Soc., 87, 1833 (1965).

51. P. J. Flory, B. E. Eichinger, and R. A. Orwoll, Macromolecules, 1, 287 (1968).

52. J. Stoelting, F. E. Karasz, and W. J. MacKnight, Polym. Eng. Sci., 10, 133 (1970).

53. W. J. MacKnight, J. Stoelting, and F. E. Karasz, "Multi-Component Polymer Systems," Amer. Chem. Soc., Washington D. C., 1971, p. 29.

54. W. M. Prest, Jr., and R. S. Porter, J. Polym. Sci., A-2, 10, 1639 (1972).

55. A. R. Shultz and B. M. Gendron, J. Appl. Polym. Sci., 16, 461 (1972).

56. A. R. Shultz and B. M. Beach, Macromolecules, 7, 902 (1974).

REFERENCES (cont.)

57. F. E. Karasz, W. J. MacKnight, and J. J. Tkacik, Polym. Prepr., 15(1), 415 (1974).

58. J. J. Tkacik, Ph.D. Dissertation, University of Massachusetts, 1975.

59. C. H. M. Jacques, H. B. Hopfenberg, and V. Stannett, Polym. Eng. Sci., 13, 81 (1973).

60. A. F. Yee, Polym. Prepr., 17(1), 145 (1976).

61. F. E. Karasz, H. E. Bair, and J. M. O'Reilly, J. Phys. Chem., 69, 2657 (1965).

62. F. E. Karasz, J. M. O'Reilly, H. E. Bair, and R. A. Kluge, Polym. Prepr., 9, 822 (1968).

63. F. E. Karasz, H. E. Bair, and J. M. O'Reilly, J. Polym. Sci., A-2, 6, 1141 (1968).

64. T. G. Fox and P. J. Flory, J. Appl. Phys., 21, 581 (1950).

65. L. Nicolais and R. F. Landel, Polym. J., 7, 259 (1975).

66. F. E. Karasz and J. M. O'Reilly, J. Polym. Sci., B, 3, 561 (1965).

67. F. N. Kelley and F. Bueche, J. Polym. Sci., 50, 549 (1961).

68. H. B. Hopfenberg, V. T. Stannett, and G. M. Folk, Polym. Eng. Sci., 15, 261 (1975).

69. A. Savolainen and P. Tormala, J. Polym. Sci., A-2, 12, 1251 (1974).

REFERENCES (cont.)

70. G. Allen, M. W. Coville, R. M. John, and R. F. Warren, Polymer, 11, 494 (1970).

71. S. de Petris, V. Frosini, E. Butta, and M. Baccaredda, Makromol. Chem., 109, 54 (1967).

72. J. Heijboer, J. Polym. Sci., C, 16, 3755 (1968).

73. A. Eisenberg and B. Cayrol, J. Polym. Sci., C, 35, 129 (1971).

74. T. Lim, V. Frosini, Z. Zaleckas, D. Morrow, and J. A. Sauer, Polym. Eng. Sci., 13, 51 (1973).

75. N. G. McCrum, B. E. Read, and G. Williams, "Anelastic and Dielectric Effects in Polymeric Solids," Wiley, New York, 1967, pp. 409-412.

76. E. Wellinghoff and E. Baer, Preprints, Org. Coat. Plastics Chem., 36, 140 (1976).

77. F. E. Karasz, W. J. MacKnight, and J. Stoelting, J. Appl. Phys., 41, 4357 (1970).

78. A. Wambach, K. Trachte, and A. Dibenedetto, J. Comp. Mater., 2, 266 (1968).

79. L. Nicolais and A. T. Dibenedetto, J. Appl. Polym. Sci., 15, 1585 (1971).

80. R. P. Kambour and A. S. Holik, J. Polym. Sci., A-2, 7, 1393 (1969).

81. L. Kleiner, unpublished results.

82. T. Ree and H. Eyring, J. Appl. Phys., 26, 793 (1955).

REFERENCES (cont.)

83. B. J. MacNulty, J. Mater. Sci., 6, 1070 (1971).

84. C. H. M. Jacques and H. B. Hopfenberg, Polym. Eng. Sci., 14, 449 (1974).

85. W. A. Butte, C. C. Price, and R. E. Hughes, J. Polym. Sci., 61, S28 (1962).

86. W. Wenig, R. Hammel, W. J. MacKnight, and F. E. Karasz, Macromolecules, 9, 253 (1976).

87. A. Factor, G. E. Heinsohn, and L. H. Vogt, Jr., J. Polym. Sci., B, 7, 205 (1969).

88. W. Wenig, F. E. Karasz, and W. J. MacKnight, J. Appl. Phys., 46, 4194 (1975).

89. R. Hammel, W. J. MacKnight, and F. E. Karasz, J. Appl. Phys., 46, 4199 (1975).

CHAPTER II

COMPATIBILITY STUDIES OF THE BLEND: POLY(STYRENE-CO-PARA-CHLOROSTYRENE)/PPO

Experimental Background

In the previous chapter, substantial evidence for the compatibility of PS and PPO has been presented. Recently, Shultz and Beach[1,2] have reported that poly(para-chlorostyrene) (PpClS) and PPO are incompatible. Films made from blends of these two homopolymers were opaque and two T_g's corresponding in temperature to those of pure PpClS and PPO were detected by thermo-optical analysis (TOA), differential scanning calorimetry (DSC), and dynamic mechanical analysis (Vibron measurements).

By contrast, random copolymers of styrene (S) and para-chlorostyrene (pClS) were found to be either compatible or incompatible with PPO depending only upon copolymer composition. Copolymers with 65.3 mole % pClS content or less were compatible with PPO while those with 68 mole % pClS or more were not. In other words, blends of poly(S-co-pClS) and PPO exhibited a compatibility-incompatibility transition between copolymer compositions of 65.3 and 68 mole % pClS.

Below 65.3 mole % pClS, T_g(TOA) versus blend composition followed the same concave curve for poly(S-co-pClS)/PPO

as was shown in Chapter I for PS/PPO (Figure 2). Near the composition range marking the compatibility-incompatibility transition, the relation of T_g(TOA) to blend composition changed in character from being concave to nearly sigmoid. As previously noted in Chapter I, a similar sigmoid relation was found for the dielectric α peak temperature by MacKnight, Stoelting, and Karasz[3] for mechanically mixed PS/PPO blends. The interpretation applied to the observed sigmoid dependence was that the major component by weight in these nearly incompatible blends was contributing slightly more than its weight fraction share toward the apparent T_g(TOA). At higher pClS content, the individual T_g's of PPO and the copolymer were evident although a slight lowering of the T_g of the predominantly PPO phase was observed in blends of PPO and a copolymer of 69.5 mole % pClS. In addition, partial miscibility of this copolymer with PPO was apparent in blends with small PPO content (W_{PPO}=0.125). This coincides with the observed clarity of films at W_{PPO} of 0.125 as well as 0.250 and 0.875 although films of intermediate PPO compositions (0.375, 0.500, and 0.625) appeared hazy.

The DSC results of Shultz and Beach were similar to their TOA findings; however, the minor component by weight in the incompatible blends was difficult to detect or was absent. For all the incompatible blends at $W_{PPO} \leq 0.375$, only the major component, copolymer or PpClS, was evident. For blends of PPO and 69.5 mole % pClS copolymer, the blend

composition range over which the minor component was absent was enlarged; at $W_{PPO}>0.50$, only the T_g of PPO was evident. These observations were tentatively attributed to a lack of sensitivity in the DSC measurements. In addition, blends of PPO and copolymers within the compatibility transition range, between 66.6 and 68.0 mole % pClS, showed some elevation of the lower T_g by incorporation of some PPO in the predominantly copolymer-rich phase and slight lowering of the upper T_g due to the presence of some copolymer in the PPO-rich phase.

The dynamic mechanical studies (Vibron, 110 Hz.) indicated two dynamic storage tensile modulus (E') decrease regions and tan δ peaks corresponding in temperature to that of PpClS in the PpClS/PPO blends. The tan δ for PPO was not reached due to the high temperatures involved (>250°C) and the consequent softening of the tensile specimens. The blends of PPO and 69.5 mole % pClS copolymer, at the edge of the compatibility-incompatibility transition, exhibited a shoulder in tan δ. Such shoulders were observed by Stoelting, Karasz, and MacKnight[4] by measurements of the dynamic loss tensile moduli (E") of their physically mixed PS/PPO blends.

Karasz, MacKnight, and Tkacik[5] have studied compatibility in the poly(S-co-pClS)/PPO system by transmission electron microscopy and by dielectric analysis in addition to the DSC and dynamic mechanical techniques employed by

Shultz and Beach. In agreement with the conclusions of Shultz and Beach, they detected two T_g's by DSC for blends of PPO and PpClS and blends of PPO and a copolymer with 68 mole % pClS composition. They also observed some elevation of the lower T_g and a lowering of the upper T_g but no trends were discerned. In addition, transmission electron microscopy of the high temperature (170°C) fracture surfaces of the incompatible blends revealed macroscopic phase separation absent in the compatible PS/PPO blends. Blends of PPO and a copolymer with 47 mole % pClS content were found to be compatible by the presence of a single DSC T_g.

The dielectric loss in PpClS or in the copolymers was about three orders of magnitude greater than PPO due to the high polarity of these molecules for which the chlorine dipoles (ca. 1.94 Debye) are oriented perpendicular to the main chain. Due to this disparity in the dielectric loss, the dielectric measurements of these blends reflected only the motions of the pClS component to a good approximation. The temperatures at maximum dielectric loss (ε'') for the compatible blends of PPO and the copolymer with 47 mole % pClS were found to increase linearly with increasing W_{PPO}. By contrast, temperatures at maximum ε'' were independent of blend composition for the incompatible blends. In addition, the compatible blends exhibited a composition-independent Arrhenius activation energy of about 145 kcal $mole^{-1}$ as calculated from the slope of the frequency of ε'' maximum versus reciprocal temperature.

In an extended study, Tkacik[6] revealed from transmission electron microscopy that at 25% PPO, blends of PPO and PpClS or the copolymer with 68 mole % pClS were characterized by ridgelike structures as a result of the extended ductile fracture surface of PPO in the PpClS or copolymer phase. At 75% PPO, phase inversion was observed with aggregates of PPO, ca. 2μ, dispersed in a PpClS or copolymer matrix. Another copolymer, 60 mole % pClS, was investigated by Tkacik and was found to be compatible with PPO by DSC, dielectric, and dynamic mechanical techniques.

The most interesting finding of Tkacik's study came from an analysis of the dielectric data by the Fröhlich[7] equation which relates a dipole orientation function, g, to the limiting dielectric constants at high and low frequencies, ε_R and ε_U respectively. This equation was given as

$$g = \frac{9kT}{4\pi N \mu_o^2} \frac{(2\varepsilon_R+\varepsilon_U)(\varepsilon_R-\varepsilon_U)}{\varepsilon_R(\varepsilon_R+2)^2} \qquad (7)$$

where

k, Boltzmann's constant

T, absolute temperature

N, number of dipole per cc

μ_o, dipole moment of an isolated dipole unit

ε_R, relaxed dielectric constant

ε_U, unrelaxed dielectric constant

For no orientation correlation between molecules, g is unity. For most macromolecules, g is less than unity due to chain configuration and hindered rotation. As the effective dipole concentration is decreased as it is by dilution with a low molecular weight solvent, g increases. The dipole orientation function also increases if the effective dipole concentration is reduced by copolymerization of the polar entity with a nonpolar one. Mikhailov et al.[8] have observed an increase in g for copolymerization of para-chlorostyrene with styrene by dielectric measurements in solution. Tkacik showed that while g was independent of blend composition for the incompatible blends, g increased with increasing W_{PPO} for the compatible blends from about 0.40 to 0.80. This was interpreted to indicate that mixing in the compatible poly (S-co-pClS)/PPO blends was as intimate as for poly(S-co-pClS) in a low molecular weight solvent. In the case of the blends, PPO could be viewed as the solvent and therefore g increased with increasing dilution, i.e. increasing W_{PPO}.

Dissertation Objectives

Besides this advantage of using polar poly(S-co-pClS) for dielectric studies, there is an additional opportunity afforded by the poly(S-co-pClS)/PPO system to study the dependence of the mechanical properties of these blends upon the state of compatibility. It is well recognized that incompatible blends in general have poor mechanical integrity.

The dispersed phase acts as a stress concentrator leading to crazing, shear banding, or both, and failure often occurs by interfacial delamination as a consequence of weak bonding between the dispersed phase and the incompatible matrix.[9] In addition to the poly(S-co-pClS)/PPO blends, there are several other systems consisting of a homopolymer and a copolymer that undergo one or more compatibility-incompatibility transitions at certain copolymer compositions. These include PVC/polu(ehtylene-co-vinyl acetate)[10] and the important PVC/poly(butadiene-co-acrylonitrile)[11] blends. Due to the very different monomers comprising the copolymers, the properties of the copolymers themselves change significantly with copolymer composition. This is especially true for copolymers like poly(butadiene-co-acrylonitrile) for which one of the corresponding homopolymers is rubbery, e.g. polybutadiene, and the other is glassy, e.g. polyacrylonitrile. Therefore it is difficult to completely isolate the effects of changing blend compatibility upon mechanical properties from changes in the copolymer properties with varying copolymer composition. This difficulty is not as severe for the poly(S-co-pClS)/PPO system because PS and PpClS have very similar properties and therefore copolymer properties do not significantly change with copolymer compositions. It is therefore possible to obtain a one-to-one correspondence between blend compatibility and properties for this system. This is a unique opportunity and is one not previously taken.

In addition to the absence of mechanical property data, the studies of Shultz and Beach and those of Tkacik and others leave several important questions still unanswered. These are:

(1) In terms of mole % PClS, how sensitive is the compatibility-incompatibility transition to copolymer composition?

(2) Can specific trends be discerned in the observed lowering of the high T_g of the PPO-rich phase and the raising of the low T_g of the copolymer-rich phase reported for some incompatible blends?

(3) What are the reasons for the apparent difficulty in detecting the T_g's of the minor components reported by Shultz and Beach in their DSC studies of the incompatible poly(S-co-pClS)/PPO blends?

(4) Does the negative excess volume of mixing reported for PS/PPO (Chapter I) go to zero as incompatible copolymer compositions are approached?

(5) Can classical free volume theory (i.e. Kelley and Bueche treatment, Chapter I) be used to predict the relation of blend T_g to composition for all the compatible blends in the poly(S-co-pClS)/PPO system?

(6) Does the position at which chlorine is attached to the aromatic styrene sites affect blend compatibility? For example, is poly(ortho-chlorostyrene) (PoClS) compatible with PPO?

The objectives of the present work were to answer the above questions with the goal of obtaining a generalized picture of blend compatibility. To improve the sensitivity of DSC measurements in the detection of minor transitions, techniques were borrowed in part from the recent studies of Landi.[12] Landi showed that two phases of closely spaced T_g's could be resolved by DSC for heterogeneous copolymers of butadiene and acrylonitrile by using large samples (25-35 mg) and a point-wise correction of relative heat absorption to optimize the signal-to-noise ratio and thereby increase sensitivity. As outlined in the following chapters, these techniques of large sample sizes, baseline correction, and in addition better instrumentation (Perkin-Elmer DSC II) are used to follow quantitative and qualitative changes in the glass transitions of blends of PPO and copolymers whose compositions span the range from compatibility to incompatibility and particularly those within the 65 to 68 mole % pClS range which mark the compatibility-incompatibility transition. The parameters of the glass transition reported in this study are the temperature, the width, and the height (ΔC_p) of the glass transition from which significant information concerning the state of molecular homogeneity can be deduced.

In addition, the compatibility (or incompatibility) of blends of PoClS and PPO is investigated, apparently for the first time. The densities of all blends are measured and

compared to those observed for other compatible systems. Finally, Young's modulus, tensile strength (stress at break or yield), and percent elongation at break (or yield) are determined for all blends. From this information, conclusions on the relation between blend compatibility and mechanical properties are reached.

REFERENCES

1. A. R. Shultz and B. M. Gendron, paper presented at the Biennial Polymer Symposium, Ann Arbor, June, 1972.
2. A. R. Shultz and B. M. Beach, Macromolecules, 7, 902 (1974).
3. W. J. MacKnight, J. Stoelting, and F. E. Karasz, "Multi-Component Polymer Systems," Amer. Chem. Soc., Washington, D. C., 1971, p. 29.
4. J. Stoelting, F. E. Karasz, and W. J. MacKnight, Polym. Eng. Sci., 10, 133 (1970).
5. F. E. Karasz, W. J. MacKnight, and J. J. Tkacik, Polym. Prepr., 15(1), 415 (1974).
6. J. J. Tkacik, Ph.D. Dissertation, University of Massachusetts, 1975.
7. H. Fröhlich, "Theory of Dielectrics," Oxford University Press, Oxford, 1958.
8. G. P. Mikhailov, A. M. Lobanov, and M. P. Platonov, Polym. Sci. USSR, 9, 2565 (1967).
9. A. F. Yee, Polym. Prepr., 17(1), 145 (1976).
10. C. F. Hammer, Macromolecules, 4, 69 (1971).
11. G. A. Zakrzewski, Polymer, 14, 347 (1973).
12. V. R. Landi, Rubber Chem. Technol., 45, 222 (1972).

C H A P T E R I I I

POLYMERIZATIONS AND EXPERIMENTAL TECHNIQUES

Materials and Method of Polymerizations

PPO was obtained as an additive-free powder through the courtesy of A. Katchman of General Electric. It was purified by filtration of a dilute solution of PPO in toluene (3-5%) prior to precipitation into a large volume (10:1) of methanol. Molecular weights of the purified polymer were determined in chloroform by gel permeation chromatography (GPC) at 25°C, courtesy of C. Orlando of General Electric. GPC results were $\bar{M}_n$=16,900, $\bar{M}_w$=34,800, and $\bar{M}_z$=54,300 with polydispersities of 2.05 ($\bar{M}_w/\bar{M}_w$) and 1.56 ($\bar{M}_z/\bar{M}_w$). A viscosity-average molecular weight ($\bar{M}_v$) of 23,000 was determined in toluene at 25°C.[1]

Monomers for the polymerizations were styrene (Eastman, lot C28), para-chlorostyrene (Aldrich, lot 110137), and ortho-chlorostyrene (Aldrich, lots 051817 and 090347). These were purified prior to polymerization by washing with a 10% aqueous solution of sodium hydroxide (Baker reagent 1-3722) in equal volumes with the monomers. The washed monomers were dried by decanting them over activated (100°C in vacuum) molecular sieves (MCB Mx1583-80, L1167, Linde Type 3A, 1/16") and were then distilled under vacuum (15-25

mm Hg). Only halocarbon (25-5S) stopcock grease was used to seal the ground-glass joints of the microware distillation apparatus and separatory funnels used in the purification procedures.

With the exception of one thermal polymerization at 110°C (Copolymer F), all polymerization were free-radical in solution, spectral-grade toluene (Burdick and Jackson, lot 5946), at 60°C. The initiator was 2,2'-bisazoisobutyronitrile (AIBN, Polysciences) which was purified by crystallization from methanol. Quantities of purified monomer and toluene were pipetted into predried 250 ml round-bottom flasks which contained about 0.400 mole % (of monomer composition) AIBN. These flasks were sealed with rubber serum stoppers, which had been leached of pigments in boiling toluene by Soxhlet extraction, and then tightly covered with parafilm. They were then immersed and agitated in a controlled temperature (±1°C) shaking water bath. At the beginning of each polymerization, dried nitrogen (passed through Drierite) was rapidly bubbled into the reaction mixture for about five min. During the polymerizations, the flasks were purged by a continuous stream of dried nitrogen at approximately 50 cc min^{-1}.

At the end of the polymerizations, the viscous mixtures of polymer, solvent, initiator, and monomer were diluted with additional toluene to bring the total polymer concentration to about 4% and then dropwise precipitated

into a 10:1 ratio of rapidly stirring, filtered methanol. The fine white precipitates were collected in a sintered glass Buchner funnel (450ml-C), washed with additional methanol, and dried at 100°C for 48 hrs. (80°C for PS). The dried polymers were weighed to determine yield and then purified by redissolving them in toluene, filtering, and reprecipitating in methanol. The reprecipitated and purified polymers were then dried in vacuum as before and reweighed to determine final yield.

Copolymer Drift Study. Reactivity ratios (r) reported for styrene (S) and para-chlorostyrene (pClS) suggest that the arrangement of monomer units in copolymers of S and pClS should be nearly random with some tendency toward alternation. In an early reference, Lewis et al.[2] calculated reactivity ratios for styrene and pClS to be 0.74±.03 and 1.025±.05, respectively, for bulk copolymerization at 60°C with 0.1 mole % benzoyl peroxide initiator. These are compared to 0.62 for S and 1.35 for pClS as reported more recently by Okumoto et al.[3] for AIBN initiated bulk copolymerization at 60°C. Copolymer composition in mole fraction pClS (F_{pClS}) was calculated from the instantaneous copolymerization equation[4] given in eq. (8) for both pairs of reactivity ratios and is plotted versus monomer batch composition (f_{pClS}) in Figure 4. The solid line represents ideal or statistical copolymerization for which both reactivity ratios equal unity.

Figure 4. Copolymer composition (F_{pClS}) in mole fraction pClS versus mole fraction pClS in monomer mixture (f_{pClS}). Curve A, calculated from the reactivity ratios of Okumoto et al., ref. (3); curve B, calculated from the reactivity ratios of Lewis et al., ref. (2); curve C, ideal copolymerization line.

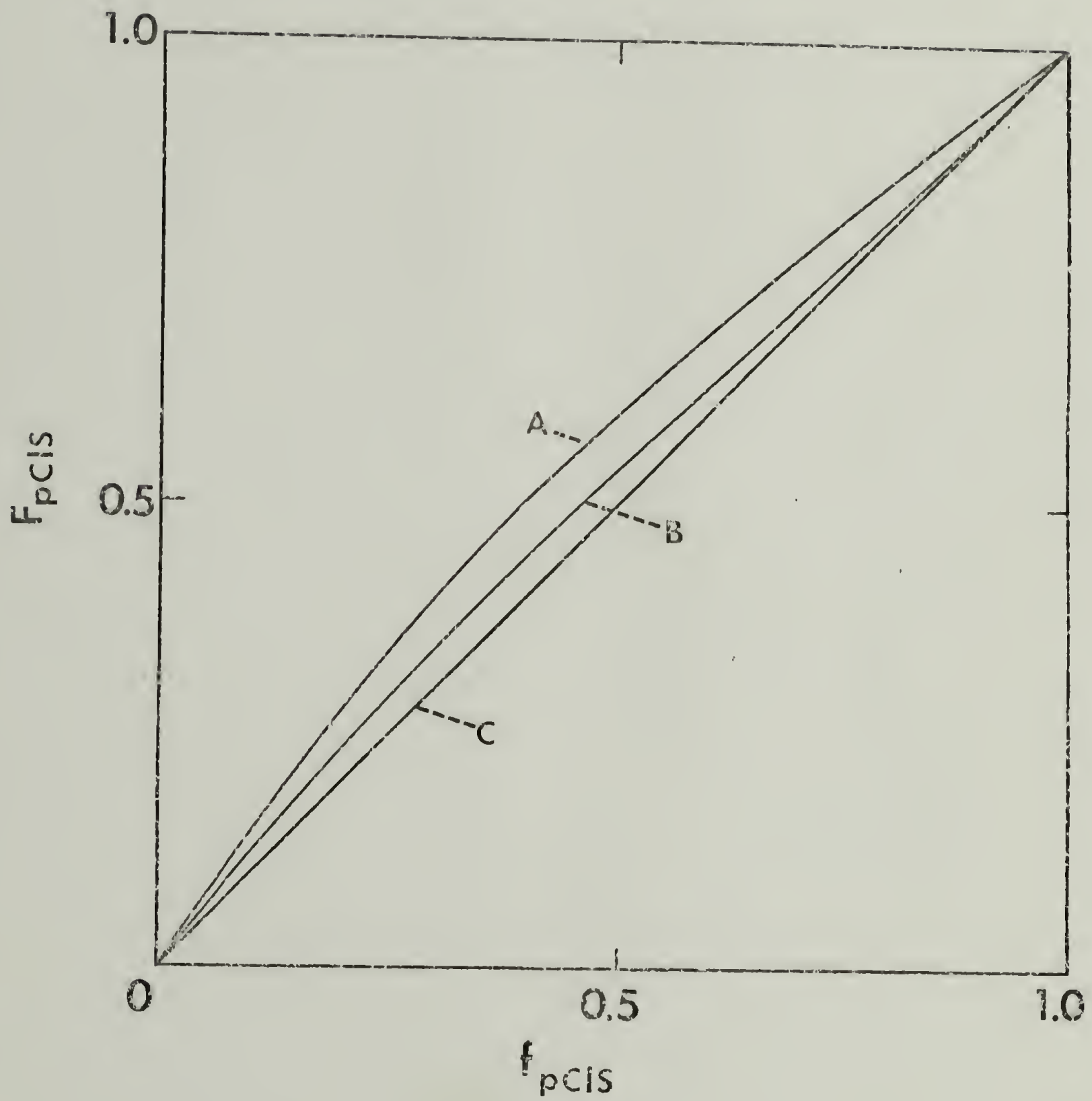
1.0
0.5
0
0.5
1.0
F_{pCIS}
f_{pCIS}
A
B
C

$$F_{pClS} = \frac{(r_{pClS}-1)f_{pClS}^2 + f_{pClS}}{(r_{pClS}+r_S-2)f_{pClS}^2+2(1-r_S)f_{pClS}+r_S} \qquad (8)$$

The values of Lewis et al. are shown to more closely approach ideal copolymerization than those of Okumoto et al.

The difference between the reactivity ratios of S and pClS and the ideal or purely random copolymerization values of unity indicates that the batch monomer mixture will become progressively richer in the less reactive monomer, styrene, with increasing conversion. As a result of these changes in the monomer ratio of the batch, the copolymer at a given conversion of monomer will contain a continuous distribution of copolymer compositions. The breadth of this distribution or copolymer heterogeneity consequently increases with greater conversion. Due to the apparent sharpness of the compatibility-incompatibility transition region, less than 3 mole % pClS in copolymer composition from the results of Shultz and Beach[5], it is important that copolymers in this range be polymerized to low enough conversion to insure that the heterogeneity of their compositions does not in itself span the transition range. Otherwise meaningful interpretation of the compatibility characteristics of blends of these copolymers and PPO is not possible.

To assess copolymer drift defined as the difference between the initial and final copolymer composition at a given conversion, small quantities of monomer mixtures

containing 64.32 mole % pClS were copolymerized in test tubes by the polymerization procedures outlined in the previous section. Four identical copolymerization batches were prepared by pipetting 5.0 ml of a masterbatch into individual test tubes. The composition of this masterbatch is given in Table III (Batch A). The copolymerization mixtures were withdrawn from the shaking water bath (60°C) at times of 1.0, 5.0, 9.0, and 15.0 hrs. and precipitated in methanol. The yield, % theoretical, or conversion at each polymerization time is given in Table IV. In addition, the composition of the purified and dried copolymers were determined by chlorine analysis and are given in terms of wt % chlorine and mole % pClS in Table IV. To obtain more complete polymerization rate data, four other monomer batches at 64.32 mole % pClS composition (Batch B in Table III) were polymerized and removed at times of 0.25, 1.0, 2.0, and 6.0 hrs. Corresponding yields are given in Table IV. In addition, the two homopolymers, PS (Batch D) and PpClS (Batch C), were polymerized at times of 16.0 and 6.0 hrs., respectively. Percent yield for the copolymers, PS and PpClS is plotted versus polymerization time in Figure 5. The conversion data for the copolymer was fitted by a smooth curve. PpClS appears to polymerize to higher conversion (above copolymer curve) and PS to lower conversion (below curve) than the copolymer (ca. 68 mole % pClS) at comparable times.

Table III. Batch Compositions for Rate and Drift Studies

Batch	Composition of Test Tube Batch	pClS mole %	Toluene ml mole^{-1}	AIBN mole %
A	5.0 ml of a masterbatch: 5.0 ml S, 10.0 ml pClS, 10.0 ml toluene, 0.0810 gm AIBN	64.32	82.0	0.400
B	1.0 ml S, 2.0 ml pClS, 2.0 ml toluene, 0.016 gm AIBN	64.32	82.0	0.405
C	3.0 ml pClS, 3.0 ml toluene, 0.0160 gm AIBN	100.	127.6	0.414
D	3.0 ml S, 3.0 ml toluene, 0.0171 gm AIBN	0	114.9	0.399

Table IV. Polymerization Rate and Copolymer Drift Study

Batch	Time hrs.	Yield % Theor.	Copolymer Composition Wt. % Chlorine		mole % pClS
B	0.25	0.69			
B	1.0	4.2			
A	1.0	4.8	19.28 19.27	ave. 19.28	69.57
B	2.0	8.6			
A	5.0	23.0	18.91 19.01	ave. 18.96	68.27
B	6.0	23.8			
C	6.0	29.6			100.
A	9.0	36.3	18.99 19.08	ave. 19.04	68.64
A	15.0	53.3	18.91 19.13	ave. 19.02	68.55
D	16.0	53.1			0

Figure 5. Copolymer yield (%) versus time (hrs.). Curve is fitted to data (●) from the copolymer drift study for which the monomer batch was 64.3 mole % pClS in composition. (■) and (◆) represent yields for polymerization of the homopolymers, PS and PpClS.

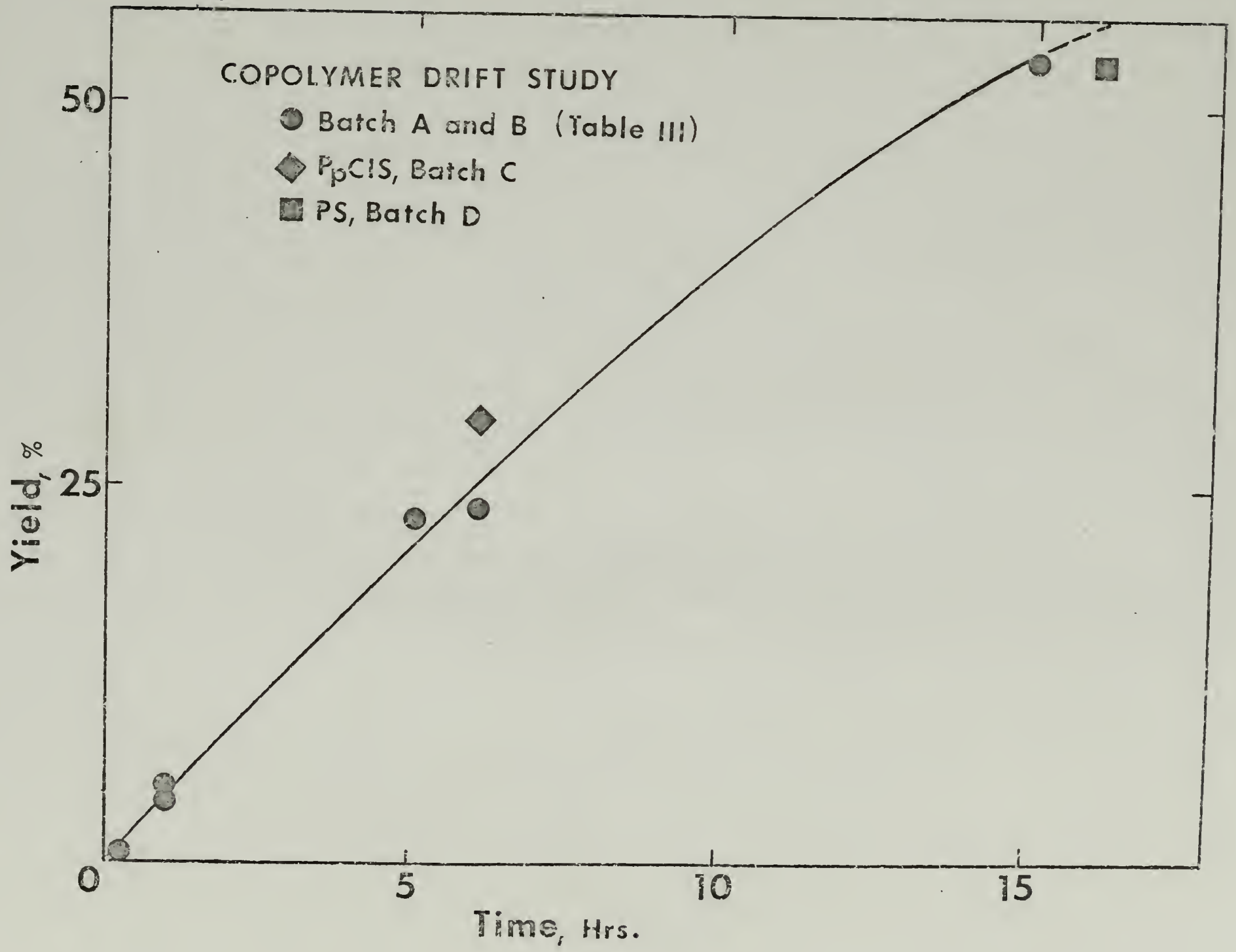
COPOLYMER DRIFT STUDY
Batch A and B (Table III)
PpCIS, Batch C
PS, Batch D
50
25
0
5
10
15
Yield, %
Time, Hrs.

In Figure 6, copolymer composition is plotted versus yield. The data points represent the average of two chlorine analyses and the error bars indicate the maximum error bounds of 0.2 wt. % (±0.8 mole % pClS) for routine chlorine analysis (single potentiometric titration). The best straight line was fitted to these data points by the method of least squares. Although curvature of the line is expected for high conversions, a linear relation is a suitable approximation at moderate yeilds (50-60%). The open circle represents a copolymer composition (Copolymer E) obtained for a 15 hr. copolymerization at the same monomer composition (64.32 mole % pClS) as for the drift study batches but at a 15:1 scaleup in quantity. As shown in Figure 6, the composition of this copolymer agrees very closely with the solid line fitted to the drift study data.

The slope of the line in Figure 5 indicates a copolymer drift of 0.89 mole % pClS at 50% conversion. Copolymer drift also can be calculated from the instantaneous copolymerization equation, eq. (8), and the reactivity ratios of Lewis et al.[2] and Okumoto et al.[3] by assuming a constant copolymer composition over a 10% conversion interval.[6] The drifts calculated for a corresponding conversion of 50% are 0.75 and 2.10 mole % pClS for the Lewis and the Okumoto results, respectively. Compared to the experimental drift of 0.89, the drift of 0.75 calculated from the Lewis et al. reactivity ratios appears to be the better prediction, but both

Figure 6. Copolymer composition in mole % pClS (●) versus yield (%) for a monomer batch of 64.3 mole % pClS composition (copolymer drift study). (○) represents the composition of Copolymer E, for the same monomer batch composition but for 15X scale-up in material.

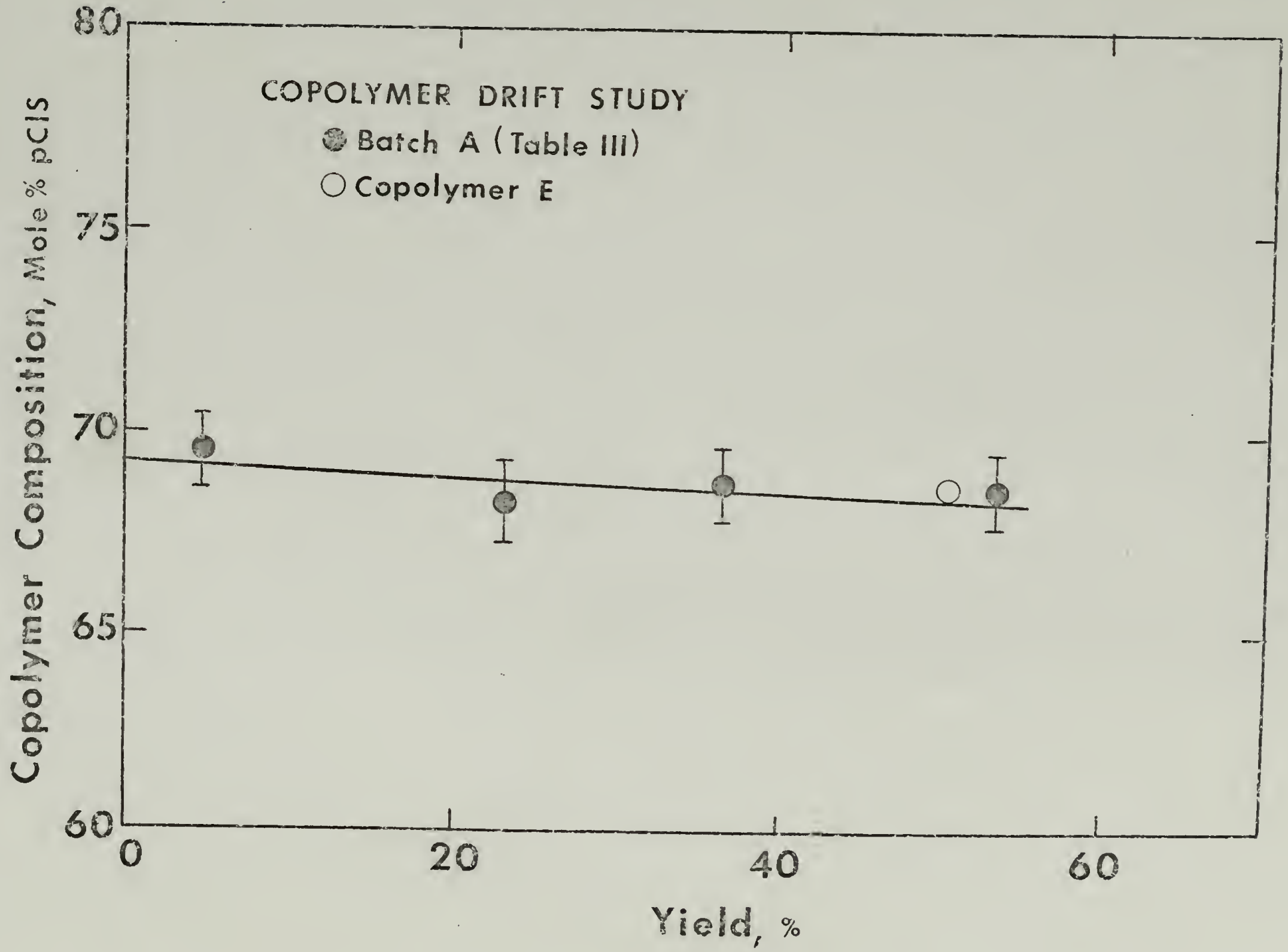
COPOLYMER DRIFT STUDY
Batch A (Table III)
Copolymer E
Copolymer Composition, Mole % pCIS
80
75
70
65
60
0
20
40
60
Yield, %

experimental values of 0.75 and 2.10 fall within the error bounds for the slope of the experimental drift line in Figure 6 for which a regression correlation coefficient of -0.5 is calculated.

Good agreement between experimental and calculated drift is also obtained if reactivity ratios calculated from the Q-e scheme of Alfrey and Price[7] are used in the instantaneous copolymerization equation. The Q-e reactivity ratio for S is given by

$$r_S = \frac{Q_S}{Q_{pClS}} \exp[e_S(e_{pClS}-e_S)] \qquad (9)$$

By using values of -0.8 for e and 1.0 for Q of S and corresponding values of -0.33 and 1.03 for pClS,[8] the Q-e reactivity ratios are calculated from eq. (9) for S and from the corresponding equation for pClS to be 0.667 and 1.203, respectively. Using these values in the instantaneous copolymerization equation, a copolymer drift of 1.20 mole % pClS is calculated. This calculated drift is also closer to the experimental value of 0.89 than the value of 2.10 calculated from the reactivity ratios of Okumoto et al.

The above results indicate that the copolymerization of S and pClS is sufficiently ideal that relative homogeneity is insured for copolymers up to about 50% conversion. (For their studies, Shultz and Beach[5] used much higher conversions, 70-90%, in bulk copolymerizations of S and pClS.) For this reason, no attempt was made to correct for drift

by continuous addition of depleted monomer as is done commercially for highly alternating copolymers.[9]

Copolymerizations. In addition to PS, PpClS, and two different molecular weight samples of PoClS, five copolymers of S and pClS were polymerized. Three of these copolymers (C, D, and E) were expected to be within the compatibility-incompatibility transition range reported by Shultz and Beach.[5] The compositions of the polymerization mixtures used in the synthesis of all the homopolymers and copolymers in this study are given in Table V. These were calculated on the basis of the molecular weights and densities given in Table VI.[10]

The polymerizations were allowed to continue for 15 hrs. at 60°C with the exception of Copolymer F which was thermally polymerized at 110°C for 23.5 hours and the second oClS batch (PoClS-2) which was permitted to polymerize for 24 hrs. at 60°C. In the latter case, a 10:1 increase in the quantity of toluene was utilized to lower the molecular weight through solvent chain transfer. As a result of this increase in the solvent concentration, conversion per unit time was reduced. To obtain a reasonable PoClS yield, the polymerization time was extended to 24 hrs. in this case.

Polymerization yields are given in Table VII. As indicated in the copolymer drift study, yield is approximately 50% for polymerizations at the end of 15 hrs. The yield data was scattered and no significant trend on the

TABLE V. Batch Polymerization Compositions

Sample Code	Notebook	Styrene ml	Styrene moles	pClS/oClS ml	pClS/oClS moles	pClS/oClS mole %	Toluene ml	Toluene ml mole^{-1}	AIBN gm	AIBN moles	AIBN moles %
PS	II-18	70.0	0.1609	0	0	0	27.0	167.8	0.4001	0.002437	0.4002
B	II-62	20.0	0.1740	28.0	0.2196	55.8	27.0	68.6	0.2563	0.001561	0.3966
C	II-6	20.0	0.1740	37.0	0.2901	62.5	37.0	79.7	0.3407	0.001856	0.3999
D	II-36	19.4	0.1688	37.5	0.2940	63.5	37.0	79.9	0.3053	0.001859	0.4017
E	I-67	15.0	0.1305	30.0	0.2352	64.3	30.0	82.0	0.2402	0.001463	0.4001
F	I-45	5.9	0.0513	9.8	0.0786	60.0	10.0	78.0	thermal, 110°C		
PpClS	II-23	0	0	50.0	0.3921	100.	31.0	79.1	0.2563	0.001561	0.3981
PpClS-1	II-67	0	0	17.0	0.1349	100.	10.0	74.1	0.0908	0.000553	0.4099
PpClS-2	III-1	0	0	10.0	0.794	100.	60.0	756.0	0.0534	0.000325	0.4095

TABLE VI. Physical Constants of Polymerization Materials

	Density gm ml^{-1}	Molecular Weight
styrene	0.9060	104.15
p-chlorostyrene	1.0868	138.60
o-chlorostyrene	1.1000	138.60
toluene	0.8669	92.15
AIBN	-	164.21

TABLE VII. Polymerization Yields and Copolymer Compositions

Sample Code	Yield %	Monomer Mix. mole % pClS	Copolymer Compositions (mole % pClS) Calculated from reactivity ratios			Experimental
			Lewis *et al.*	Q-e scheme	Okumoto *et al.*	
PS	42.5	0	0	0	0	-
B	58.1	55.8	58.1	60.2	61.8	58.5
C	48.9	62.5	64.6	66.9	68.6	67.1
D	55.4	63.5	65.4	67.4	68.9	67.8
E	44.4	64.3	66.2	68.2	69.6	68.6
F	62.4	-	-	-	-	75.4
PpClS	53.8	100.0	100.0	100.0	100.0	100.2
PoClS-1	89.9	-	-	-	-	-
PoClS-2	29.1	-	-	-	-	-

relation of polymerization yield to pClS content of the monomer mixture could be ascertained. Ushakov and Matuzov[11] have observed a linear increase in conversion with increasing pClS content of the copolymer.

Copolymer compositions were determined from chlorine analysis and are given in the last column (Experimental) of Table VII. The technique used to obtain the most accurate copolymer compositions was a potentiometric titration of chloride followed by a gravimetric determination of silver chloride with a reported maximum error of ±0.1 wt. % Cl.* An average of these two determinations was reported in mole % pClS for each copolymer. Theoretical copolymer compositions have been calculated from the three sets of reactivity ratios previously cited and the instantaneous copolymerization equation, eq. (8), by assuming copolymer composition to be constant within a 10% conversion interval as was done in the determination of copolymer drift in the previous section. These compositions are given in mole % pClS in Table VII for comparison with chlorine analysis results. The calculated compositions are those at 50% conversion. The best agreement with the experimental values are for

---

*Performed as a commercial service by Schwarzkopf Microanalytical Laboratory, New York. Chlorine analysis on the drift study samples was a routine titration procedure performed by Baron Consulting Co., Conn.

compositions calculated from the Q-e reactivity ratios. By comparison, the reactivity ratios of Lewis et al.[2] predict copolymer compositions which are too low and those of Okumoto et al.[3] result in compositions which are too high. The three copolymers which were prepared for study of the compatibility-incompatibility transition for the copolymer/PPO blends were found to have compositions of 67.1, 67.8, and 68.6 mole % pClS (copolymers C, D, and E, respectively).

Molecular weights and molecular weight distributions for PS, PpClS, PoClS-1, and the five copolymers were determined by GPC at 25°C in tetrahydrofuran (THF). Except for PS, all molecular weights were corrected by assuming that molecules of equal contour lengths elute at equal volumes. Shultz and Beach[5] gave the equation for this correction as

$$M = M_{PS}[(1-N_{pClS})+(138.6/104.2)N_{pClS}] \qquad (10)$$

where M_{PS} is the GPC molecular weight based upon PS calibration and N_{pClS} is the mole fraction of pClS in the copolymer. In addition, the molecular weights of PoClS-1, PoClS-2, and a third PoClS sample, prepared by A. Chatterjee from bulk polymerization of oClS initiated by 0.1 wt. % benzoyl peroxide (PoClS-3), were determined from intrinsic viscosity measurements in toluene solution at 30°C. Approximately 2% solutions were made for the three PoClS samples and a copolymer of pClS and oClS with about 27% pClS (Dow Chemicals). These 2% solutions were diluted directly in a No. 1 Ubbelohde

211 viscometer by addition of toluene to obtain different concentrations;the time for measured flow was recorded at each concentration (ca. 2.0, 1.5, 1.0, and 0.5 wt. %) in a controlled-temperature (±0.5°C) water bath. Intrinsic viscosities, [η], were calculated for each of the four materials and from these values molecular weights were determined by the Mark-Houwink-Sakurada equation and the parameters given by Matsumura[12] for PoClS in toluene at 30°C. This equation is given as

$$[\eta] = 14.3 \times 10^{-5} M_v^{0.65} \qquad (11)$$

where [η] is in dl gm^{-1}. Both GPC and viscosity-average molecular weights ($\bar{M}_v$) are given in Table VIII.

Several remarks should be made about the molecular weight results given in Table VIII. First, the molecular weight of PS polymerized in this study is low ($\bar{M}_n$=38,000) compared to those of the copolymers (81,000-100,000). This was probably due to the larger amount of solvent used in the polymerization of PS. The molecular weights of the three PoClS homopolymers illustrate the significant effect of toluene as a solvent transfer agent in reducing the molecular weight of the solution-polymerized product. In terms of viscosity-average molecular weight, the bulk polymerized PoClS had the highest molecular weight of 1,213,000 followed by 571,000 for PoClS-1 polymerized in a toluene concentration of 74.1 ml per mole of oClS monomer and then 223,500

TABLE VIII. Molecular Weights of Blend Polymers

Sample	N_{pClS}	[ ]*	Uncorrected MW $\bar{M}_n$	Uncorrected MW $\bar{M}_w$	$\bar{M}_v$	Corrected MW $\bar{M}_n$	Corrected MW $\bar{M}_w$	$\bar{M}_w/\bar{M}_n$	$\bar{M}_z/\bar{M}_w$
PS	0	1.000	38,000	81,800	-	38,000	81,800	2.16	1.53
B**	0.585	1.193	79,400	174,000	-	94,700	208,000	2.19	1.92
C	0.671	1.222	72,100	118,000	-	88,100	145,000	1.69	1.41
D	0.678	1.224	81,700	156,000	-	100,000	192,000	1.92	1.42
E	0.686	1.226	66,000	145,000	-	81,000	177,000	2.19	1.53
F	0.754	1.249	216,000	390,000	-	270,000	487,000	1.80	1.50
PpClS	1.000	1.330	96,400	163,000	-	128,000	217,000	1.69	1.46
PoClS-1**	1.000	1.330	176,000	495,000	571,000	235,000	658,000	2.81	1.61
PoClS-2	-	-	-	-	224,000	-	-	-	-
PoClS-3	-	-	-	-	1,213,000	-	-	-	-
P(oClS-co-pClS)	-	-	-	-	665,000	-	-	-	-
PPO	-	-	16,900	34,800	23,000	-	-	-	-

*[ ] represents multiplicative factor in brackets, eq.(10).

**GPC by DeBell and Richardson Testing Institute, Conn.; molecular weights were calculated from results expressed in angstroms extended length of PS by MW=Q[A] where Q was 41.58.

for PoClS-2 at 756 ml toluene per mole of oClS. In addition, PoClS appeared to polymerize to higher molecular weight and conversion than PpClS under identical initiator and solvent concentrations. There is also some evidence for an increase in molecular weight with increasing mole % pClS for the copolymer. The one discrepancy in the molecular weight trend was Copolymer F which had substantially higher molecular weight ($\bar{M}_n$=270,000) than any other copolymer. Copolymer F was the only one which was thermally polymerized and due to toluene loss during reflux at 110°C, the final polymerization mixture was nearly bulk. The subsequent Trommsdorf effect at high conversion probably led to the higher observed molecular weight.

Due to the influence of molecular weight upon blend compatibility (i.e. decreasing tendency for compatibility with increasing molecular weight),[13] the differences in molecular weight between some of the copolymers and homopolymers in Table VIII may be cause for some concern. The important fact to note is that within experimental uncertainties, the three copolymers (C, D, and E) expected to be within the compatibility-incompatibility transition region of composition have nearly equal molecular weights. This means any transition would occur only as a result of the slight differences in their pClS compositions and not as a result of molecular weight effects. In fact, Shultz and Beach[5] found an almost identical transitional composition

range to that of the present study (Chapter IV) for blends of PPO and copolymers with higher molecular weights (bulk polymerizations at high conversions, 70-90%). In addition, although the molecular weight of the PS sample used in the present study is low, it is well known that PPO and PS are compatible at much higher molecular weights. For example, Yee[14] has demonstrated compatibility for blends of high molecular weight samples of PS ($\bar{M}_w$=430,000) and PPO ($\bar{M}_w$=120,000). Finally, the effects of widely differing molecular weights upon blend compatibility will be studied for blends of PPO and the three PoClS samples previously cited. In addition, whether PPO and PpClS can be made compatible by lowering the molecular weight of PPO will be investigated for blends of PpClS and a low molecular weight PPO ($\bar{M}_n$=5,760, $\bar{M}_w$=11,500, $\bar{M}_w/\bar{M}_n$=2.00) supplied through the courtesy of T. F. Rutledge of ICI United States, Inc. This sample of PPO was prepared using a palladium-carbon catalyst.[15]

Blend and Film Preparation

The copolymers and homopolymers given in Table VII were blended with PPO by coprecipitation from dilute solution (3-4% in toluene) into a large quantity of methanol (10:1). This same precipitation procedure was used in the purification of the polymers recovered from the polymerization. Prior to precipitation, all the blend solutions were

heated on ca. 50°C to remove traces of PPO crystallinity (slightly cloudy tc clear upon heating). The precipitated blends were collected in a sintered glass funnel and were then dried at 100°C in vacuum for about 48 hours.

Except for PoClS-2 and PoClS-3, blends of 20,40,60, and 80% PPO by weight were prepared in this manner. In addition to the above compositions, 50% PPO blends were prepared for Copolymer E and for PpClS. For PoClS-2 and PoClS-3, only 50% PPO blends were made. The compositions of all blends used in this study with the exception of that of PpClS and the low molecular weight PPO cited above are given in Table IX. In addition, total material loss upon precipitation is indicated in the last column at the right of Table IX. In general, total loss is minimal, 3-6%, except for blends which were prepared in small quantities and for which one of the components is low molecular weight. These material losses for the blends were about the same values for those observed in the precipitation of pure PPO and pure ClS-polymers during purification. One exception was a 50/50 blend of PpClS and the low molecular weight PPO ($\bar{M}_n$= 5,760) sample cited in the above section. This blend was prepared by coprecipitating 1.4963 gm of PpClS and 1.4954 gm of the PPO from cosolution in toluene as for the other blends. For this case, material loss was more appreciable, (21.1%), probably as a result of very low

TABLE IX. Blend Compositions

Blend Designation	PPO Component gm	PPO Component wt fraction	ClS Component gm	ClS Component wt fraction	Yield Ppt. gm	Yield Ppt. %loss
PS-b20	5.9998	0.7999	1.5006	0.2001	7.2479	3.4
PS-b40	4.5007	0.6000	3.0005	0.4000	7.2570	3.3
PS-b60	2.9997	0.4000	4.4997	0.6000	7.2682	3.1
PS-b80	1.4997	0.2000	5.9998	0.8000	7.2102	3.9
B-b20	7.1896	0.7998	1.7992	0.2002	8.4820	5.6
B-b40	5.3942	0.5998	3.5992	0.4002	8.6414	3.9
B-b60	3.5948	0.3994	5.4059	0.6006	8.7350	3.0
B-b80	1.7978	0.1997	7.2037	0.8003	8.6910	3.5
C-b20	5.990	0.800	1.500	0.200	7.694	
C-b40	4.495	0.600	3.002	0.400	6.950	7.3
C-b60	2.983	0.398	4.507	0.602	7.225	3.1
C-b80	1.503	0.200	6.000	0.800	7.230	3.6
D-b20	8.0004	0.8000	2.0006	0.2000	9.3895	6.1
D-b40	5.9872	0.5995	4.0001	0.4005	9.5786	4.1
D-b60	3.9991	0.3999	6.0018	0.6001	9.6526	3.5
D-b80	2.0140	0.2011	7.9986	0.7989	9.6656	3.5
E-b20	5.2000	0.8000	1.3000	0.2000	6.1156	5.9
E-b40	3.9000	0.6000	2.6001	0.4000	6.1090	6.0
E-b50	3.7500	0.5000	3.7500	0.5000	6.9583	7.2
E-b60	2.6000	0.4000	3.9000	0.6000	5.8031	10.7
E-b80	1.3001	0.2000	5.2000	0.8000	5.9556	8.4
F-b20	2.635	0.799	0.662	0.201	3.188	3.3
F-b40	1.979	0.600	1.321	0.400	3.160	4.2
F-b60	1.316	0.399	1.981	0.601	3.087	6.4
F-b80	0.657	0.199	2.643	0.801	2.893	12.3
PpClS-b20	5.9990	0.8000	1.5000	0.2000	7.2131	3.8
PpClS-b40	4.4943	0.5996	3.0011	0.4004	7.2656	3.1
PpClS-b50	1.5065	0.5008	1.5016	0.4992	2.7724	7.8
PpClS-b60	3.0042	0.4004	4.4996	0.5996	7.2670	3.2
PpClS-b80	1.4991	0.1999	6.0004	0.8001	7.2149	3.8
PoClS-1-b20	4.7974	0.7997	1.2014	0.2003	5.2998	11.7
PoClS-1-b40	3.6056	0.6004	2.4000	0.3996	5.6844	5.3
PoClS-1-b60	2.4083	0.4005	3.6047	0.5995	5.6749	5.6
PoClS-1-b80	1.2172	0.2022	4.8029	0.7978	5.5395	8.0
PoClS-2-b50	0.6018	0.5003	0.6011	0.4997	1.0638	11.6
PoClS-3-b50	1.4999	0.5002	1.4988	0.4998	2.5964	13.4

molecular weight PPO remaining in solution. This suggests that the actual PPO composition in this blend is somewhat less than 50%.

The dried, precipitated blends were compression molded at 10,000 psi into square films, approximately 3 in. along a side and 0.12 in. in thickness. All unblended components except PPO, i.e. PS, PoClS, PpClS, and the copolymers, were molded at 180°C while the blends and PPO were molded at 280°C. A ten step procedure of alternately applying and removing pressure in 2 min. periods provided films free from voids. Films used for density and DSC measurements were allowed to cool under pressure for about 90 min. until mold temperature was just below T_g before removal from the press.

For preparation of specimens for tensile testing, the blend and pure component precipitates were pressed into irregular films in small aluminum foil packets at the temperatures given above and at 10,000 psi. These packets were immediately removed from the press after a few minutes of alternately applying and removing pressure and were allowed to cool at room temperature out of the press. The aluminum foil was then stripped off, and the thin films were cut into small pieces for injection molding into small tensile dumbbells.

Characterization of Blends

Differential Scanning Calorimetry. A Perkin-Elmer DSC II was used to study the glass transitions of the blends and the blend components. DSC samples were punched from the compression molded films. Two disks from each film were pressed into aluminum DSC pans which were then sealed. The combined weight of the two disks was 20-30 mg as measured by a Perkin-Elmer AD-2 Autobalance with a precision of 0.01 mg. A heating rate of 20° min^{-1} and a range of 5 mcal sec^{-1} was used for each sample while chart settings (Perkin-Elmer model 56 recorder) were 10 mv at a speed of 20 mm min^{-1}. Samples were heated from $330^{\circ}K$ to $530^{\circ}K$ under a nitrogen purge at 20 psi and were immediately cooled back to $330^{\circ}K$ at 80° min^{-1}. After several minutes of equilibration at $330^{\circ}K$, the samples were then reprogrammed to $530^{\circ}K$ at 20° min^{-1} and again cooled at $330^{\circ}K$. A blank (sealed, empty pan) was then run to $530^{\circ}K$ at 20° min^{-1} with identical instrumental settings except for changes in the zero positioning of the pen.

The DSC thermograms for the sample (the second of two runs) and the blank were placed one over the other on an illuminated screen for intersection at $350^{\circ}K$. A piece of millimeter graph paper (10 mm cm^{-1}) was placed over the two thermograms so that each mm division coincided with 1° on the DSC traces. The two thermograms were then traced on the graph paper by placing points at each 2° interval along the curves while at the glass transition these intervals were

reduced to 1° for better accuracy in determination of T_g. When the vertical distance between corresponding points on the sample and blank thermograms was plotted against temperature on another piece of graph paper, the shape of the original sample thermogram was accurately reproduced and deviation from baseline linearity was automatically corrected. The entire procedure is illustrated in Figure 7 for a 22.93 mg sample of Copolymer C selected as an example. The uncorrected DSC thermogram for Copolymer C is shown in Figure 7(a), while the point-traces for this thermogram and for the blank and the final corrected trace (vertical distance versus temperature) are illustrated in Figures 9(b) and 7(c) respectively. The above procedure improves accuracy in the determinations of T_g defined as the temperature at the half height of the transition, the transition width (TW), and the transition height (ΔC_p) through better extrapolation of the linear portions of the thermogram through the glass transition. These parameters are indicated in Figure 7(c).

Before each series of DSC measurements, the baseline was optimized by conventional DSC techniques and the temperature calibration was checked by reference to the standard melt temperatures of indium (429.78°K), tin (505.06°K), and occasionally lead (600.65°K). Any small curvature in the baseline remaining after optimization was automatically corrected by the point-tracing method outlined above, and minor deviations from the standard reference temperatures were

Figure 7. Example of the point-correction technique used to analyze the DSC thermograms. (a) DSC thermogram of Copolymer C (unblended); (b) point traces of Copolymer C and blank pan thermograms; (c) final adjusted point trace with identification of the parameters of T_g, transition width (TW), and the height (ΔC_p) of the glass transition.

COPOLYMER C

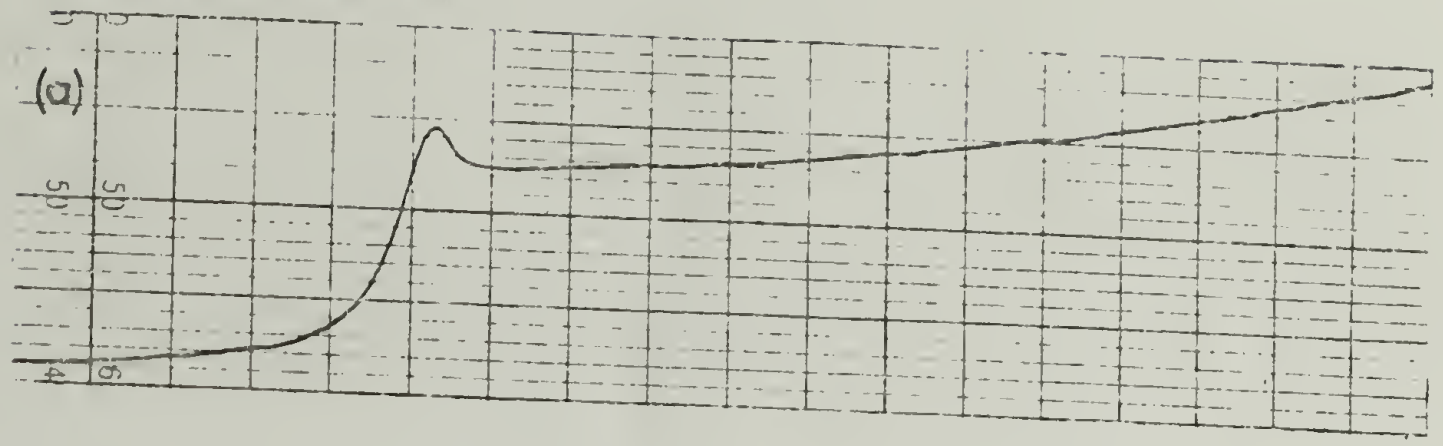

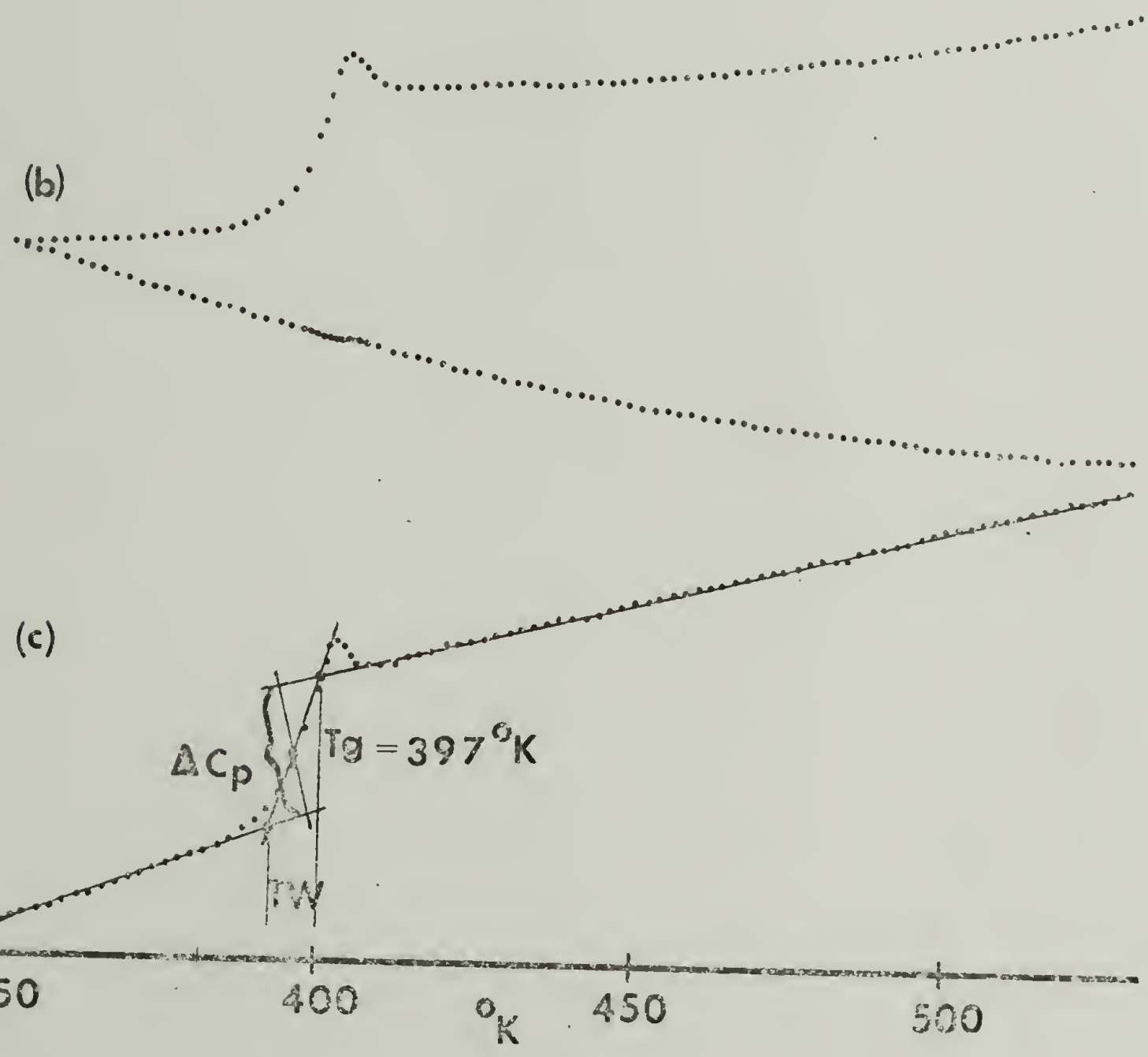

accomodated by either adding or subtracting the appropriate error, 1^{o} or 2^{o}, to the T_g measured for each sample. This error was obtained from a linear plot of the difference between the measured and true melt temperatures for each of the standard reference materials (tin and indium) versus temperature.

Density Measurements. The densities of the blends and the unblended materials were measured at room temperature in gradient columns of sodium nitrate in distilled water. Several columns with different density ranges were used. In each case, gradients were about 0.04 gm cc^{-1}. These columns were calibrated by three or four glass bead standards whose positions within the 1000 ml graduate columns were determined by means of a Gaertner cathetometer. The best linear relation between column position and density was obtained by the method of least squares. The positions of four to six disks punched from different locations on the same film sample were used to calculate a mean density for all samples except PPO for which 19 samples taken from different films were used. Error analysis for these density measurements is outlined in the Appendix.

Tensile Measurements. Small dumbbells of all the blended and unblended samples were molded from about 0.3 gm packets of pieces cut from compressionmolded films. These were fabricated by injection molding the films melted in a

pre-mixing cup into steel molds.* Cup and mold temperatures were elevated 20° for each blend increment of 20 wt. % PPO from 250°C for the copolymers, PS, PoClS, and PpClS to 340°C for pure PPO. The molder used in these experiments was a rotating head Mini-Max Injection Molder from Custom Scientific Instruments. The molded dumbbells had a gauge length of 8.9 mm and a cross-sectional diameter of 0.157 cm (8.9 mm) giving a cross-sectional area of 0.0195 cm^2. In addition to the blends which are given in Table IX, a high molecular weight PS sample and three of its blends (25, 50, and 75% PPO) were studied.[16] This PS was Monsanto HH 101 with a $\bar{M}_n$ of 92,600, a $\bar{M}_w$ of 270,000, and $\bar{M}_z$ of 485,000.

The tensile tests were performed at a constant cross-head speed of 0.2 mm min^{-1} on a Tensilon UTM-1 (Toyo Baldwin Co., Ltd.) at room temperature. Based on an effective sample length of 8.9 mm, this cross-head speed yields a strain rate of 3.75×10^{-4} sec^{-1}. For each test, a 20 kg load cell was used. The load-deformation curve was recorded on a SS-105D-B-UTM recorder (Toyo Measuring Instrument Co., Ltd.) at a chart speed of 200 mm min^{-1}. Measurements were made immediately after the molded dumbbell had cooled to room tempera-

---

*Prior to each molding, the mold was sprayed with a thin coat of MS 136 Fluorocarbon Release Agent for Injection Molding and Hot Molds (Miller-Stephenson Chemical Co., Inc.).

ture. For the majority of samples, at least 5 and as many as 15 dumbbells molded from the same blend or unblended component were tested for statistical treatment.

Modulus, strength at break (or yield), and elongation at break (yield) were calculated from the recorded load-deformation curves. Yielding or cold drawing was indicated by a maximum in stress-strain curve. Young's modulus was arbitrarily defined as the ratio of stress over strain at 100% pen deflection at a recorder range of 1 (4 kg maximum deflection). Tensile strength or stress at break was calculated from the ratio of force at break over dumbbell cross-sectional area. Percent elongation or strain at break was calculated from knowledge of chart and cross-head speed, the pen position in cm along the abscissas at break, and the sample gauge length. Strain defined in this way was engineering strain, i.e. change in gauge length divided by original gauge length.

The actual strain was corrected from measured strain by accounting for instrumental compliance and applying a clamp correction. A load-deformation curve was obtained for a steel bolt. Assuming an essentially infinite modulus for steel, the elongation or strain of the bolt in the tensile mode should be negligible; however, a finite elongation was recorded due to the softness of the Tensilon. For the polymer samples, this elongation or strain (ε_i) was subtracted from the measured strain (ε_m) to give the actual strain (ε_a).

Gauge length also has an effect on measured strain. Modulus was measured for PS at two gauge lengths (8.9 and 12.8 mm) and was plotted against reciprocal gauge length. The difference between the measured modulus for 8.9 mm gauge length samples and the extrapolated modulus at infinite gauge length was used to determine a clamp correction strain factor (ε_c). The final corrected strain is then

$$\varepsilon_a = \varepsilon_m - \varepsilon_i - \varepsilon_c \quad . \tag{12}$$

A typical set of corrections for ε_m at break for HH 101 PS at the same instrumental settings used in all measurements was $\varepsilon_a = 5.28-1.46-2.3=1.69\%$ in the order of terms given in eq. (12). Young's modulus was then corrected from the relation

$$E = \frac{\sigma}{\varepsilon_a} . \tag{13}$$

Statistical treatment of the tensile data is outlined in detail in the Appendix.

Electron Microscopy. Scanning electron micrographs were taken of the fracture surfaces of dumbbells of a blend of Copolymer C with 40% PPO (C-b60). A dumbbell of this blend and one of the same blend composition but which had been annealed at 135°C (20° below its T_g) for 17 hrs. in vacuum were fractured perpendicular to the thin section of the dumbbell after immersion in liquid nitrogen. The

fracture surfaces were coated with gold and the samples were fastened to platforms with Dog 154 adhesive. Sample magnification was 1000X at a secondary scatter mode (Micro II-2 Scanning Electron Microscope). Microscope settings were 250 mA emmission current, 2.5 contrast, dark level 5, and 20 KV secondary scatter. Film type 57 was used for the unannealed blend and type 55 for the annealed.

REFERENCES

1. R. Hammel, W. J. MacKnight, and F. E. Karasz, J. Appl. Polym. Phys., 46, 4199 (1975).
2. F. M. Lewis, C. Walling, W. Cummings, E. R. Briggs, and R. F. Mayo, J. Amer. Chem. Soc., 70, 1519 (1948).
3. T. Okumoto, T. Takeuchi, and S. Tsuge, Macromolecules, 6, 922 (1973).
4. S. L. Rosen, "Fundamental Principles of Polymeric Materials for Practicing Engineers," Barnes and Noble, New York, 1973, p. 123.
5. A. R. Shultz and B. M. Beach, Macromolecules, 7, 902 (1974).
6. B. Vollmert, "Polymer Chemistry," Springer-Verlag, New York, 1973, p. 127.
7. T. Alfrey, Jr., and C. C. Price, J. Polym. Sci., 2, 101 (1947).
8. B. Vollmert, op. cit., p. 139.
9. R. J. Hanna, Ind. and Eng. Chem., 49, 208 (1957).
10. R. C. Weast, ed., "Handbook of Chemistry and Physics," Chemical Rubber Co. Press, Cleveland, 54th ed., 1973.
11. S. N. Ushakov and P. A. Matuzov, J. Appl. Chem. USSR, 14, 120 (1944).
12. K. Matsumura, Makromol. Chem., 124, 204 (1969).
13. S. Krause, J. Macromol. Sci.-Revs. Macromol. Chem., C7, 251 (1972).

REFERENCES (cont.)

14. A. Yee, Polym. Prepr., 17(1), 145 (1976).

15. T. F. Rutledge, U. S. Patent 3,804,865 (assigned to ICI America, Inc.), March 23, 1973.

16. L. Kleiner, unpublished results.

C H A P T E R I V

DIFFERENTIAL SCANNING CALORIMETRY AND DENSITY STUDIES

Homopolymers and Copolymers Used in Blends

The glass transition temperatures (T_g) of PS, PpClS, PoClS, PPO, and the five copolymers of styrene and <u>para</u>-chlorostyrene whose polymerizations were described in Chapter III were determined at 20^{o} min^{-1} (Perkin Elmer DSC II) by the point-correction technique outlined in Chapter III. In addition, the densities of each of these polymers were measured in liquid gradient columns of aqueous sodium nitrate solution (Chapter III). The results of these measurements are given in Table X. The compositions of the copolymers determined by chlorine analysis (Table VII, Chapter III) are included in Table X in units of mole fraction <u>para</u>-chlorostyrene (N_{pClS}).

TABLE X. T_g's and Densities of Blend Polymers

Polymer	N_{pClS}	T_g ^{o}K	T_g ^{o}C	Density gm cc^{-1}
PS	0	378	105	1.0476±.0008
B	0.585	398	125	1.1630±.0043
C	0.671	400	127	1.1715±.0019
D	0.678	399	126	1.1738±.0038
E	0.686	399	126	1.1762±.0019
F	0.754	401	128	1.1885±.0024
PpClS	1.0	405	132	1.2230±.0012
PoClS-1	-	408	135	1.2506±.0049
PPO	-	489	216	1.0656±.0006

The T_g's of PS and PPO given in Table X agree with those determined by DSC by Bair[1] at 40° min^{-1} and Prest and Porter[2] at 10° min^{-1} as given in Table I of Chapter I. In addition, agreement is good between the densities measured for PS and PPO in this study and those reported in the literature. For example, Karasz et al.[3] determined the density of PS as 1.047 gm cc^{-1} by hydrostatic weighing at 25°C in comparison to 1.0476±.0008 gm cc^{-1} measured in the present study. For PPO, the density of 1.0656±.0006 gm cc^{-1} given in Table X is close to the density of 1.06 gm cc^{-1} reported by de Petris et al.[4] (flotation method using aqueous cuprous sulfate solution at 20°C) and Hay[5] (ASTM D792 at 73°F) and to the density of 1.063 gm cc^{-1} from the data of Jacques and Hopfenberg[6] (density gradient column of aqueous sodium chloride at 25°C). A much higher density of 1.157 gm cc^{-1} has been reported by Lim et al.[7] for PPO but no method of determination was given in that source. The error bounds for all the densities given in Table X represent conservative values for the standard deviation of the mean which were determined by the propagation of error analysis given in the Appendix.

As shown by Table X, the densities of the copolymers increase monotonically with increasing PClS content from a low of 1.0476 gm cc^{-1} for pure PS to a high of 1.2230 gm cc^{-1} for pure PpClS. Due to this large difference in densities between homopolymers corresponding to the two comonomers,

copolymers with very small differences in composition have measurably different densities. For example, a total difference of 1.5 mole % pClS in composition between Copolymer C and E coincides with a difference of 0.0047 gm cc^{-1} in density. In this regard, density measurements appear to be a good secondary measure of copolymer composition once the primary correlation between density and copolymer composition has been determined from elemental analysis.

By contrast, copolymer T_g appears relatively insensitive to composition over the range between 58.5 and 75.4 mole % pClS for Copolymers B through F. The difference between T_g's at the edges of this region is about 3° ($\pm 1^{\circ}$) while over the entire composition range, between pure PS and PpClS, the difference between T_g's is appreciably larger, i.e. 27°C. The values for T_g given in Table X agree within experimental error with those determined by Shultz and Beach[8] whose DSC, TOA, and dynamic mechanical studies of the poly(S-co-pClS)/PPO system have been reviewed in Chapter II. By DSC at the same heating rate of 20° min^{-1} used in the present study, they determined the T_g of PpClS as 130°C (132°C in this study) and the T_g of PPO as 212°C (216°C in this study). To compare T_g's of copolymers between the two studies, it should be first noted that the compositions of their copolymers, which were thermally polymerized in bulk at 111°C, were calculated from the copolymerization equation, eq. (8), Chapter III, and reactivity ratios at 111°C from an

Arrhenius-type extrapolation between values reported by Lewis et al.[9] for 60 and 131°C. As was shown in Table VII of Chapter III, these Lewis reactivity ratios result in calculated copolymer compositions which are about 3-4% lower in mole % pClS content than those determined from the precision chlorine analysis employed in the present study. After allowing for these composition differences, the T_g of a copolymer comparable to Copolymer B in composition was found to be 120°C by Shultz and Beach (125°C in this study) and one comparable to Copolymer C was 124°C (127°C in this study).

Determination of Blend Compatibility by DSC

Each of the blends whose compositions were given in Table IX of Chapter III were compression molded into thin films from which small disks were punched and placed in DSC pans. The techniques of sample preparation have been given in Chapter III. DSC thermograms for each of these samples were obtained at 20° min^{-1} (DSC II) and the temperature (T_g), width (TW), and height (ΔC_p) of each glass transition were determined by the point-correction method cited in Chapter III. A single T_g intermediate between those of the pure components was indicative of blend compatibility.

The actual DSC traces of heat capacity (C_p) versus temperature (°K) for PS, Copolymers B through F, PpClS, and PoClS and their blends with PPO are grouped together in

Figures 8 through 15. The weights of the DSC samples used to obtain these thermograms are given in Table XI.

TABLE XI. Weights of DSC Samples

Sample	Wt. % PPO	Weight(mg)	Sample	Wt. % PPO	Weight(mg)
PS	0	18.08	E	0	23.80
PS-b80	20	20.22	E-b80	20	20.46
PS-b60	40	19.11	E-b60	40	20.53
PS-b40	60	21.56	E-b40	60	19.78
PS-b20	80	23.39	E-b20	80	22.28
PPO	100	24.81	PPO	100	24.05
B	0	31.68	F	0	22.37
B-b80	20	22.64	F-b80	20	21.28
B-b60	40	19.96	F-b60	40	21.85
B-b40	60	24.83	F-b40	60	22.07
B-b20	80	26.29	F-b20	80	22.90
PPO	100	25.74	PPO	100	24.57
C	0	22.93	PpClS	0	22.01
C-b80	20	22.19	PpClS-b80	20	19.89
C-b60	40	21.37	PpClS-b60	40	21.44
C-b40	60	23.57	PpClS-b40	60	21.13
C-b20	80	25.02	PpClS-b20	80	21.73
PPO	100	23.51	PPO	100	26.40
D	0	22.21	PoClS-1	0	34.96
D-b80	20	23.80	PoClS-b80	20	23.85
D-b60	40	21.66	PoClS-b60	40	23.28
D-b40	60	21.73	PoClS-b40	60	25.04
D-b20	80	23.19	PoClS-b20	80	25.98
PPO	100	23.10	PPO	100	24.81

Only blends of PS, Copolymer B, and Copolymer C with PPO exhibit single glass transitions over the entire blend composition range. For Copolymer D/PPO and Copolymer E/PPO, single glass transitions are apparent only when one of the components is present in small quantity, i.e. 20 and 80% PPO, while two glass transitions are exhibited at intermediate

Figure 8. DSC thermograms of PS and the PS/PPO blends.

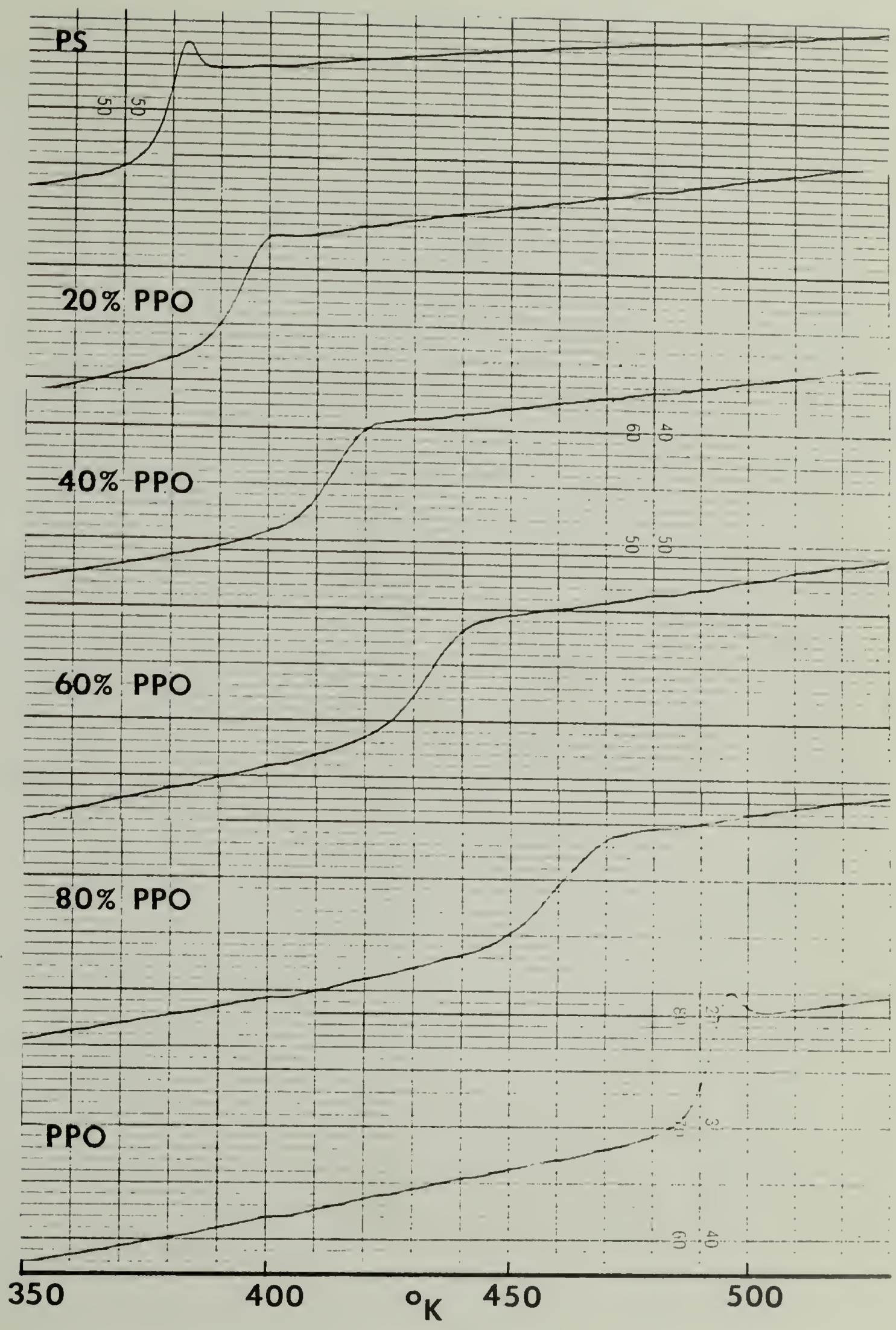
PS
20% PPO
40% PPO
60% PPO
80% PPO
PPO
350
400
450
500
°K

Figure 9. DSC thermograms of Copolymer B and Copolymer B/PPO blends.

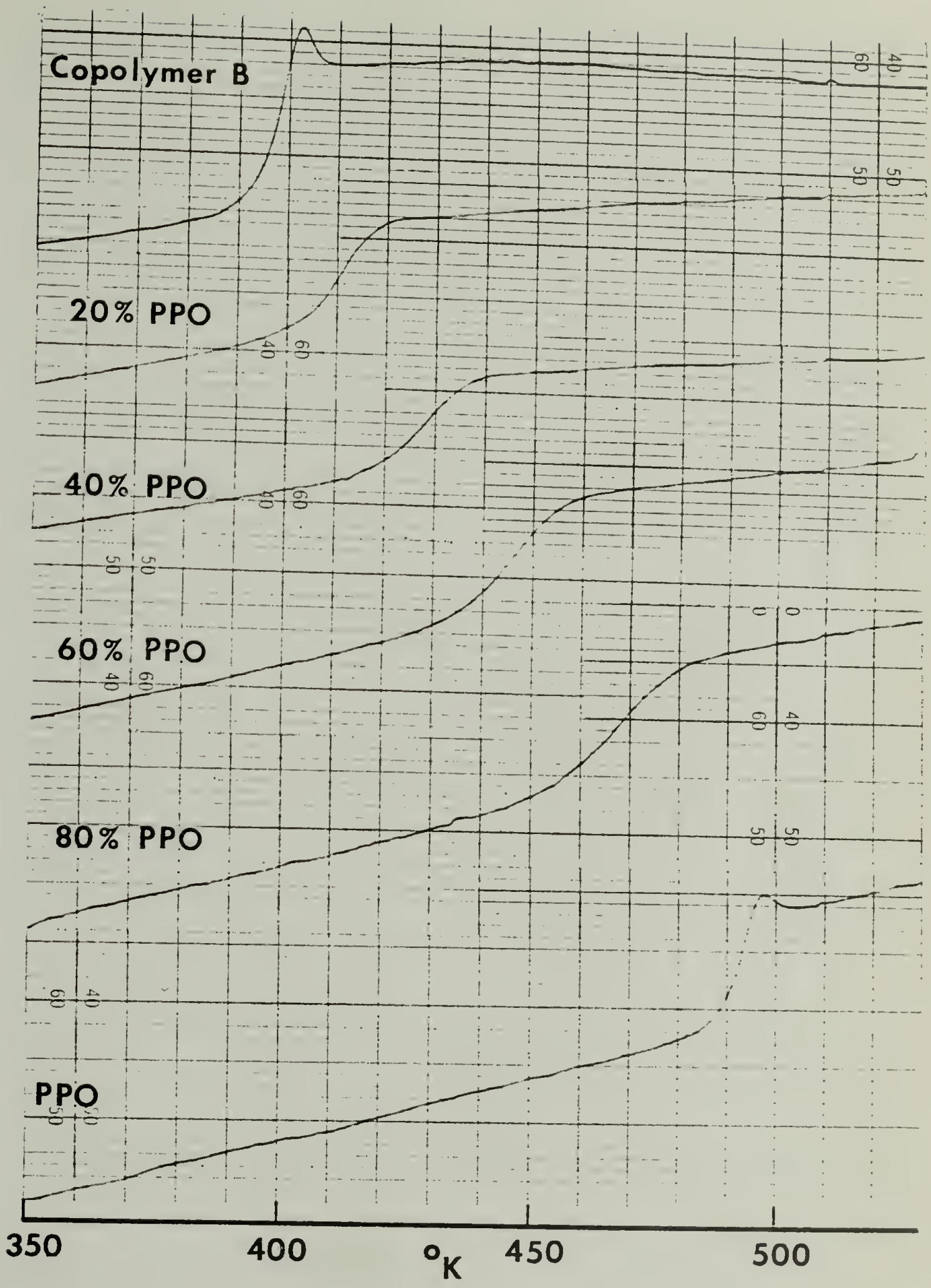
Copolymer B
20% PPO
40% PPO
60% PPO
80% PPO
PPO
350
400
°K
450
500

Figure 10. DSC thermograms of Copolymer C and Copolymer C/PPO blends.

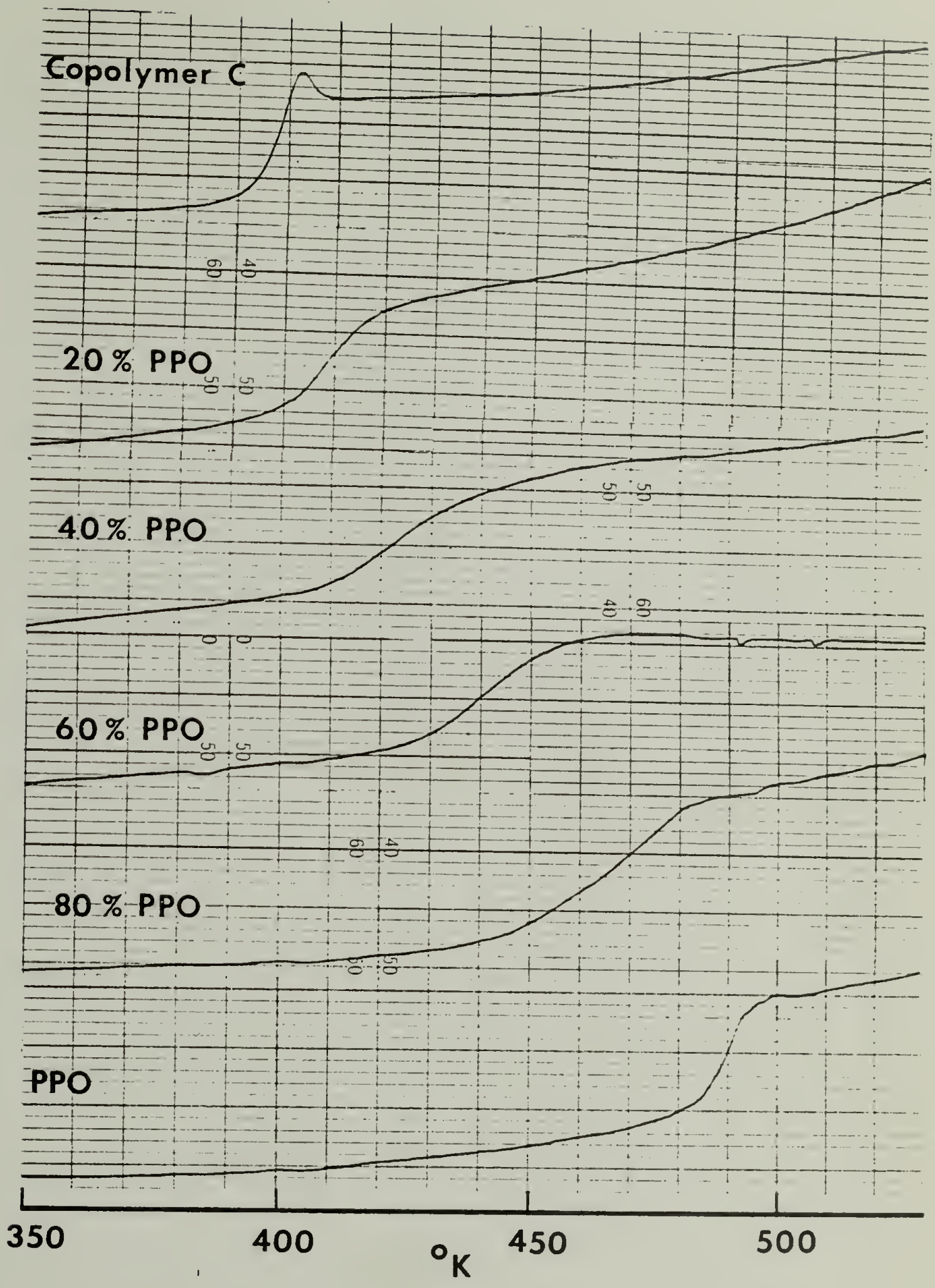
Copolymer C
20 % PPO
40 % PPO
60 % PPO
80 % PPO
PPO
350
400
450
500
°K

Figure 11. DSC thermograms of Copolymer D and Copolymer D/PPO blends.

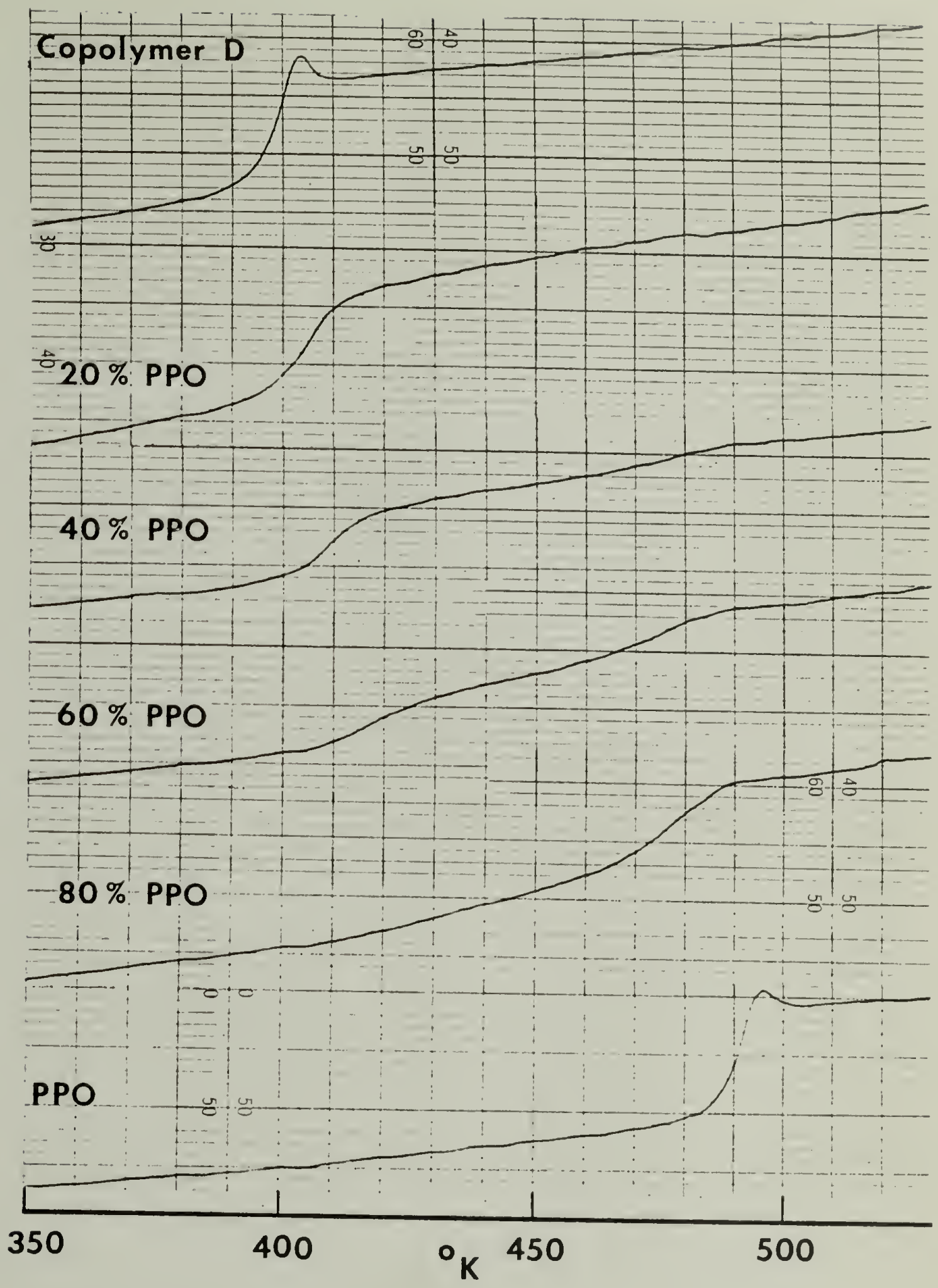
Copolymer D
20 % PPO
40 % PPO
60 % PPO
80 % PPO
PPO
350
400
450
500
°K

Figure 12. DSC thermograms of Copolymer E and Copolymer E/PPO blends.

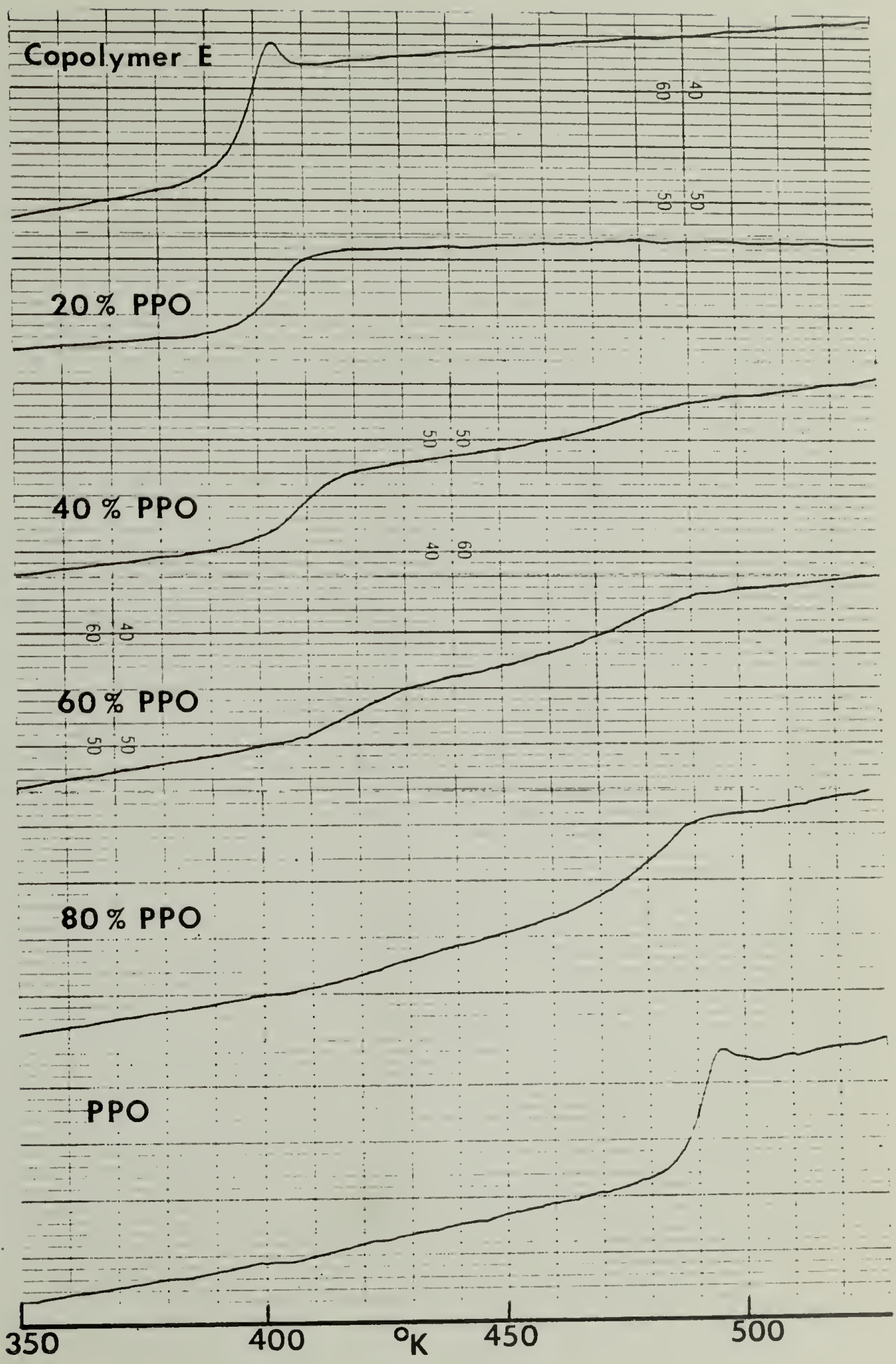
Copolymer E
20 % PPO
40 % PPO
60 % PPO
80 % PPO
PPO
350
400
°K
450
500

Figure 13. DSC thermograms of Copolymer F and Copolymer F/PPO blends.

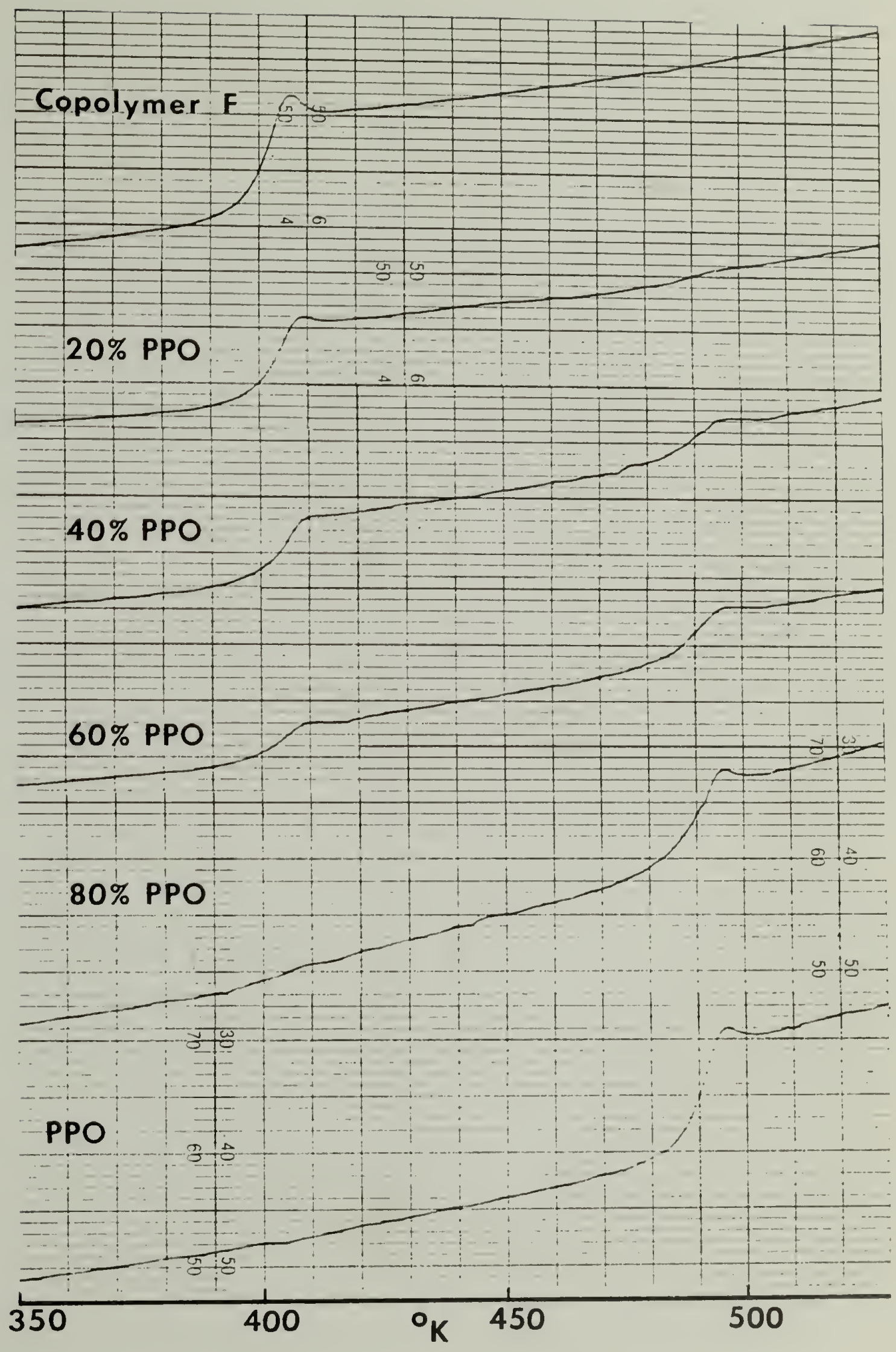
Copolymer F
20% PPO
40% PPO
60% PPO
80% PPO
PPO
350
400
°K
450
500

Figure 14. DSC thermograms of PpClS and PpClS/PPO blends.

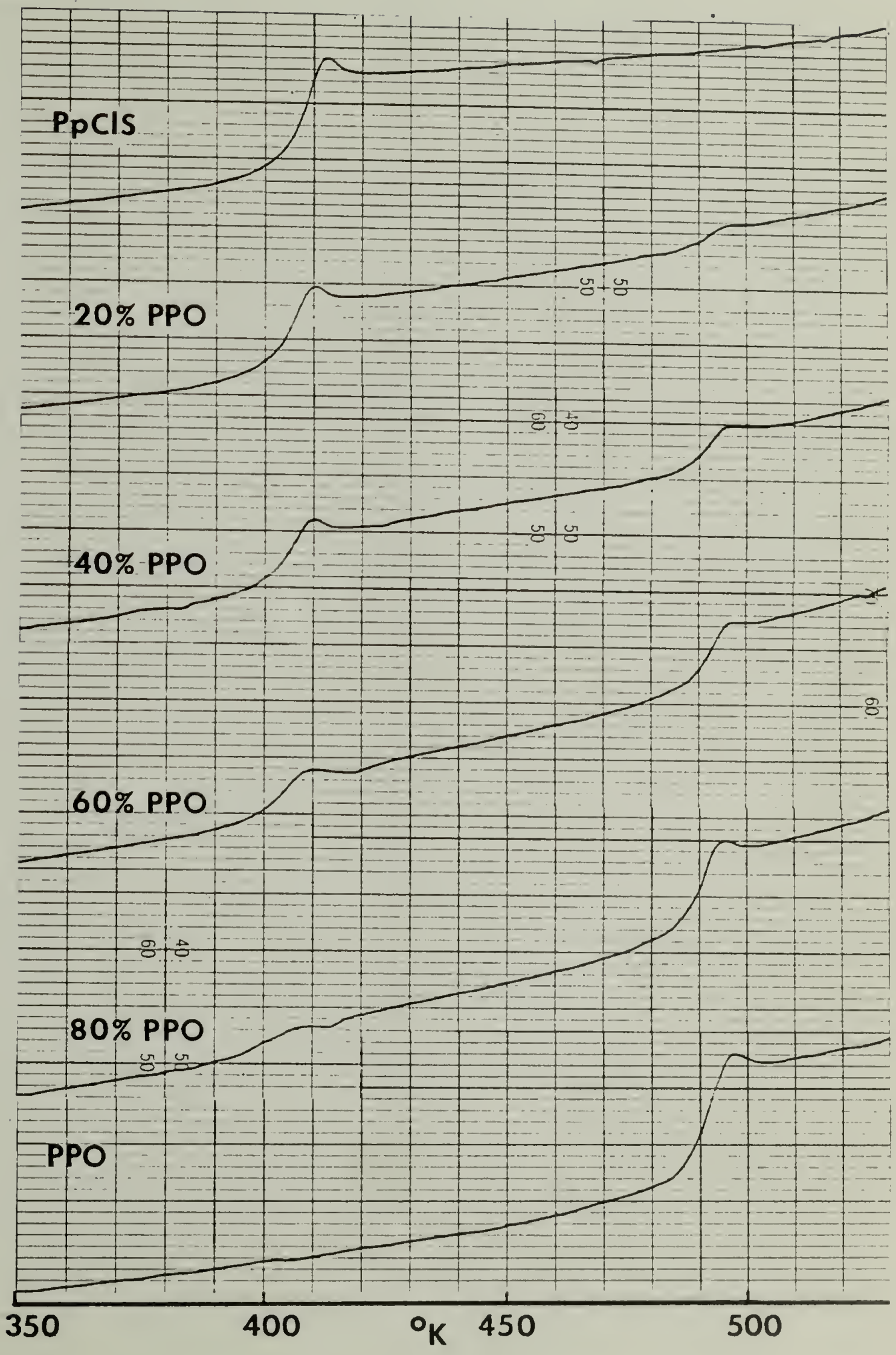
PpClS
20% PPO
40% PPO
60% PPO
80% PPO
PPO
350
400
°K
450
500

Figure 15. DSC thermograms of PoClS-1 and PoClS-1/PPO blends.

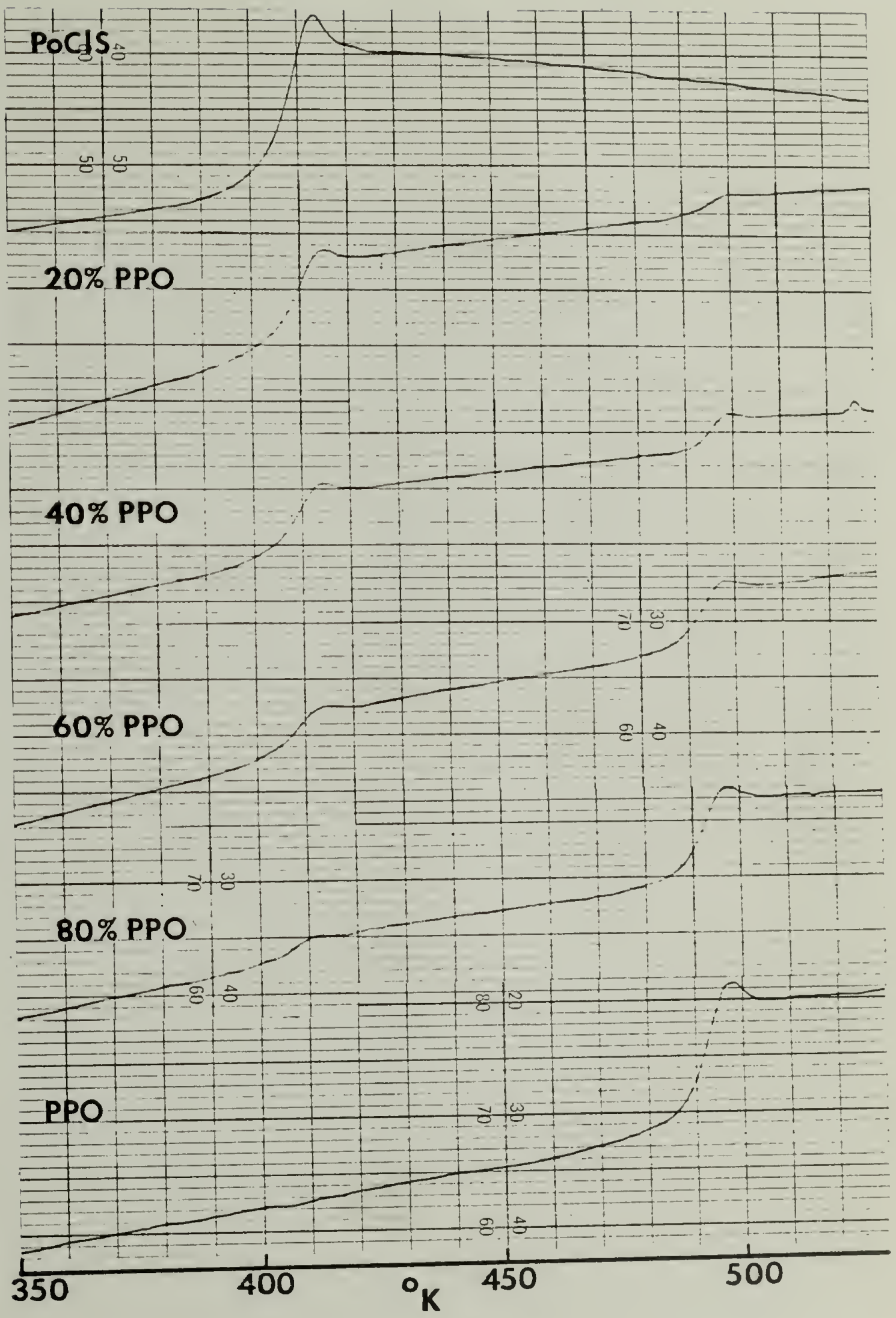
PoCIS
40
50
50
20% PPO
40% PPO
30
70
60
40
60% PPO
30
70
40
60
80% PPO
20
80
40
60
PPO
30
70
40
60
350
400
°K
450
500

compositions of 40 and 60% PPO where both components are present in nearly equal amounts. The same difficulty in the detection of the minor component transition was reported by Shultz and Beach.[8] As mentioned in Chapter II, they found that at $W_{PPO} \leq .375$, only the major component, i.e. copolymer or PpClS, was evident in all the incompatible blends. These observations were attributed to instrumental insensitivity; however, with better instrumentation (DSC II) and much larger sample sizes in the present study, it is evident that instrumental sensitivity is only partly the answer. For the most incompatible blends, those of Copolymer F/PPO, PpClS/PPO, and PoClS/PPO, all the transitions are evident although the minor transitions for Copolymer F/PPO are very small and would be impossible to detect if not for the use of large samples. Implications of these findings will be discussed shortly.

Analysis of these thermograms indicates that the compatibility-incompatibility transition occurs between 67.1 and 67.6 mole % pClS copolymer composition which agrees with the 65.3 to 68 mole % pClS range reported by Shultz and Beach. In addition, PoClS was found to be incompatible with PPO as was PpClS. The effect of varying the molecular weight of PoClS in the PoClS/PPO blends and the molecular weight of PPO in the PpClS/PPO blends will be discussed in a latter section.

Three features of the DSC thermograms are particularly noteworthy. First, the glass transition of each of the

compatible blends increases monotonically in temperature with increasing PPO content. For the two incompatible blends closest to the compatibility-incompatibility transition, Copolymer D/PPO and Copolymer E/PPO in Figures 11 and 12, respectively, there is an apparent elevation of the T_g corresponding to the copolymer and a depression of the T_g corresponding to PPO. This is not the case for the other incompatible blends of Copolymer F/PPO, PpClS/PPO, and PoClS/PPO for which the T_g's of the phases corresponding to the blended components appear almost identical to those of the unblended components. Second, there is a broadening of the width of the glass transition for the compatible blends with increasing PPO content and more particularly with increasing pClS composition, i.e. moving toward less compatible compositions. The width of each of the transitions for the incompatible blends increases with decreasing pClS composition, i.e. moving toward less incompatible compositions. Finally, the small peak appearing at the end of the glass transitions of the pure components (PS, the copolymers, PpClS, PoClS, and PPO) is absent or is less pronounced in all blends except for the most incompatible blends of PpClS/PPO and PoClS/PPO for which each phase corresponds to pure PpClS (PoClS) or PPO. Each one of these observations will be discussed in turn in the following sections.

Glass Transition Temperatures. As noted in Chapter I, Prest and Porter[2] reported excellent agreement between T_g (DSC) of PS/PPO blends and T_g calculated from the free volume theory of Kelley and Bueche.[10,11] By applying a blend nomenclature to the polymer-diluent equations of Bueche, the following equation is obtained for the free volume of a blend (f_B):

$$f_B = f_{g,B} + \Delta\alpha_B (T - T_{g,B}) \qquad (14)$$

where $f_{g,B}$ is the free volume of the blend at T_g, $\Delta\alpha_B$ is the difference between thermal expansion coefficients of the blend above and below T_g ($\Delta\alpha_B = \alpha_{r,B} - \alpha_{g,B}$), T is some specified temperature, and $T_{g,B}$ is the T_g of the blend. Eq. (14) is in the familiar Williams-Landel-Ferry (WLF) form[12] which assumes an iso-free volume at T_g. A further assumption of the Kelley-Bueche treatment is that the free volume of a binary blend (f_B) is equal to the volume fraction sum of the free volumes of the components

$$f_B = v_1 f_{g_1} + v_2 f_{g_2} + v_1 \Delta\alpha_1 (T - T_{g_1}) + v_2 \Delta\alpha_2 (T - T_{g_2}) \qquad (15)$$

where v is the volume fraction of component 1 or 2 and $\Delta\alpha$ is the corresponding difference between thermal expansion coefficients above (α_r) and below (α_g) T_g. In addition, the assumption was made that the free volume of the blend at T_g ($f_{g,B}$) and $\Delta\alpha_B$ can be expressed simply as the volume fraction sums

of the corresponding component properties, i.e. eqs. (15) and (17).

$$f_{g,B} = v_1 f_{g_1} + v_2 f_{g_2} \qquad (16)$$

$$\Delta\alpha_B = v_1 \Delta\alpha_1 + v_2 \Delta\alpha_2 \qquad (17)$$

By rearranging eq. (14) and substituting eqs. (15), (16), and (17) for f_B, $f_{g,B}$, and $\Delta\alpha_B$, respectively, and $1-v_2$ for v_1, the Bueche[11] expression for the glass transition temperature of the blend ($T_{g,B}$) is obtained as

$$T_{g,B} = [T_{g_1} + (KT_{g_2} - T_{g_1})v_2]/[1+(K-1)v_2] \qquad (18)$$

where

$$K = \Delta\alpha_2/\Delta\alpha_1 \quad . \qquad (19)$$

The shape of the curve relating blend T_g to composition, i.e. whether concave or convex, is determined by the value of K and therefore by the thermal expansion coefficients for the two components. Values for $\Delta\alpha$ of PS often reported are 3.0×10^{-4} (Fox and Flory),[13] 3.33×10^{-4} (Fordon and Macnab),[14] and 3.6×10^{-4} (Ueberreiter and Kanig),[15] in units of reciprocal degrees Kelvin. These are lower than the so-called universal value of 4.8×10^{-4}. For PPO, $\Delta\alpha$ has been calculated from dilatometry data[16] as 5.7×10^{-4}. Sharma et al.[17] give a substantially lower thermal expansion coefficient of 3.09×10^{-4} for PPO; however, their value for the thermal expansion coefficient above T_g ($\alpha_r = 5.13\times10^{-4}$) appears questionably low

when compared with other sources.[16,18] Designating PS as component 1 and PPO as component 2 and using an average value of $3.3x10^{-4}$ as the expansion coefficient for PS and $5.7x10^{-4}$ for PPO, the Bueche parameter, K, as defined by eq. (19) is calculated as 1.73 for PS/PPO. Using this value for K in eq. (18), blend T_g's for PS/PPO were calculated and are plotted versus volume fraction PPO (v_2 or V_{PPO} for simplicity) in Figure 16 (broken curve). The data points (filled circles) in Figure 16 represent actual T_g's measured by DSC for PS/PPO in this study and are fitted by a smooth curve.

As shown by Figure 16, the Kelley-Bueche assumptions predict a convex dependence of blend T_g upon composition in contrast to the concave dependence actually observed. The agreement reported by Prest and Porter[2] was probably a result of a fortuitous choice of thermal expansion coefficients for PPO and PS. For $\Delta\alpha$ of PS, they used $6.9x10^{-4}$ given by Plazek[19] and as an approximation for $\Delta\alpha$ of PPO, they used $4.5x10^{-4}$ reported by Eisenberg and Cayrol[20] for poly (2-methyl-6-phenyl-phenylene oxide). For these thermal expansion coefficients, the Bueche parameter, K, was calculated to be 0.68 as compared to 1.73 for the $\Delta\alpha$ values used in the present study. An empirical value for K can be calculated from the experimental T_g data by rearranging eq. (18) to give

$$K=[v_1(T_{g,B}-T_{g_1})]/[v_2(T_{g_2}-T_{g,B})]. \qquad (20)$$

Figure 16. Plot of PS/PPO T_g's versus volume fraction PPO (V_{PPO}) as predicted by the Kelley-Bueche theory and as experimentally observed by DSC.

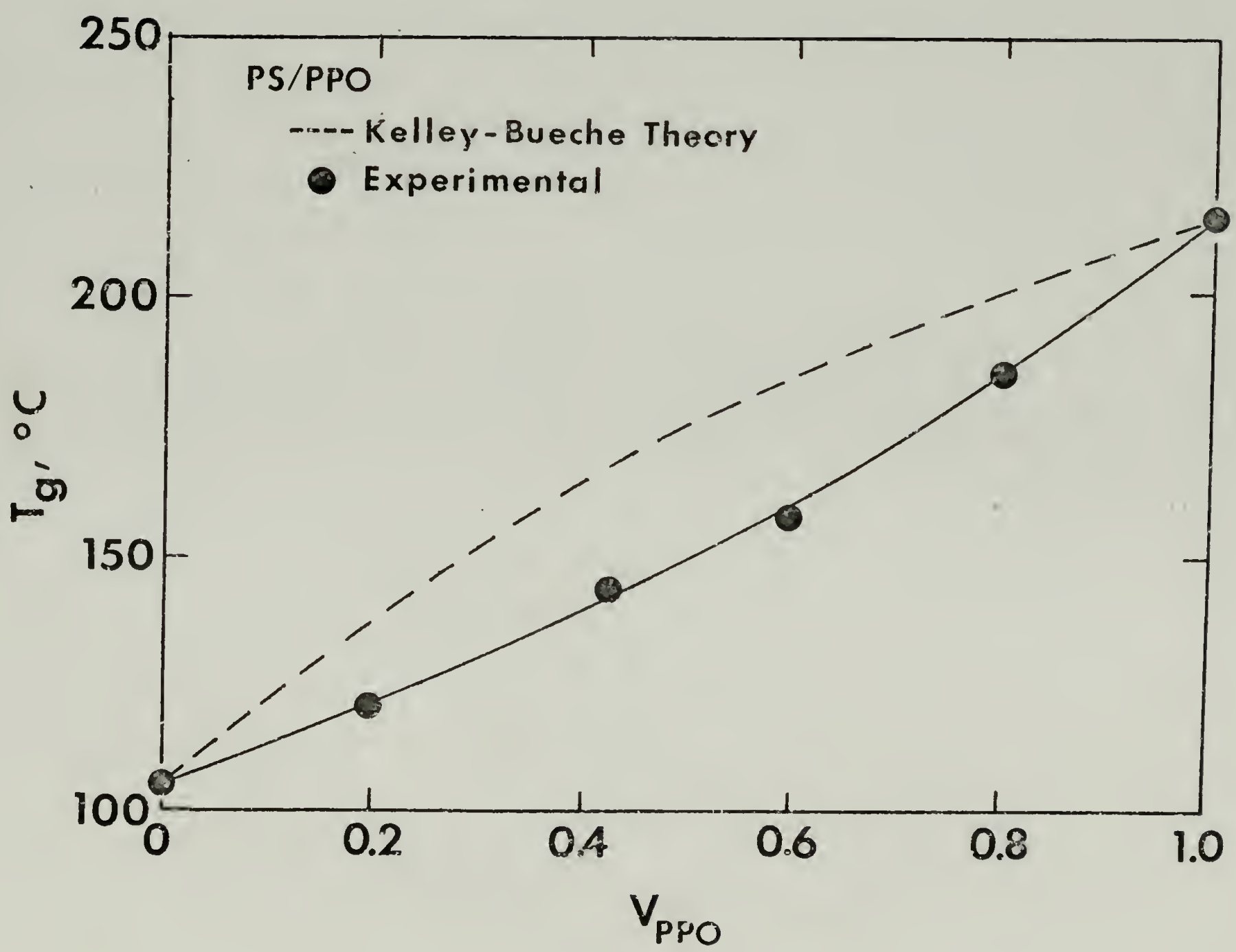
PS/PPO
---- Kelley-Bueche Theory
Experimental
250
200
150
100
T_g, °C
0
0.2
0.4
0.6
0.8
1.0
V_{PPO}

Calculated in this way, the experimental or empirical K was found to be independent of blend composition and had a value between 0.62 and 0.70. This range compares favorably with that of between 0.66 and 0.71 calculated by Prest and Porter from their data.

Several expressions relating the T_g of random copolymers to copolymer composition and the T_g's of the corresponding homopolymers have appeared in the literature. Alternately, these can be applied to determine the dependence of blend T_g upon blend composition and component T_g. The most general of these has the form given by Wood[21]

$$T_{g,B}=[T_{g_1}+(kT_{g_2}-T_{g_1})W_2]/[1+(k-1)W_2] \qquad (21)$$

where K is an arbitrary constant and W_2 is the weight fraction of component 2 in the blend. It is noted that the Wood equation written in the form of eq. (21) is nearly identical to the Kelley-Bueche relation given in eq. (18) except for the arbitrariness of the Wood constant and the use of weight instead of volume fractions in the Wood relation. Most other well known relations such as those proposed by Gordon and Taylor,[22] Fox,[23] and Gibbs and Dimarzio[24] can be obtained from the general Wood expression by applying certain restrictions on the significance of the parameter, k. For example, the Gordon-Taylor (G-T) equation can be obtained from eq. (21) by equating k to K as defined by eq. (19). Except for the use of weight fractions, the G-T equation is therefore

identical to the one obtained by Kelley and Bueche, eq. (18). Similarly, the Fox equation given by

$$\frac{1}{T_{g,B}} = \frac{W_1}{T_{g_1}} + \frac{W_2}{T_{g_2}} \qquad (22)$$

can be obtained by rearranging the Wood equation and setting $k=T_{g_1}/T_{g_2}$. Finally, the Gibbs-Dimarzio (G-D) equation may be written in the form of eq. (21) by allowing $k=n_2M_1/n_1M_2$ where n is the number of rotational bonds of a monomeric unit having the molecular weight, M.

In some recent studies, Krause and Roman[25] investigated the T_g-composition dependencies of random copolymers of isopropyl acrylate and isopropyl methacrylate in addition to compatible blends of the two corresponding homopolymers. Although the T_g's of the copolymers and the blends followed identical composition dependencies, they could not be fitted by the Fox, G-T, or Kanig[26] equations. Daimon et al.[27] also found that the Fox, G-T, and G-D expressions could not adequately represent the relation of T_g to composition for some random copolymers of styrene and cyclododecyl acrylate. They attributed these failures to the inability of these simple theories to take into account the influences of adjacent dissimilar monomeric units on the steric and energetic terms in the copolymer backbone. The nearly identical dependencies of copolymer and blend T_g upon composition reported by Krause and Roman indicate that steric

and energetic interactions are nearly the same for dissimilar monomers along the main chain of the copolymer as for the identical monomers but on different homopolymer chains in the blend. This can be interpreted as evidence for segmented mixing in this blend.

The adequacy of the G-T, Fox, G-D, Wood, and Kanig equations for the PS/PPO system has been determined. The Kanig equation used by Krause and Roman is given by

$$\frac{T_{g_1} - T_{g,B}}{\phi_{f_1}} = C_1 \phi_{f_1} + C_2 \qquad (23)$$

where C_1 and C_2 are empirical constants and

$$\phi_{f_1} = W_1/(W_1 + KW_2) \quad . \qquad (24)$$

The Kanig parameter, K, in eq. (24) is the same as defined by eq. (19) and used in the Kelley-Bueche and Gordon-Taylor equations. If eq. (23) is applicable for a given system, copolymer or blend, then the plot of $(T_{g_2} - T_g)/\phi_{f_1}$ versus ϕ_{f_1} must be linear. As shown in Figure 17, this plot for PS/PPO shows significant curvature indicating the inadequacy of the Kanig relation for this system. In addition, for the same K value of 1.73 used previously for the Kelley-Bueche equation, the Gordon-Taylor (G-T) relation gives blend T_g's for PS/PPO which are substantially higher than actually observed. Better agreement between experimental and calculated blend T_g is obtained by using the Fox and

Figure 17. Plot of the Kanig parameters, $(T_{g_2}-T_g)/\phi_{f_1}$ versus ϕ_{f_1}, for PS/PPO.

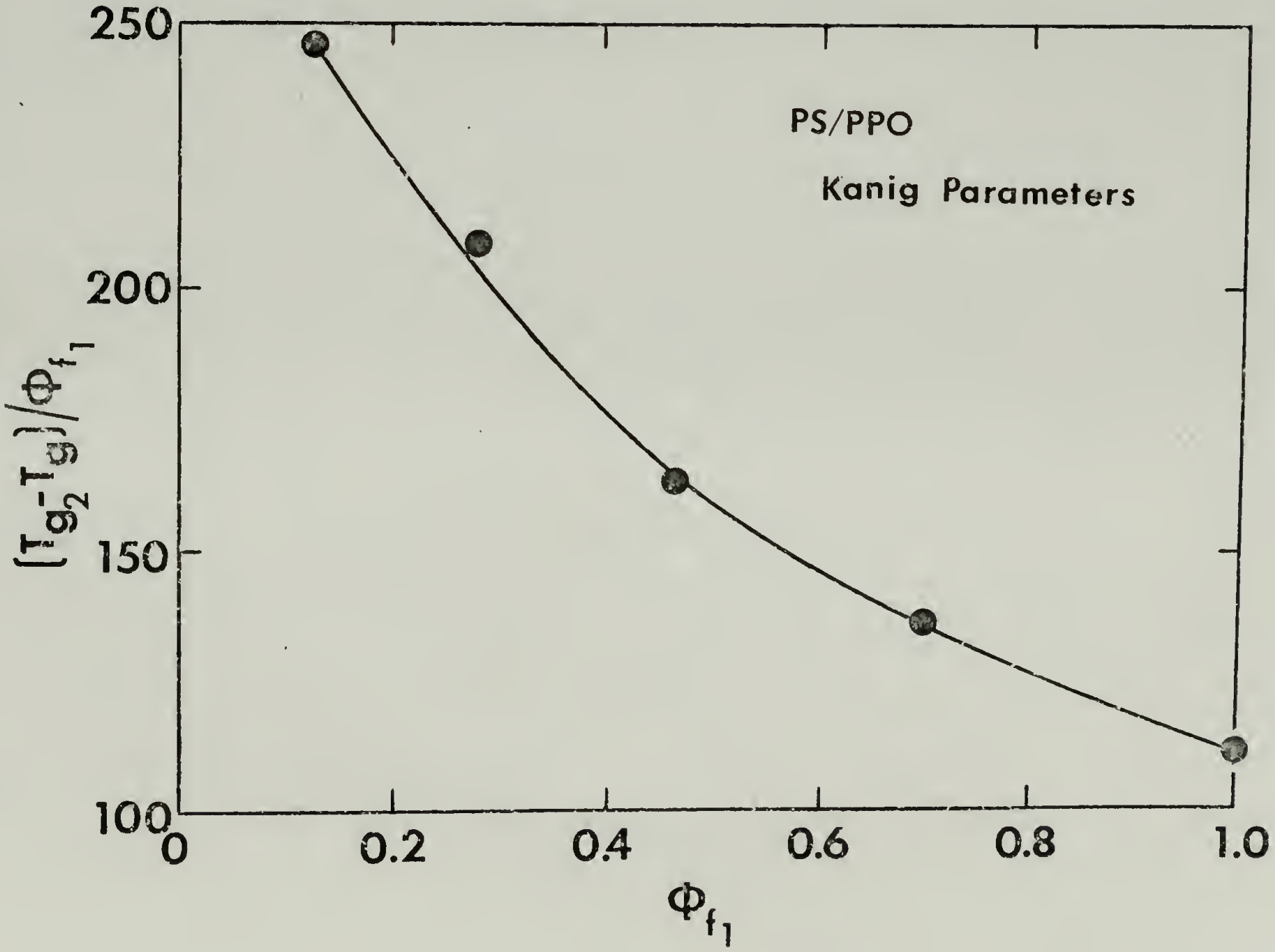
PS/PPO
Kanig Parameters
250
200
150
100
0
0.2
0.4
0.6
0.8
1.0
$[T_{g_2}-T_{g_1}]/\Phi_{f_1}$
Φ_{f_1}

the Gibbs-Dimarzio (G-D) equations. For the latter calculations, M_1 was 104.2 and M_2 was 120.2. If n_1, the number of rotatable bonds in PS, is taken to be 3 and n_2 for PPO to be 4, then k is calculated as 0.65. As previously mentioned, the experimental range was between 0.62 and 0.70 in this study and between 0.66 and 0.71 from the results of Prest and Porter. A comparison of the predictions of PS/PPO T_g from the G-T, Fox, and G-D theories is given in Table XII.

TABLE XII. Theoretical Predictions of Blend T_g

Blend	W_1	W_2	T_g (^oC) of PS/PPO Blend			
			G-T	Fox	G-D	Experimental
PS-b80	0.800	0.200	139	123	121	121
PS-b60	0.600	0.400	165	143	139	140
PS-b40	0.400	0.600	185	165	160	158
PS-b20	0.200	0.800	202	189	185	185

For each calculation, T_g was computed in ^oK with $T_{g_1}=378^oK$ and $T_{g_2}=489^oK$. The value of k in the Fox expression was 0.77 (T_{g_1}/T_{g_2}). As mentioned, the poorest predictions of blend T_g were for the G-T, Kanig, and Kelley-Bueche equations for which K in the generalized Wood equation was equal to the ratio of the thermal expansion coefficients of the components. This is not surprising because it is unrealistic to assume that the free volume per monomer unit is exactly the same for pure PPO and PS as for the PS/PPO

blends in the presence of any intermolecular interactions. For this reason, the relation between k and $\Delta\alpha_2/\Delta\alpha_1$ cannot be predicted and k must be assumed an empirical constant. The good approximations of the Fox and G-D equations may be, in fact, fortuitous because they have been reported to be less adequate for other blend and copolymer systems as previously mentioned.[25,27] Shultz and Gendron[28] also found that the Fox equation in the form of eqs. (3) and (4) given in Chapter I fitted their DSC and TOA data for PS/PPO. What is needed is a general theory than can predict the T_g-composition relationship for all copolymers and blends from physical and molecular parameters. A step in this direction is the modified Gibbs-Dimarzio equation offered by Uematsu and Honda[29] for copolymers and the modified Fox relationship of Johnston,[30] also for copolymers. The former treatment is based upon the estimation of the different chain stiffness energies for A-B type bonds along the copolymer backbone while the latter weights corresponding homopolymer T_g's to the diad probabilities of monomer pairs. An adequate blend theory must be able to take into account changes in volume upon mixing, i.e. the negative excess free volume of mixing noted for PS/PPO in Chapter I and further detailed in this Chapter, and the steric and energetic factors involved in intermolecular contacts between dissimilar molecules. For now, the empirical Wood equation, eq. (21), appears to be the only adequate expression to fit blend data.

As shown in Figures 18 and 19, the T_g data for all three compatible blends (PS/PPO and Copolymer B/PPO in Figure 18 and Copolymer C/PPO in Figure 19) is fitted closely by the Wood equation for a single k value of 0.679 and the values of T_{g_1} given for PS, Copolymer B, and Copolymer C in Table X. As a check on the graphical techniques used to determine T_g (Chapter III), the T_g and the transition height (ΔC_p) for a 24.5 mg sample of C-b40 were electronically calculated by means of a Tektronic Model 31 Programmable Calculator coupled to a Perkin Elmer DSC II through a Perkin Elmer Calculator Interface.* In addition to the temperature at the half-height of the transition ($1/2\Delta C_p$) used for the definition of T_g in the graphical procedure, the electronic technique also prints out the temperature at the inflection point of the transition (T_{inf}) and the temperature marking the intersection of the extrapolated linear portion of the transition with the baseline (T_{extr}). The values of T_g calculated by these definitions are T_{extr}=433.59°K (160.43°C), T_{inf}=442.3°K (169.14°C), and $T_{1/2\Delta C_p}$=441.96°K (168.8°C); and ΔC_p=0.061 cal $^{\circ}C^{-1}$ g^{-1}. The calculated values of T_{extr} and $T_{1/2\Delta C_p}$ agree within about 2° to those of 431°K (158°C) and 444°K (171°C) determined from the point-correction graphical procedure for this

---

*Measurements performed through the courtesy of Perkin Elmer.

Figure 18. Plot of T_g versus weight fraction PPO (W_{PPO}) for PS/PPO and Copolymer B/PPO blends. Curves were drawn from values calculated from the Wood eq. for k=0.679.

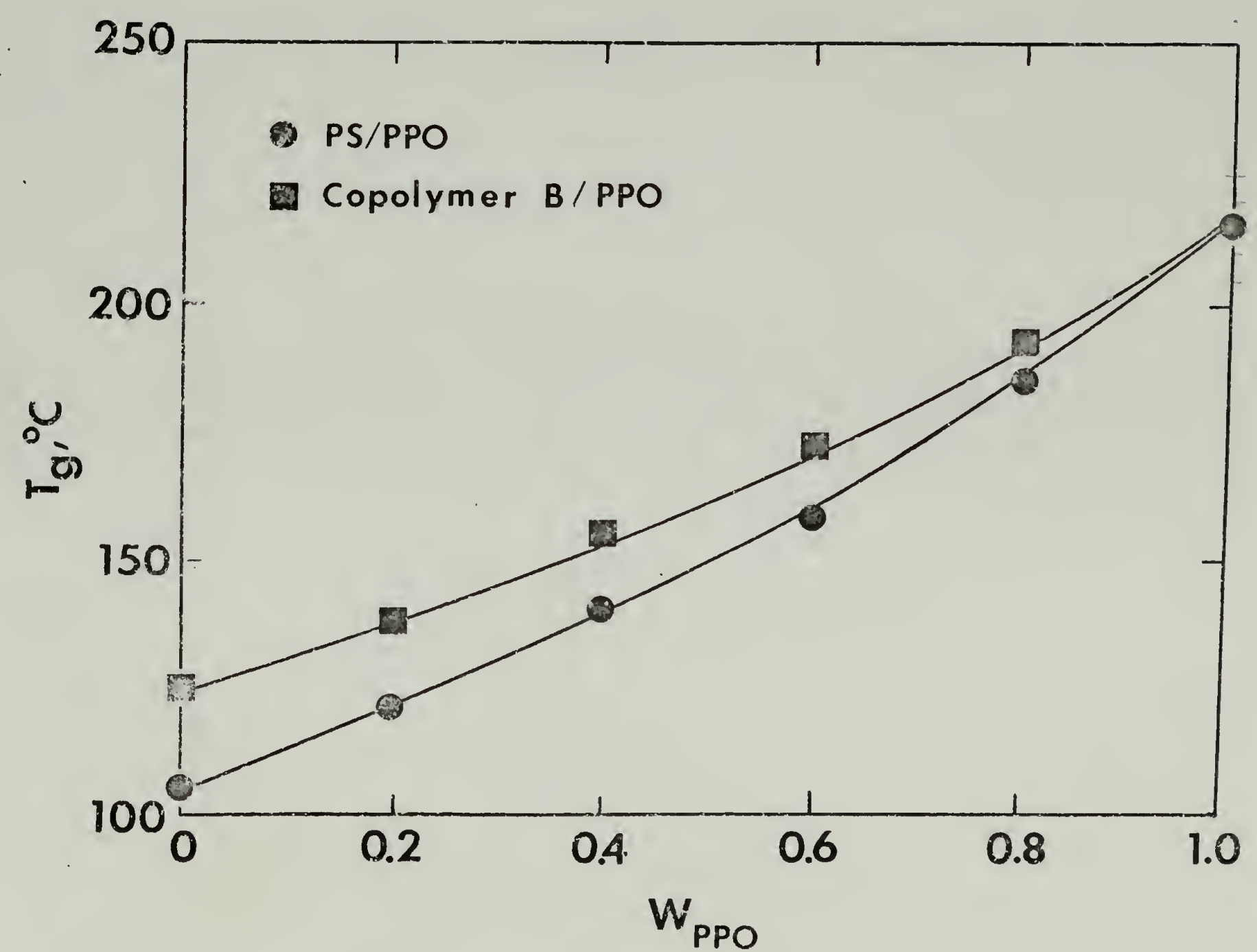
250
200
150
100
PS/PPO
Copolymer B / PPO
T_g, °C
0
0.2
0.4
0.6
0.8
1.0
W_{PPO}

Figure 19. Plot of T_g versus weight fraction PPO (W_{PPO}) for Copolymer C/PPO. Curve was drawn from values calculated from the Wood eq. for k=0.679.

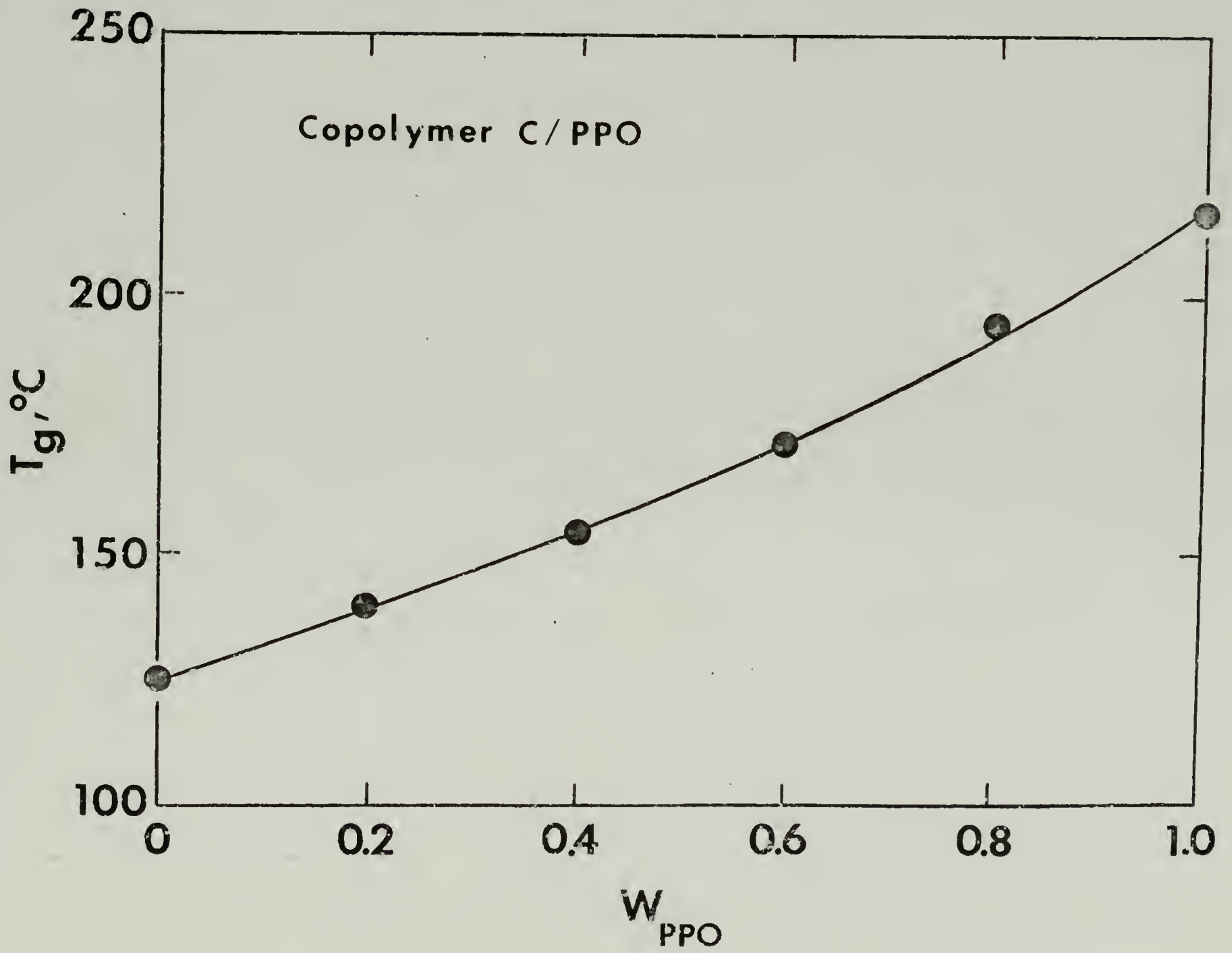
Copolymer C/PPO
250
200
150
100
T_g, °C
0
0.2
0.4
0.6
0.8
1.0
W_{PPO}

extremely broad, ca. 27°C, blend glass transition. As indicated from the values given above, the temperature at the inflection point of the transition corresponds very closely with the temperature at the half-width of the transition.

Glass transition temperatures for the incompatible blends are plotted versus weight fraction PPO (W_{PPO}) in Figures 20 through 24. The broken lines represent the T_g's of the pure components in each blend. As shown in Figures 20 and 21, the blends of Copolymer D and Copolymer E with PPO exhibit two glass transitions whose temperatures are displaced from those of unblended copolymer and PPO. By contrast, there is only slight evidence for a depression of the T_g of the PPO phase and elevation of the T_g of the copolymer phase for Copolymer F/PPO in Figure 22 while the T_g's of both phases in PpClS/PPO and PoClS/PPO blends in Figures 23 and 24, respectively, correspond almost exactly with those of the unblended homopolymers.

This movement of the T_g's of the two phases in the Copolymer D/PPO and Copolymer E/PPO blends toward an eventual single glass transition in Copolymer C/PPO blends indicates a state of partial compatibility. This means that the high T_g phases should be classified as PPO-rich phases which contain some of the lower T_g copolymer while the low T_g phases are actually copolymer-rich phases containing some PPO. As shown in Figures 20 and 21, annealing these blends at temperatures about 20° below T_g (20° below the high T_g for 30 to 120 min. followed by annealing at 20° belo-

Figure 20. Plot of T_g versus weight fraction PPO (W_{PPO}) for Copolymer D/PPO blends. Broken lines indicate expected T_g's of pure components, Copolymer D and PPO, for complete incompatibility. Solid lines were fitted to the actual T_g's of the Copolymer D-rich and PPO-rich phases by the method of least squares. (◯) indicates T_g's of blends annealed for 30 min at about 20° below each T_g.

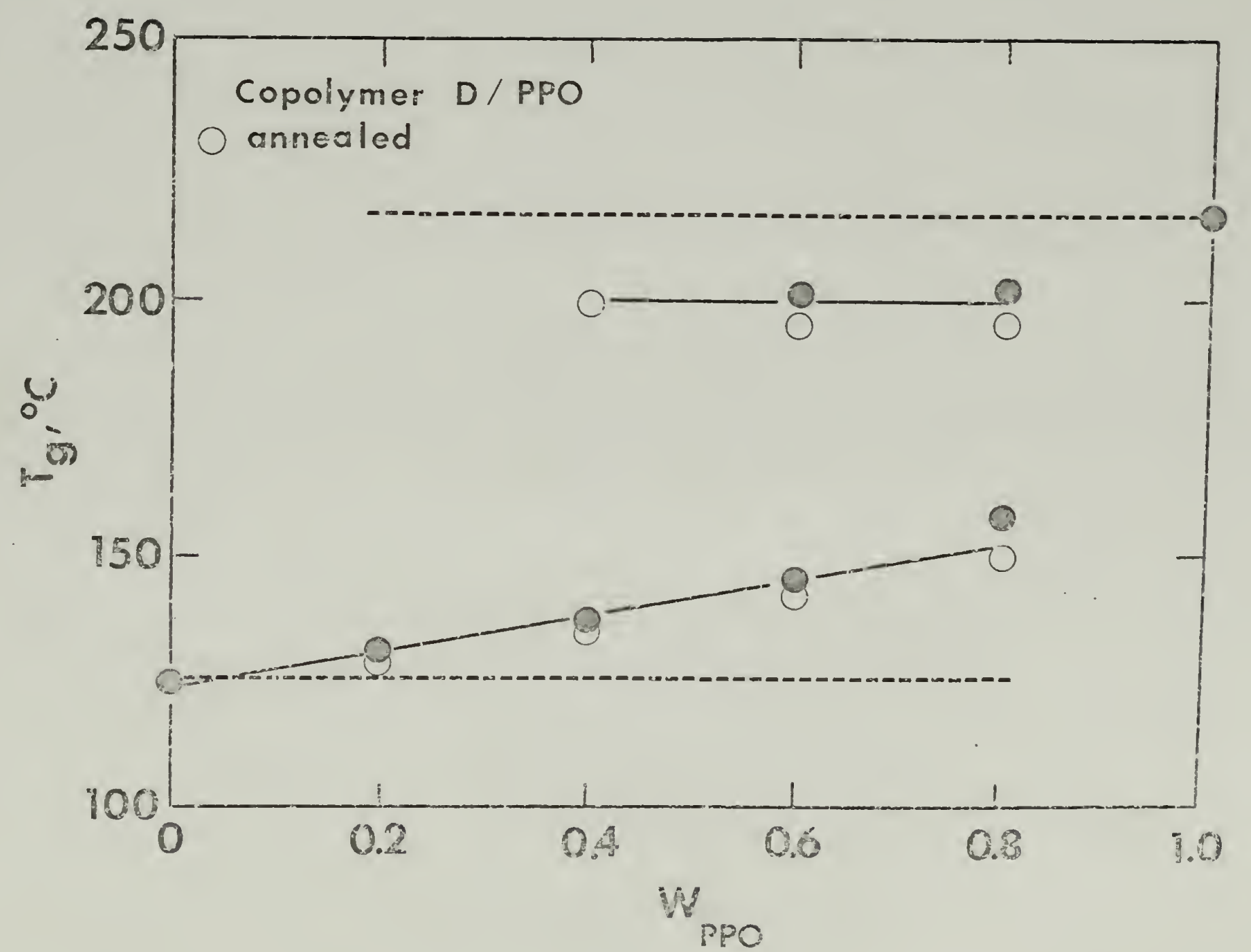
Copolymer D / PPO
○ annealed
250
200
150
100
T_g, °C
0
0.2
0.4
0.6
0.8
1.0
W_{PPO}

Figure 21. Plot of T_g versus weight fraction PPO (W_{PPO}) for Copolymer E/PPO blends. Broken lines indicate expected T_g's of pure components, Copolymer E and PPO, for complete incompatibility. Solid lines were fitted to the actual T_g's of the Copolymer E-rich and PPO-rich phases by the method of least squares. (○) indicates T_g's of blends annealed for 30 min. at about 20° below each T_g.

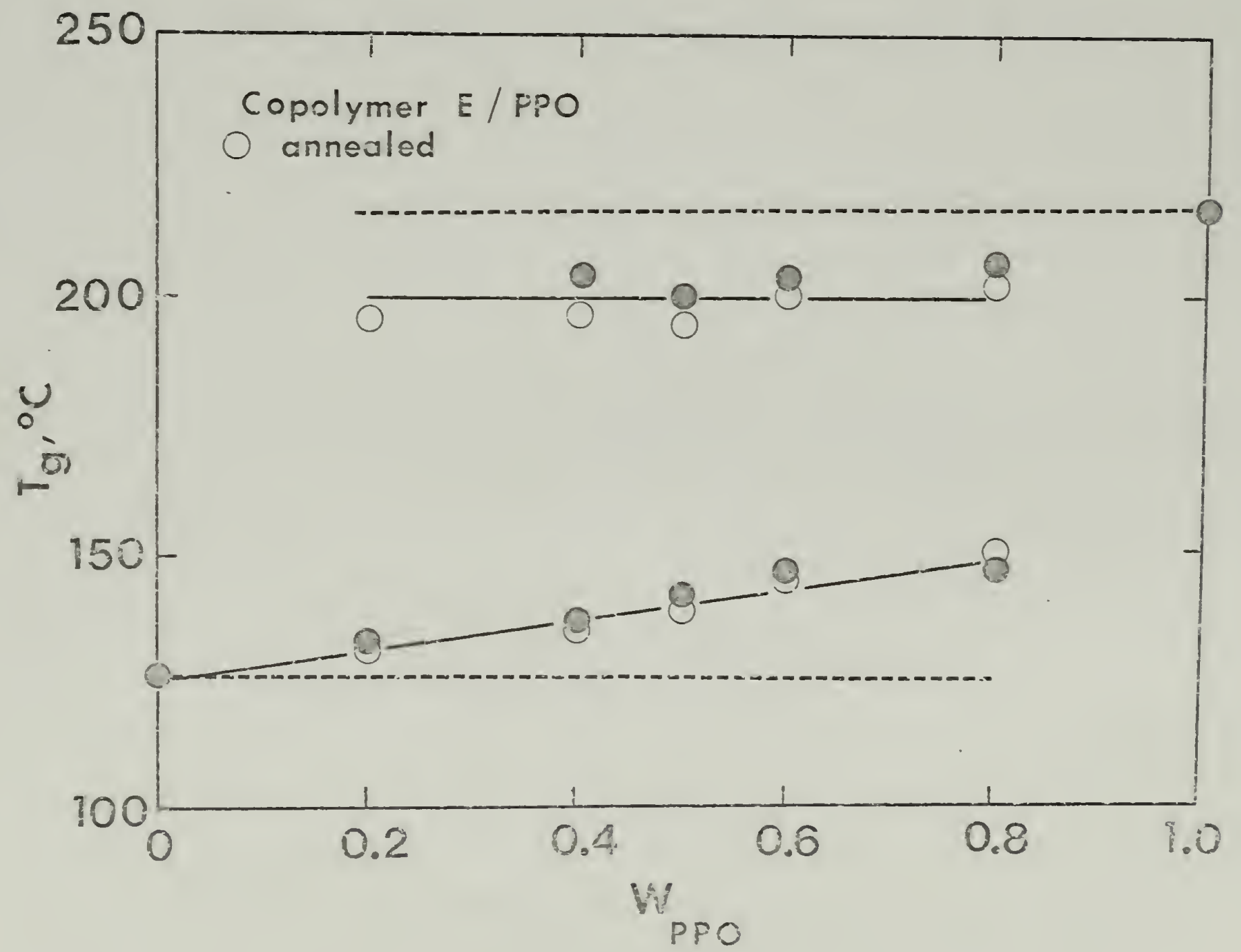
Copolymer E / PPO
○ annealed
250
200
150
100
T_g, °C
0
0.2
0.4
0.6
0.8
1.0
W_{PPO}

Figure 22. Plot of T_g versus weight fraction PPO (W_{PPO}) for Copolymer F/PPO blends. Broken lines indicate expected T_g's of pure components, Copolymer F and PPO, for complete incompatibility.

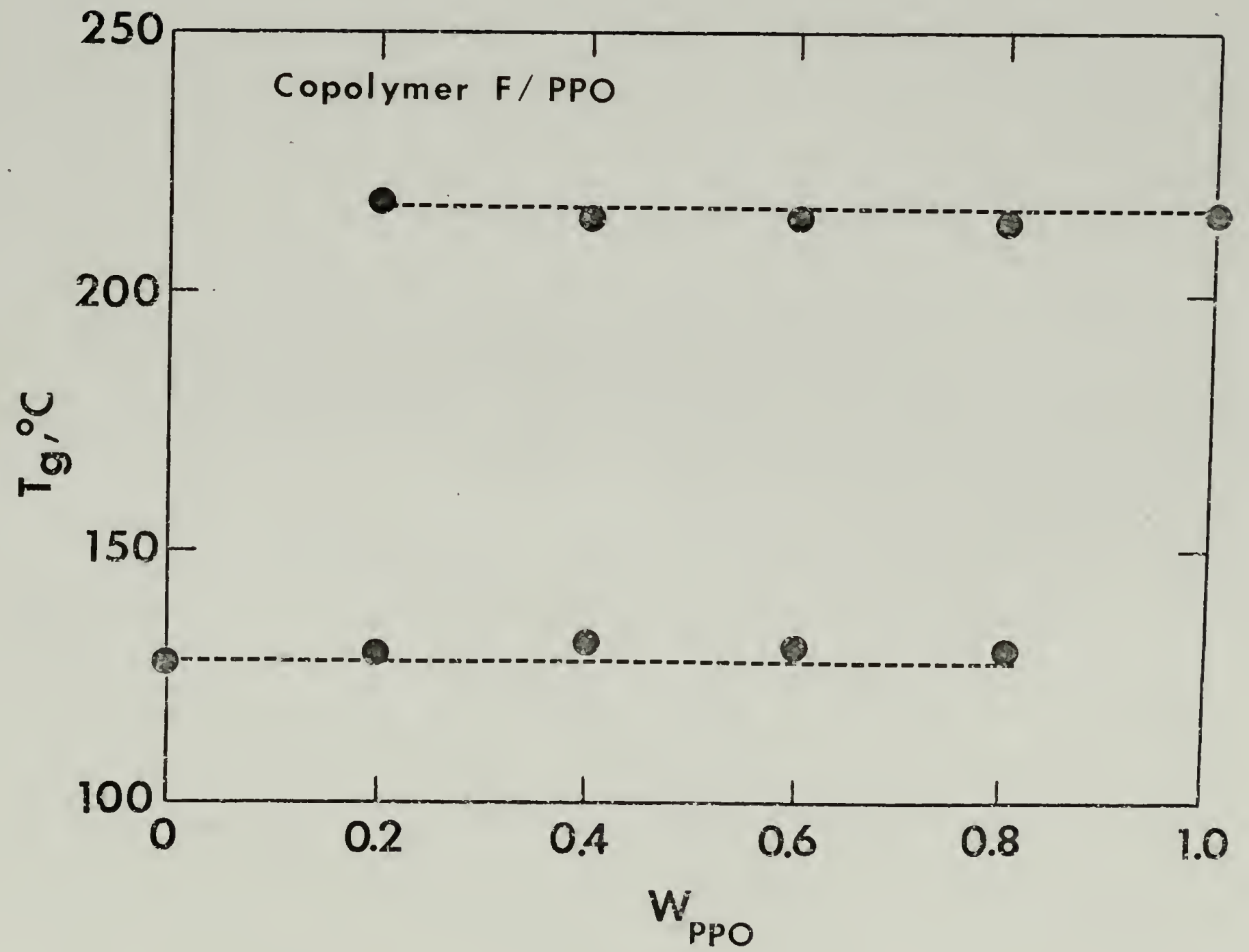
Copolymer F/PPO
250
200
150
100
T_g, °C
0
0.2
0.4
0.6
0.8
1.0
W_{PPO}

Figure 23. Plot of T_g versus weight fraction PPO (W_{PPO}) for PpClS/PPO blends. Broken lines indicated expected T_g's of pure components, PpClS and PPO, for complete incompatibility.

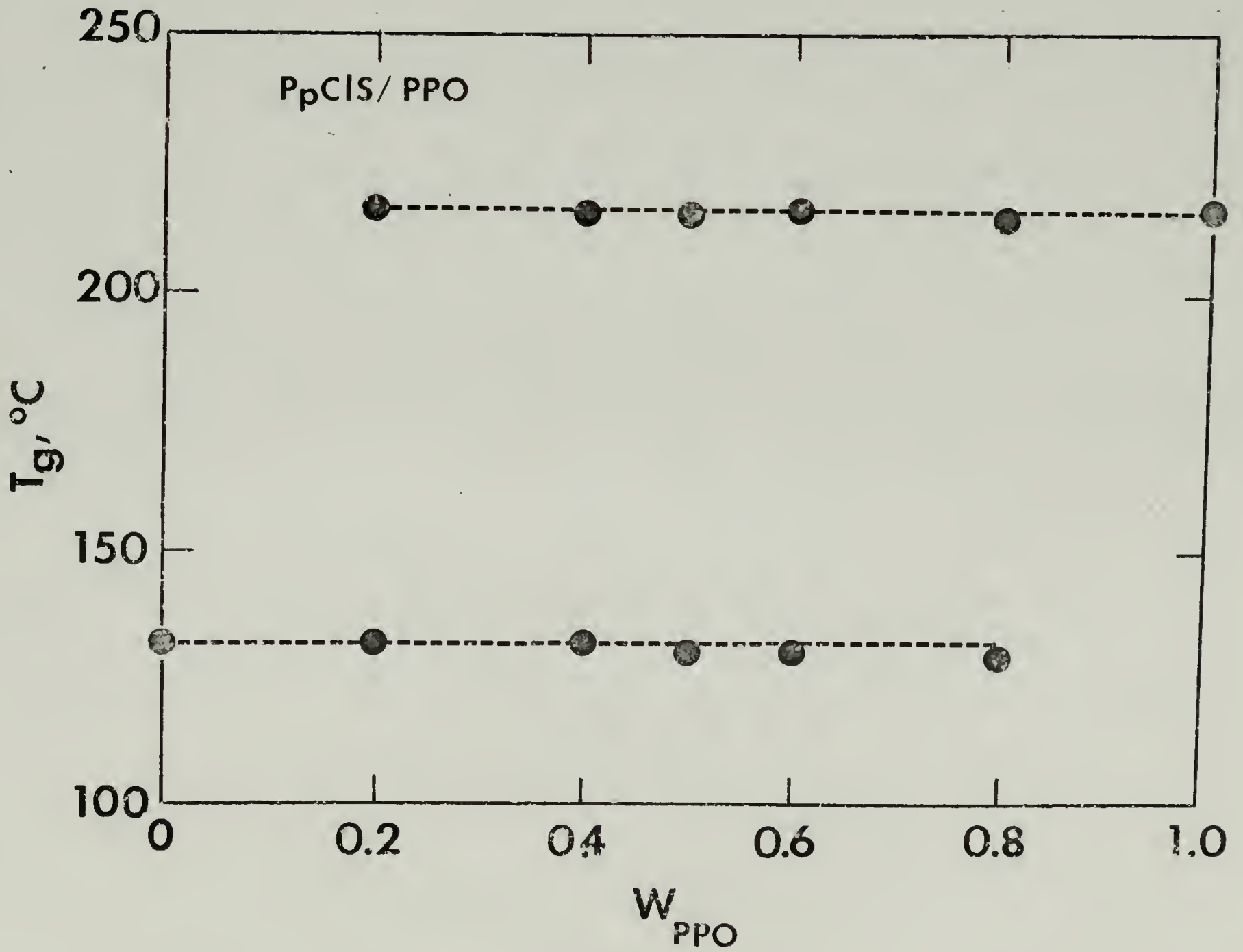
250
200
150
100
T_g, °C
P_pCIS/PPO
0
0.2
0.4
0.6
0.8
1.0
W_{PPO}

Figure 24. Plot of T_g versus weight fraction PPO (W_{PPO}) for PoClS/PPO blends. Broken lines indicate expected T_g's of pure components, PoClS and PPO, for complete incompatibility.

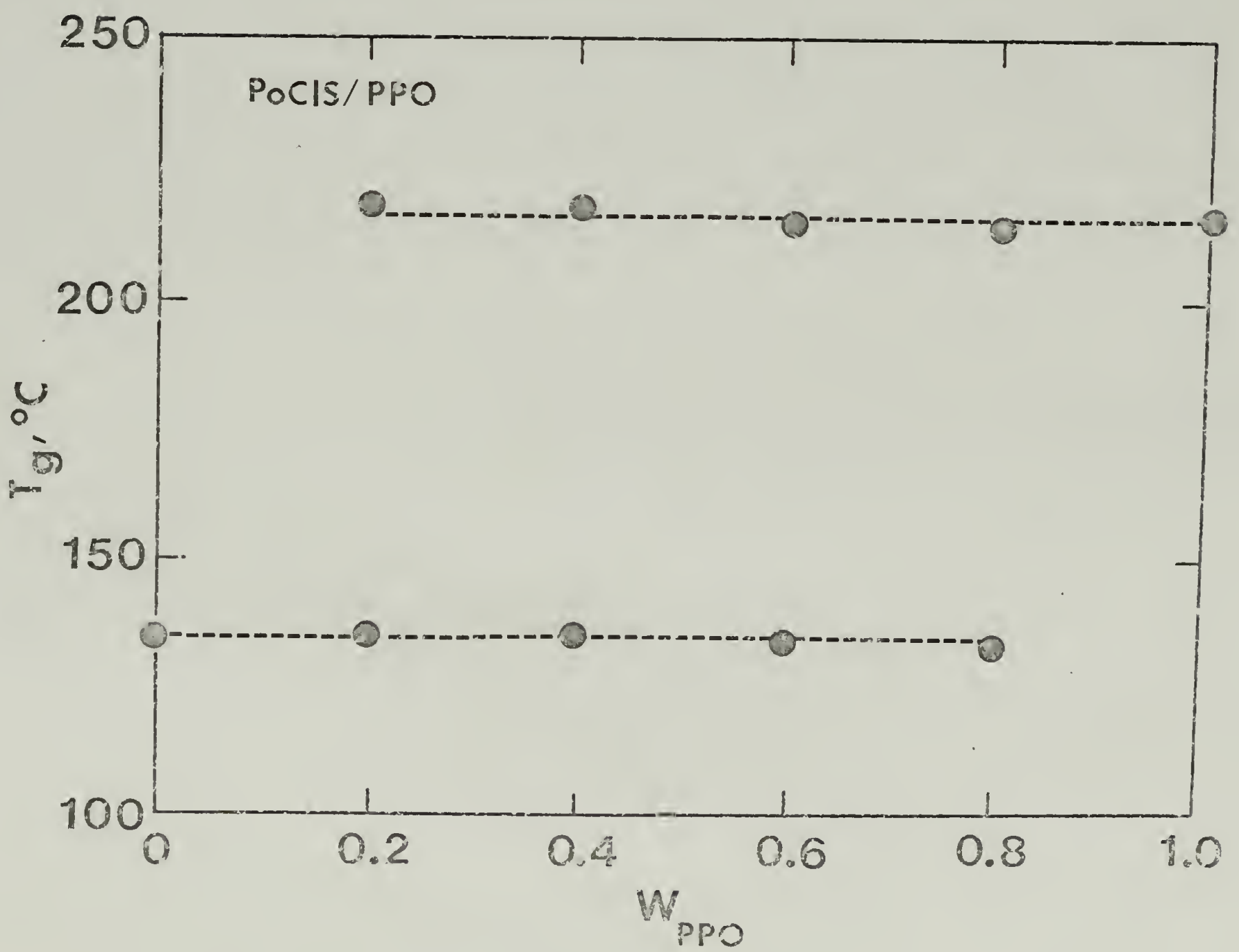
250
200
150
100
PoCIS/PPO
T_g, °C
0
0.2
0.4
0.6
0.8
1.0
W_{PPO}

the low T_g for identical times) has little affect on the temperature of these transitions but their widths decrease with increasing annealing time and detection of the transition is made somewhat easier. For those blend compositions for which one component is present in small quantity, e.g. for 20% PPO, compatibility appears complete and the transition corresponding to the minor component is completely absent.

The actual compositions of each of the phases of the Copolymer D/PPO and Copolymer E/PPO blends can be calculated from the observed T_g and use of the Wood equation, eq. (21), for which the parameter, k, is taken to be 0.679 as for the completely compatible blends. The weight fraction of PPO (W_{PPO}) in the copolymer-rich and PPO-rich phases are given in Table XIII.

TABLE XIII. Apparent Weight Fractions of PPO in the Copolymer-Rich and PPO-Rich Phases of Copolymer D/PPO and Copolymer E/PPO

W_{PPO}	W_{PPO} of Copolymer-Rich Phases		W_{PPO} of PPO-Rich Phases
Blend	Copolymer D	Copolymer E	Copolymers D and E
0.20	0.08	0.08	0.86
0.40	0.19	0.17	0.86
0.60	0.28	0.26	0.86
0.80	0.37	0.34	0.86

In comparison, W_{PPO} in the low T_g phases of the Copolymer F/PPO, PpClS/PPO, and PoClS/PPO blends is approximately zero, while W_{PPO} of the high T_g phases is unity. The results given in Table XIII indicate that the compositions of the PPO-rich phases in the Copolymer D/PPO and Copolymer E/PPO blends are both about 86% PPO and are independent of overall blend composition. In contrast, the concentration of PPO in the copolymer-rich phase linearly increases with increasing overall PPO content of the blend. At equal overall blend compositions, the weight fraction of PPO in the copolymer-rich phases is slightly greater in the Copolymer D/PPO blends than in the Copolymer E/PPO blends. This would be expected because Copolymer D due to its slightly lower pClS content (67.8 mole % pClS) should be more compatible than Copolymer E (68.6 mole % pClS).

The observation that the T_g of the copolymer-rich phase linearly increases with increasing W_{PPO} while the T_g of the PPO-rich phase is depressed by a constant factor was totally unexpected but may be explained by consideration of the different molecular weights of PPO and those of the two copolymers given in Table VIII of Chapter III. The number-average molecular weight of PPO was approximately 17,000 which is substantially smaller than those of about 99,000 for Copolymer D and 80,000 for Copolymer E. Since the entropy of mixing is greater for low molecular weight molecules, the free energy of mixing is therefore lower and thus

compatibility is encouraged. This means that the lower molecular weight PPO would be expected to be preferentially soluble in the higher molecular weight copolymer phase, while the copolymer apparently reaches a saturation concentration in the PPO-rich phase before an overall composition of 20% PPO is reached in the blend. In terms of the average molecular weight of both components in each phase, adding PPO to the copolymer in the copolymer-rich phase results in an overall decrease in phase molecular weight therefore favoring miscibility. The lower molecular weight end of the polydisperse PPO probably is involved in this interphase miscibility while the higher molecular end remains in the PPO-rich phase. More lower molecular weight PPO is available as the overall amount of PPO in the blend is increased and therefore the amount of PPO in the copolymer-rich phase linearly increases with W_{PPO}. The reversed situation exists for the PPO-rich phase. As the copolymer is added to the PPO phase, the average molecular weight of this phase increases therefore discouraging miscibility. Up to 14% copolymer can be tolerated in the PPO-rich phase before no additional copolymer can be dissolved and is independent of the overall composition of the copolymer in the blend. Shifting of the miscibility gap for binary polymer mixtures towards the axis of the constituent with the shorter chains has been noted by Koningsveld.[31,32] If the molecular weight of PPO and the copolymers were equal, then the T_g's of both

phases would be expected to exhibit a constant, composition independent shift from those of the unblended components (constant depression of the high T_g phase and elevation of the low T_g phase).

Such partial miscibility or compatibility of two polymers as exhibited by the Copolymer D/PPO and Copolymer E/PPO blends has been observed for several other systems. For example, Shultz and Gendron[33] reported a 5-7° elevation of the T_g of a PS-rich phase in blends of PS and poly (2-methyl-6-phenyl-1,4-phenylene oxide). Robeson et al.[34] have observed that blends of high molecular weight PS and poly (α-methyl styrene) are totally incompatible; however, blends of high molecular weight poly (α-methyl styrene) and lower molecular weight PS ($\bar{M}_w$=36,000) exhibit both broadened transitions and shifts in T_g indicating slight mutual solubility. The extreme closeness of the compositions of Copolymer D and E to the compatible composition of Copolymer C (67.1 mole % pClS), i.e. 0.7 mole % pClS between Copolymer D and C, suggests that other blends for which T_g shifts are observed are critically close to being totally compatible and therefore lowering the molecular weight of one or both components may be all that is needed to induce compatibility. It is possible for example, that PS and poly (α-methyl styrene) may become totally compatible at sufficiently low molecular weights.

Transition Heights and Interfacial Mixing. It has been mentioned previously that Shultz and Beach[8] reported difficulty in the detection of the transitions of the minor components in the incompatible poly(S-co-pClS)/PPO blends. This was attributed to instrumental insensitivity; however, as exhibited for Copolymer D/PPO (Figure 11), Copolymer E/PPO (Figure 12), and to a lesser extent for Copolymer F/PPO (Figure 13), the minor transitions are still difficult to detect even though larger samples (20-30 mg) and better instrumentation (DSC II in place of the DSC I) were employed. Since the minor transitions in the incompatible blends of pPClS/PPO and PoClS/PPO are clearly evident in Figures 14 and 15, respectively, instrumental insensitivity is apparently not the full answer.

The qualitative observations concerning the heights of the blend transitions can be expressed quantitatively by measurement of the change in heat capacity (ΔC_p) at the glass transition. Although absolute value of the heat capacity, C_p, can be obtained only from reference to a standard material such as pure sapphire (α-Al_2O_3)[1,35,36] the change in heat capacity, ΔC_p, can be obtained directly from the relation[1] given by

$$\Delta C_p = \frac{\Delta\ S}{MR} \qquad (25)$$

where

Δ, fractional increase in the ordinate at

the transition

S, full scale value of the power (ordinate) in mcal sec^{-1}

M, sample mass in mg

R, heating rate in degrees sec^{-1}

In all the DSC results in this study, R was 20^{o} min^{-1} or 0.33^{o} sec^{-1}, DSC range or S was 5 mcal sec^{-1}, and a full-scale deflection corresponded to 230 mm along the chart ordinate. For these values, ΔC_p could be calculated by

$$\Delta C_p = 0.0652 \frac{H}{M} \qquad (26)$$

where H is the transition height in mm and M is the sample weight in mg as before. The values of ΔC_p calculated by eq. (26) for all the polymers used in the blends, except PPO, are given in Table XIV.

TABLE XIV. DSC Values for ΔC_p of Blend Polymers

Sample	M(mg)	H(mm)	ΔC_p (cal $^{o}C^{-1}$ g^{-1})
PS	18.08	18.6	0.0671
Copolymer B	31.68	28.8	0.0593
Copolymer C	22.93	20.7	0.0589
Copolymer D	22.21	20.2	0.0593
Copolymer E	23.80	19.3	0.0563
Copolymer F	22.37	19.6	0.0571
PpClS	22.01	19.5	0.0578
PoClS-1	34.96	28.3	0.0528

For PS, ΔC_p was found to be 0.0671 cal $^{o}C^{-1}$ g^{-1} as indicated in Table XIV. This compares well with the value

of 0.069 determined by Bair[1] for DSC and 0.0707 reported by Karasz et al.[3] for their adiabatic calorimetry results. As indicated in Table XIV, ΔC_p for the copolymers, PpClS, and particularly PoClS are lower than for PS. For PPO, seven samples from separately purified (Chapter III) and molded films were used to obtain ΔC_p and to calculate a standard deviation of the mean. The weights of these samples were given in Table XI at the beginning of this chapter. The calculated mean for ΔC_p of PPO was 0.0528±.0007 cal $^{o}C^{-1}$ g^{-1} which falls between the values of 0.048 and 0.057 determined by Bair[1] and Karasz,[3] respectively.

The ΔC_p of the compatible blends can be calculated from a weighted average of the ΔC_p of the two components in the following manner:

$$(\Delta C_{p,B})_{calc} = W_2 \Delta C_{p1} + W_2 \Delta C_{p2} \qquad (27)$$

where W_1 is the weight fraction of component 1 (PS, Copolymers B through F, PpClS, or PoClS), W_2 is the weight fraction of PPO ($W_2 = 1 - W_1$), and ΔC_{p1} and ΔC_{p2} are the corresponding heat capacities of the pure polymers; ΔC_{p_i} are those given in Table XIV. The principal source of error in these determinations is in the measurement of the transition height (H) especially for the very small transitions in some of the incompatible blends and the propagation of errors of ΔC_p for the unblended components in eq. (27). As

mentioned in the previous chapter, ΔC_p was computed for blend C-b40 by means of Tektronic Programmable Calculator and a Perkin Elmer Calculator Interface coupled to the DSC II. This calculated value of 0.061 agrees within about 11% with that of 0.055 determined from the actual DSC thermogram and eq. (27).

For the compatible blends, ΔC_p can be measured directly from the transition height (H) and use of eq. (26). The ratio of measured to calculated ΔC_p, eq. (27), for the compatible blends is plotted versus weight fraction PPO (W_{PPO}) in Figure 25. As Figure 25 shows, this ratio for the compatible blends is close to unity within experimental error. This means that all the material in the blend contributes to the observed transition.

For the incompatible blends, the equivalent ratio given by

$$\frac{W_1(\Delta C_{p_1})_{meas} + W_2(\Delta C_{p_2})_{meas}}{W_1 \Delta C_{p_1} + W_2 \Delta C_{p_2}} \qquad (28)$$

is plotted versus W_{PPO} in Figure 26. The denominator has the same significance as eq. (27). Within experimental error, the value of this ratio for the most incompatible blend, that of PpClS/PPO, is close to unity. This indicates that the two phases correspond to pure PpClS and pure PPO and that the entire PpClS content is contributing to the apparent PpClS transition while the entire PPO content is contributing

Figure 25. Plot of the ratio of measured to calculated transition heights for the compatible blends versus weight fraction PPO (W_{PPO}).

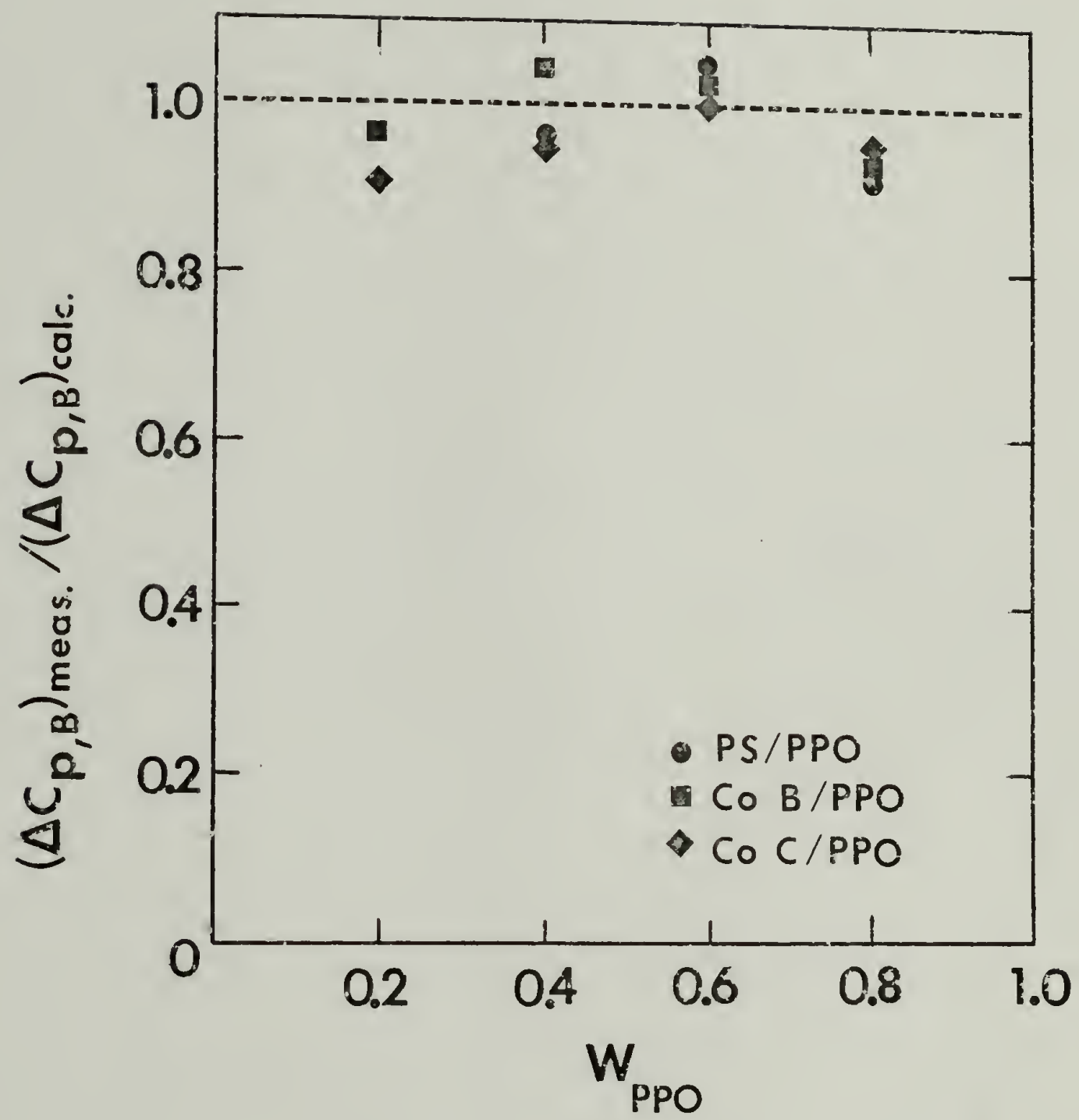
1.0
0.8
0.6
0.4
0.2
0
0.2
0.4
0.6
0.8
1.0
$(\Delta C_{p,B})_{meas.}/(\Delta C_{p,B})_{calc.}$
W_{PPO}
PS/PPO
Co B/PPO
Co C/PPO

Figure 26. Plot of the ratio of measured to calculated transition heights for the incompatible blends versus weight fraction PPO (W_{PPO}).

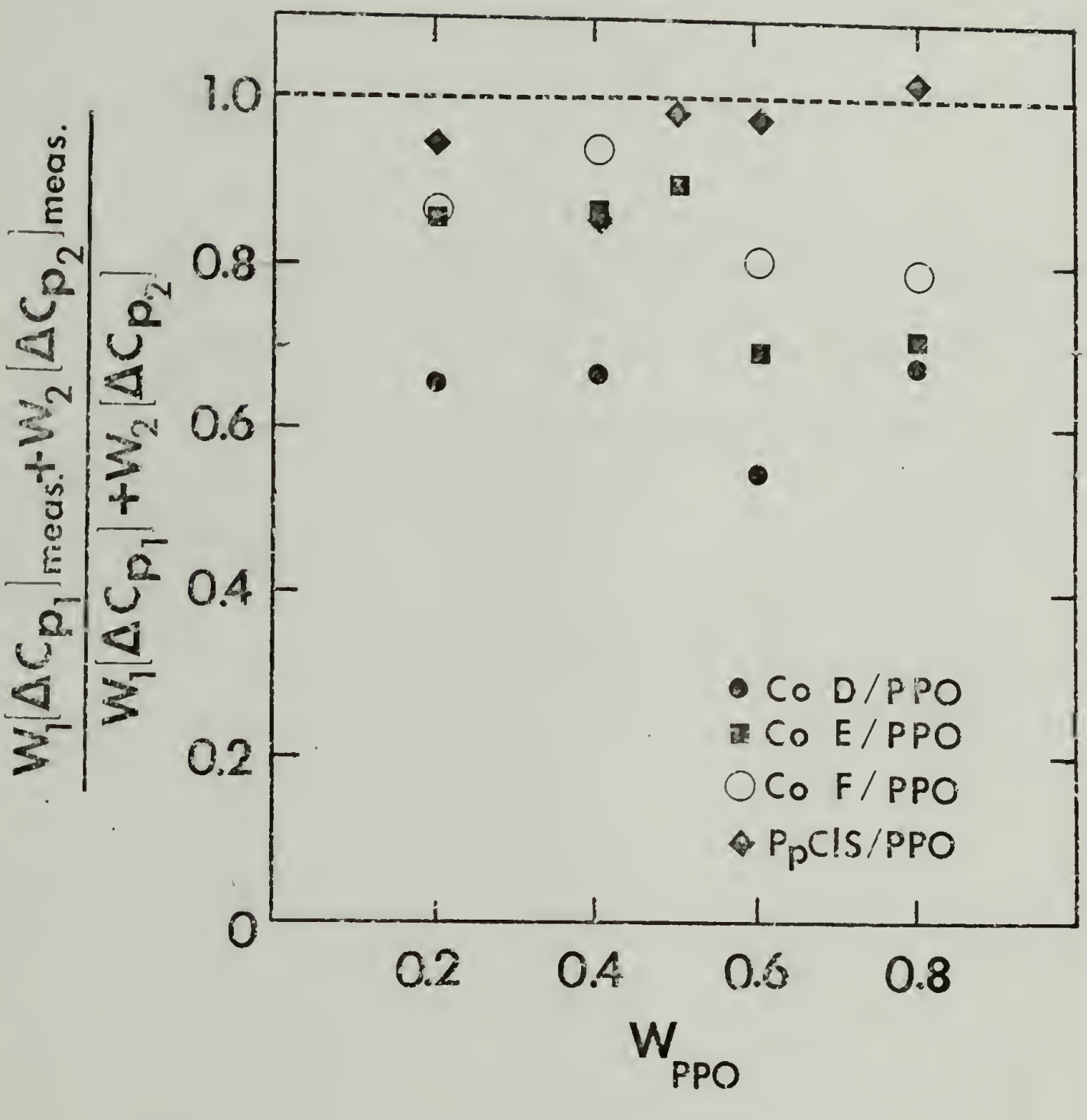
$\frac{W_1|\Delta C_{p_1}|_{meas.}+W_2|\Delta C_{p_2}|_{meas.}}{W_1|\Delta C_{p_1}|+W_2|\Delta C_{p_2}|}$
1.0
0.8
0.6
0.4
0.2
0
0.2
0.4
0.6
0.8
W_{PPO}
Co D/PPO
Co E/PPO
Co F/PPO
P_pCIS/PPO

to the apparent PPO transition. For the copolymer/PPO blends, the ratio is less than unity and roughly decreases with decreasing PClS content of the copolymer, i.e. in the direction of decreasing incompatibility. The lowest values, between 0.54 and 0.68, are observed for blends of Copolymer D whose composition is closest to the compatible Copolymer C. This means that a substantial amount of blend material is not involved in either transition and therefore the small transitions of the minor blend components appear even smaller.

These observations can be explained by applying conclusions reached by Letz[35] in a recent study of the diffuse interphase layer in microheterogeneous polymer mixtures to the poly(S-co-pClS) system. Letz found that if two incompatible polymers are allowed to interdiffuse either by bonding two films together or mixing powders in suspension and then evaporating the suspending medium and compacting the powdered mixtures, an interphase region is formed at elevated temperatures. Interdiffusion at first proceeds by Fick's law (rate proportional to the square-root of time) but after about 20 min, diffusion was retarded and finally stopped. Letz proposed that the equilibrium thickness of the interphase layer can be used as a quantitative criterion of polymer compatibility. More compatible polymer pairs would be expected to exhibit larger interphase layers while strongly incompatible pairs would have very small interphase layers and therefore sharp phase boundaries. At 160°C,

equilibrium thicknesses of 28,000 and 89,600 Å were measured by phase contrast microscopy for mixtures of isotactic polypropylene/polyethylene and PVC/polyethylene, respectively.

The results of Letz would suggest that for the most incompatible pair, that of PpClS and PPO, the interphase layer should be relatively small. Therefore, the majority of PpClS and PPO molecules exist in separate, well-defined phases characterized by sharp, quantitative glass transitions of the pure materials. As the copolymer compositions and PPO become more compatible, some miscibility probably occurs in the region between phases. It is probable that this interphase mixing occurs between low molecular weight molecules of the polydisperse components for which the thermodynamic restrictions for compatibility are less severe. As the pClS content of the copolymer is decreased, interphase mixing extends to larger molecular weight molecules and therefore the amount of material (or the size of the diffuse interphase layer) between phases increases. If the size and composition of these interphase regions varies throughout the sample, then the T_g corresponding to these regions may be so small or broad that detection is not possible. This means that the dominant transitions of the principal phases are the only detectable ones and these appear small due to depleted material participating in the interphase regions.

Transition Widths and Annealing Effects. As previously noted in the DSC thermograms (Figures 8 through 14), there is an increase in the width of the glass transitions for both the compatible and incompatible blends as the copolymer composition marking the compatibility-incompatibility transition (67.1 to 67.8 mole % pClS) is approached. Transition widths obtained by the point-correction technique (Chapter III) are plotted against copolymer composition (mole % pClS) in Figure 27. The transition widths of the incompatible blends represent an average for the two transitions. As shown, transition width reaches a sharp maximum at the compatibility-incompatibility transition.

This observed trend in transition width can be related to the extent of blend heterogeneity. The validity of this argument is supported by the early work of Nielsen[38] who showed that the width of the logarithmic decrement in the dynamic mechanical spectrum of several vinyl copolymers of broad compositional distribution increased with the chemical heterogeneity of the system although the position of the maximum remained unchanged. In addition, similar broadening of the loss peak in the dynamic mechanical spectrum of plasticized polymers has been observed.[39] For example, the width of the damping peak of PVC is observed to increase when plasticizers of decreasing solvating power are used. Buchdahl and Nielsen[40] have attributed such broadening to fluctuations in the interaction of chain segments with their

Figure 27. Plot of the width of the glass transition versus the composition (mole % pClS) of the copolymers used in the blends.

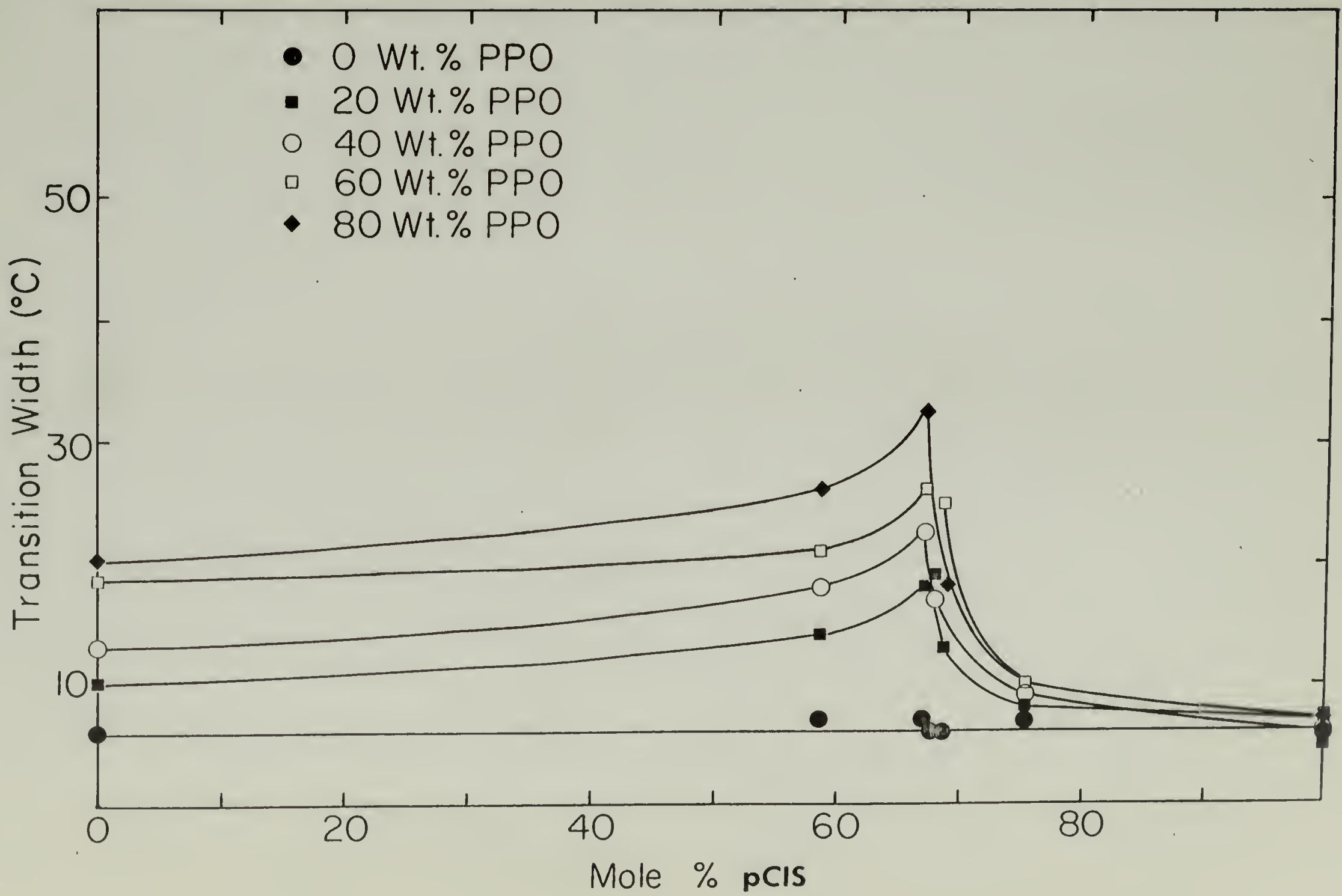
0 Wt. % PPO
20 Wt. % PPO
40 Wt. % PPO
60 Wt. % PPO
80 Wt. % PPO
Transition Width (°C)
50
30
10
0
20
40
60
80
Mole % pCIS

nearest neighbors in excess of normal thermal fluctuations. Besides the normal thermal and density fluctuations of pure polymers, polymer blends also experience local fluctuations in composition which are apparently sufficient to broaden the glass transition. For the poly(S-co-pClS)/PPO blends, as there is a greater tendency for phase separation with increasing pClS content of the copolymer, the local fluctuations in composition become larger and the glass transition broadens until final phase separation occurs. The separated phases in the incompatible blends become purer in the single components with increasing pClS copolymer composition and therefore local composition fluctuations become less and the transition becomes sharper.

A second feature of the DSC thermograms worth noting is that the small peaks at the high temperature side of the glass transitions for the unblended materials (PS, Copolymers B through F, PpClS, and PPO) is absent for all the compatible blends and all but the most incompatible blends (Copolymer F/PPO, PpClS/PPO, and PoClS/PPO) for which each phase consists of essentially pure polymer.

The significance of these transition endotherms for unblended polymers has been discussed by several authors. Wunderlich and Bodily[41] using classical hole theory[42,43] have postulated that upon slow cooling, a relatively small number of holes are frozen in the polymer structure. Upon subsequent fast heating, the equilibrium number of holes is

overshot because there is not enough time for equilibration, and the polymer glass returns to the equilibrium condition via a path which appears endothermic. More recently, Petrie[44,45] has shown that this endotherm is a result of energy absorbed in the T_g region as the glass returns from a lower excess enthalpy due to annealing or slow cooling. The cooling rate of 80° min^{-1} used in the present study prior to heating at 20° min^{-1} (Chapter III) is apparently sufficient to partially anneal the pure polymers and thereby cause a decrease in excess enthalpy, but is less effective for the molecularly heterogeneous blends. The width of these broad transitions can be sharply narrowed and endothermic peaks created by annealing below T_g. For example, Figure 28 shows a comparison between a DSC thermogram for a PS-b20 (80% PPO) sample that was cooled from the melt at 80° min^{-1} and one for a sample which had been annealed at about 20° below T_g for 2 hrs. in the DSC. As shown, the transition of the annealed sample is very narrow and has a large endothermic peak. The transitions of all the blends could be equally narrowed by annealing below T_g but to achieve equal transition widths and endotherm peak areas, longer annealing times were required for the more heterogeneous blends, i.e. those with copolymer compositions approaching the compatibility-incompatibility transition.

Figure 29 shows DSC thermograms for two Copolymer C blends, C-b40 (60% PPO) and C-b20 (80% PPO), both unannealed

Figure 28. Comparison between DSC thermograms of a blend of 20% PS and 80% PPO (PS-b20) which had been cooled from the melt (unannealed) and one which was annealed for 2 hrs. at about 20° below T_g.

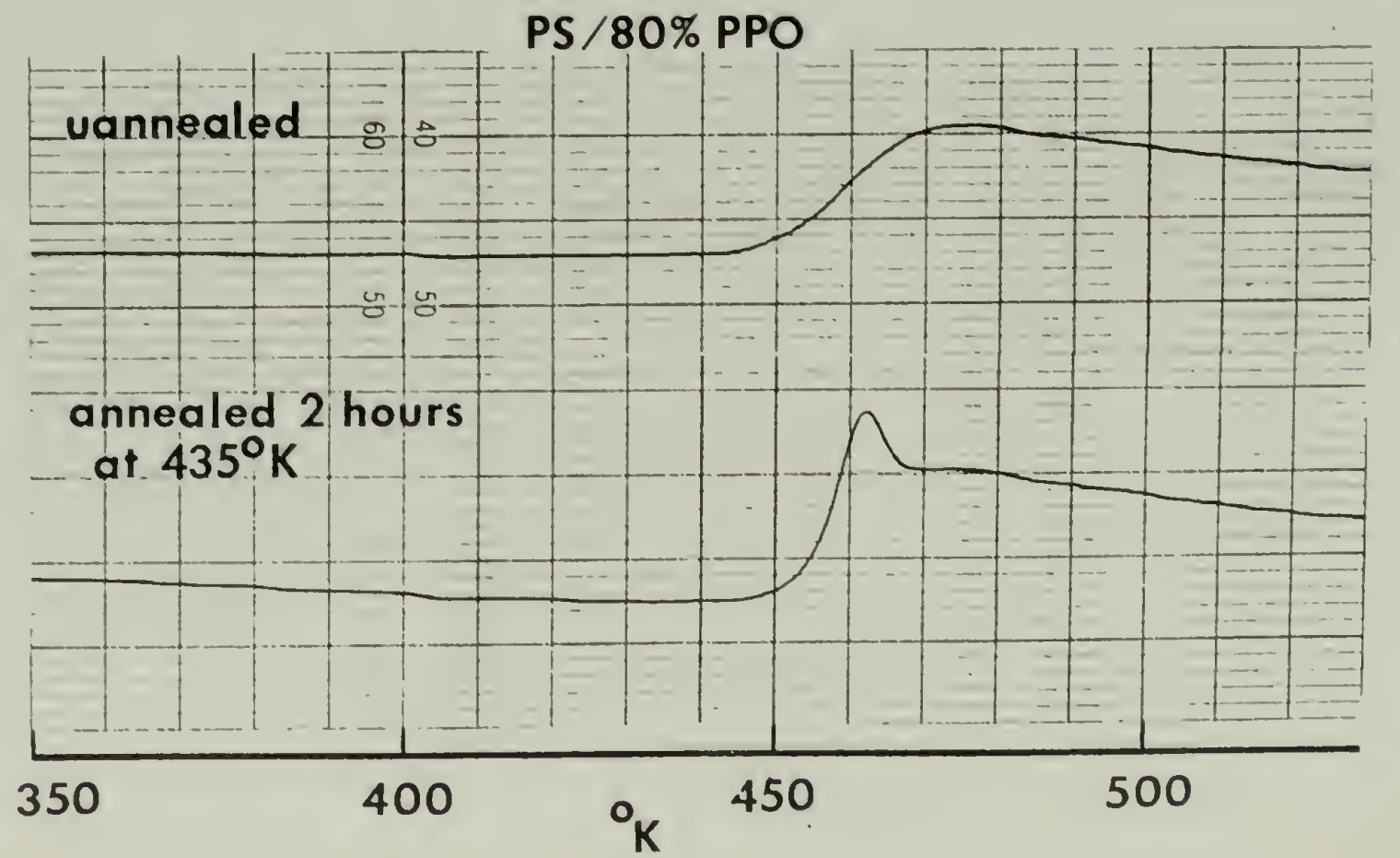
PS/80% PPO
unannealed
annealed 2 hours
at 435°K
60
40
50
50
350
400
450
500
°K

Figure 29. DSC thermograms of unannealed and annealed Copolymer C/PPO blends.

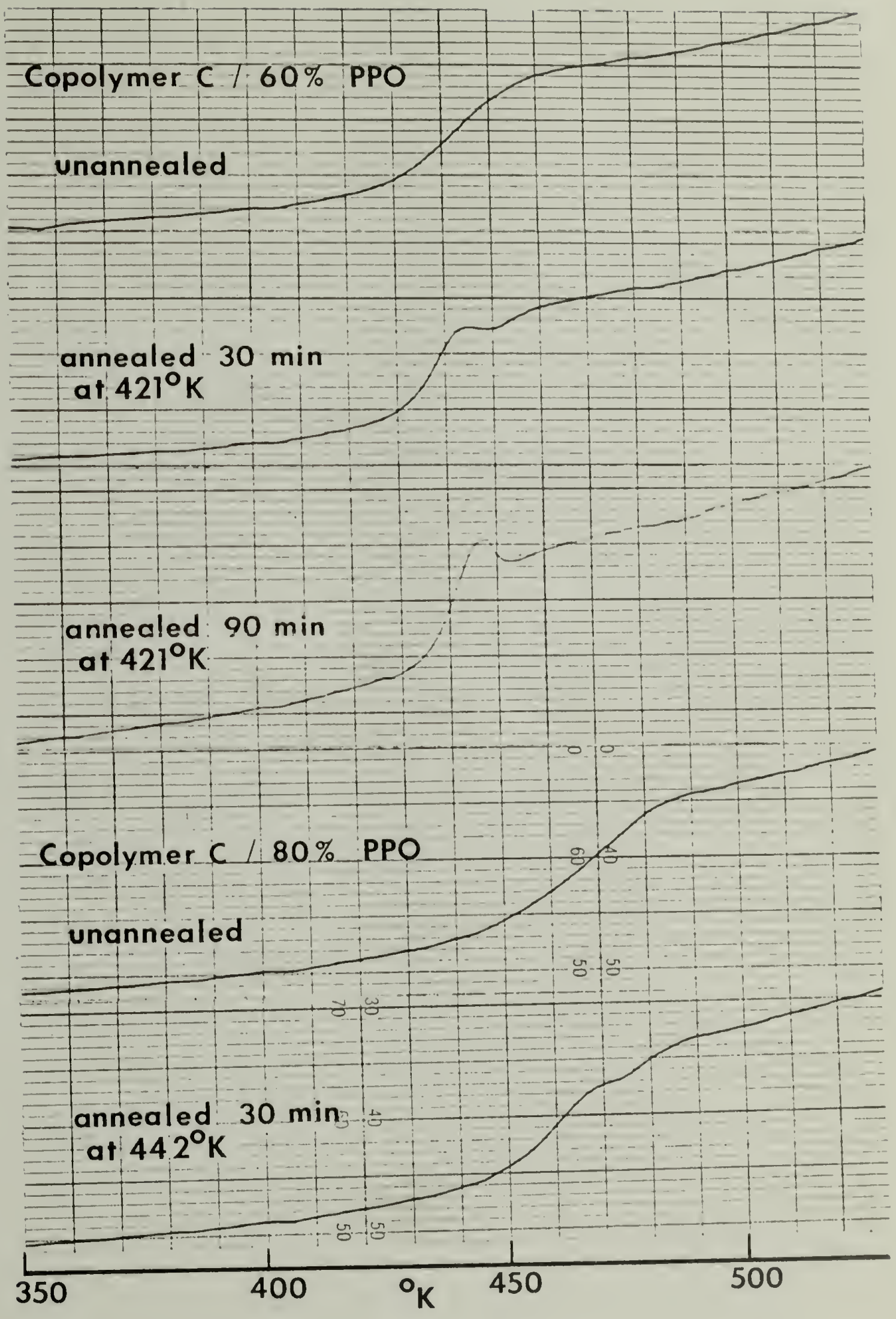
Copolymer C / 60% PPO
unannealed
annealed 30 min
at 421°K
annealed 90 min
at 421°K
Copolymer C / 80% PPO
unannealed
annealed 30 min
at 442°K
350
400
°K
450
500

and annealed. Annealing these blends at 20° below T_g for 30 min. appears to split these single broad blend transitions into two overlapping ones. Similar results were obtained for the annealed Copolymer B blends; however, in all cases annealing for longer times results in large endotherms which obscure detection of the second transition. This effect is shown in Figure 29 for C-b40 which had been annealed for 90 min. The splitting of the compatible blend transitions may be interpreted as evidence for phase separation as a result of annealing. For example, Landi[46] has demonstrated that heterogeneous copolymers of butadiene and acrylonitrile separate into two phases whose T_g's are so close that they overlap and unless very careful procedures are employed, they cannot be resolved by DSC. The thermodynamics of phase separation of heterogeneous copolymers has been discussed by Scott.[47] There is also evidence for a small shoulder in the dielectric spectrum of annealed Copolymer C blends which would confirm phase separation for this system, but data is incomplete at this point.[48] The fact that these blends appear compatible when quenched from the melt (80° min^{-1}) but phase separate when annealed at lower temperatures would indicate that this system exhibits an Upper Critical Solution Temperature (UCST) for phase separation. The compatible state in the melt is frozen-in by rapid cooling, but when annealed below T_g the equilibrium phase-separated state is achieved at lower temperatures. A

UCST for this system would be the exception to the general observation that polymer solutions and some polymer blends exhibit a Lower Critical Solution Temperature (LCST) for phase separation.[49,50,51] There is also the possibility that the break in the transition for the annealed blends may be due to factors other than phase separation. For example, Roe et al.[52] have recently shown that PVC annealed at 46°C, over 30° below T_g, for 12 hrs. exhibits a dip on the high temperature side of the endotherm peak; this dip was absent for PVC annealed at higher temperatures. This thermogram looks similar to that of C-b40 annealed for 30 min. at 20° below T_g (Figure 29). There is no good explanation for this dip as yet, but Roe's study indicates that the structure of glassy polymers annealed at different temperatures are different not only with respect to their enthalpy content but probably with respect to some other fine details of the molecular organization.

The effects of annealing the incompatible blends also has been studied. As Figure 30 shows for the example of the blend E-b40 (60% PPO), each of the two phases can be annealed separately, or alternately both phases can be annealed at the same time by applying a series of cooling and annealing steps. For example, by heating E-b40 to the melt (530°K), cooling at 80° min^{-1} to 20° below the upper T_g, and then annealing 2 hrs., the transition width of the PPO-rich phase is reduced and an endotherm is apparent. Both phases can

Figure 30. DSC thermograms of unannealed and annealed Copolymer E/PPO blends.

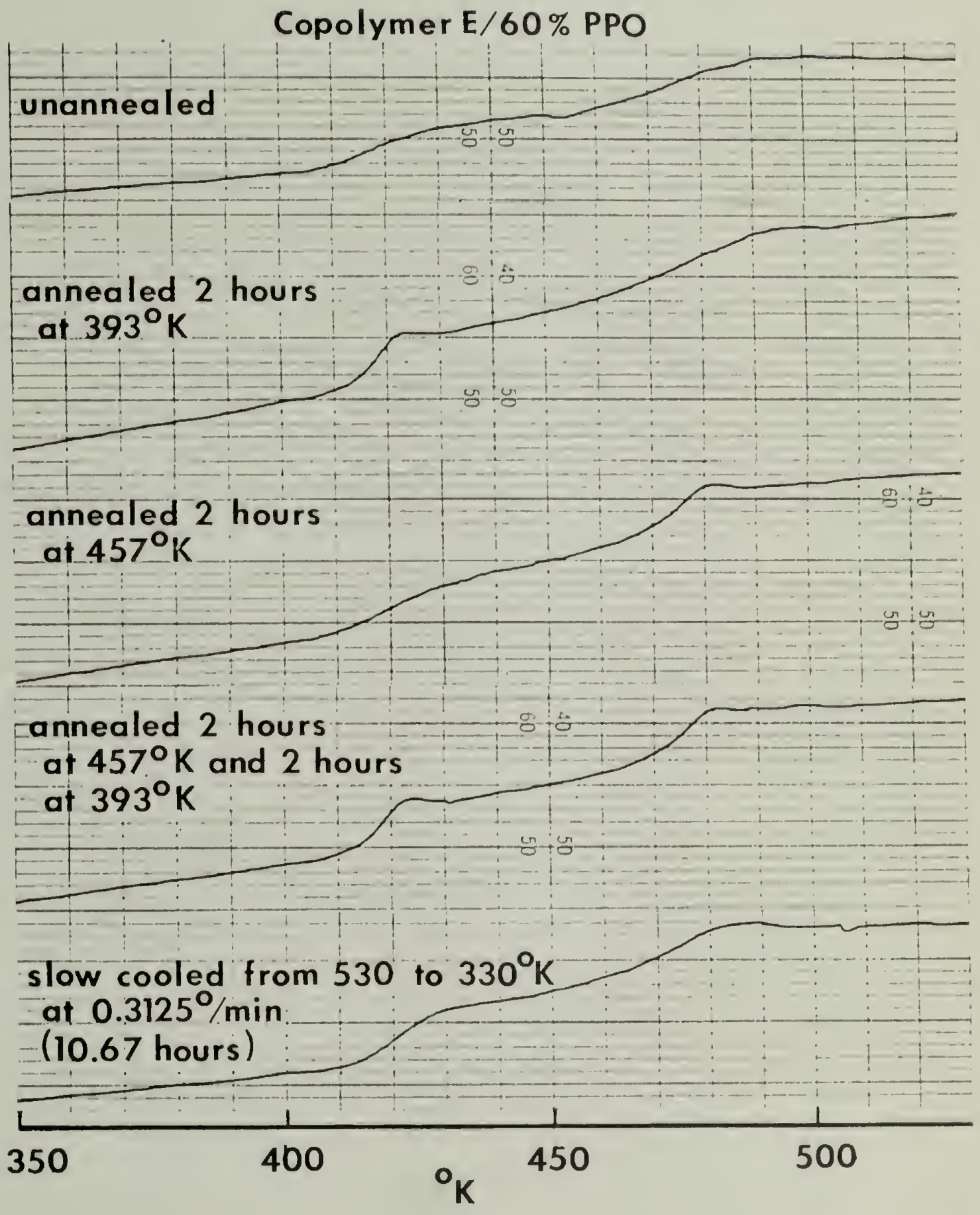
Copolymer E/60% PPO
unannealed
annealed 2 hours
at 393°K
annealed 2 hours
at 457°K
annealed 2 hours
at 457°K and 2 hours
at 393°K
slow cooled from 530 to 330°K
at 0.3125°/min
(10.67 hours)
350
400
450
500
°K

be annealed by first annealing below the upper T_g followed by cooling and annealing below the lower T_g for two intervals of 2 hrs. As shown at the bottom of Figure 30, annealing for 2 hrs. in this manner is more effective in reducing the widths of the two transitions than is slow cooling from the melt at the slowest available rate in the DSC II, 0.3125° min^{-1}.

Molecular Weight Effects in the PpClS/PPO and PoClS/PPO Blends. Figure 31 shows DSC thermograms for unblended PpClS and three 50/50 blends of PpClS and PPO of different molecular weights. The 5,760 molecular weight PPO ($\bar{M}_n$ = 5,760, $\bar{M}_w$ = 11,500, $\bar{M}_w/\bar{M}_n$ = 2.00) and the 64,200 molecular weight PPO ($\bar{M}_n$ = 64,200, $\bar{M}_w$ = 239,000, $\bar{M}_w/\bar{M}_n$ = 3.72) were supplied through the courtesy of T. F. Rutledge of ICI United States, Inc. The 16,900 molecular weight PPO was the same used for all the other blends and was characterized in Table VIII, Chapter III. As indicated by the thermograms in Figure 31, all blends exhibit two glass transitions and there is no indication of compatibility even for low molecular weight PPO. The apparent depression of the PPO T_g for the 5,760 $\bar{M}_n$ blend is due to the lower T_g of pure PPO at that molecular weight (193°C) and is not due to partial miscibility, although the broader transition width perhaps indicates some tendency toward compatibility at lower molecular weights. Similarly, the T_g of the pure high molecular weight PPO (64,200) is slightly higher (221°C) than that

Figure 31. DSC thermograms of 50/50 blends of PpCls and three different molecular weight PPO samples.

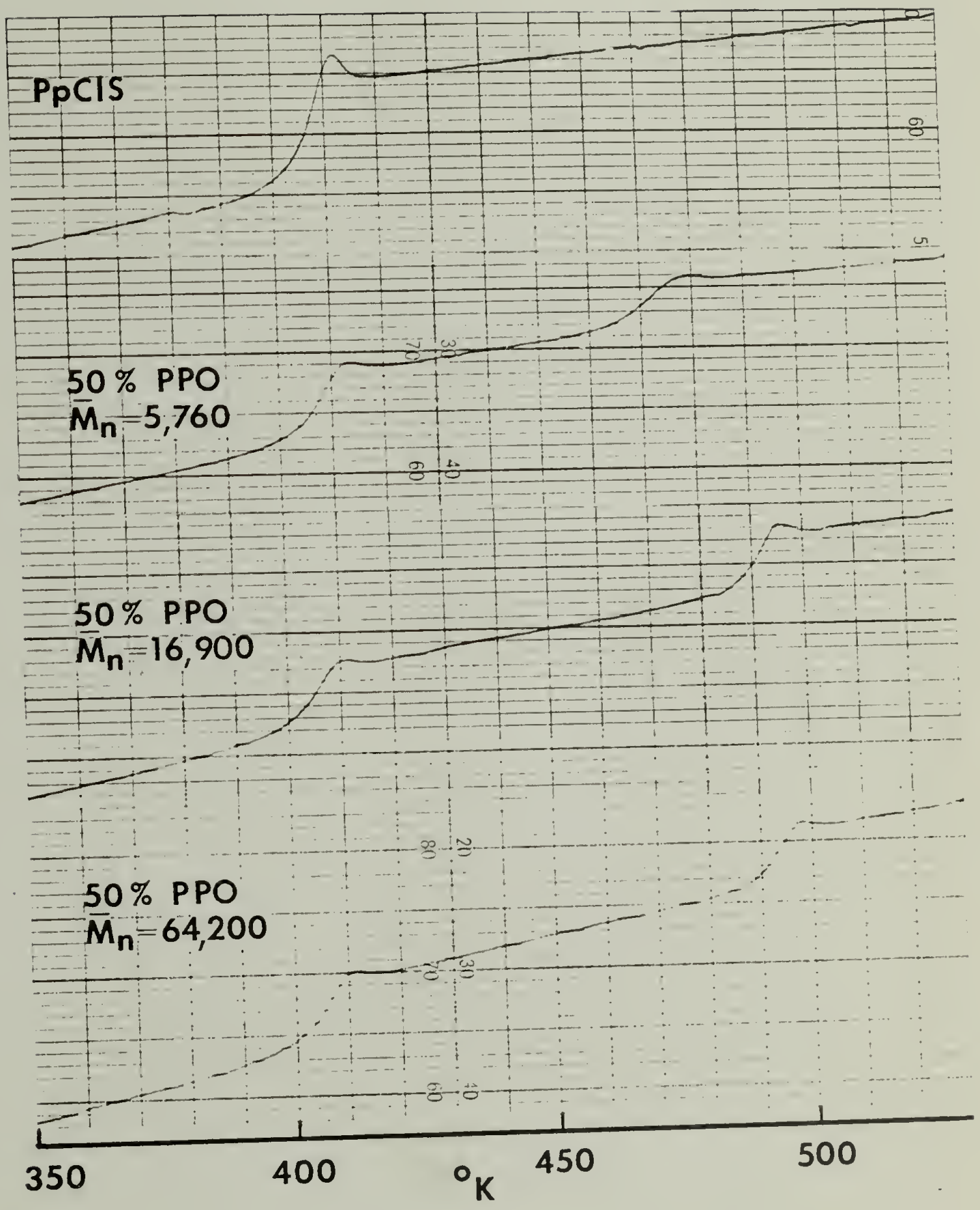
PpCIS
60
5
50 % PPO
$\bar{M}_n$=5,760
70
30
60
40
50 % PPO
$\bar{M}_n$=16,900
80
20
50 % PPO
$\bar{M}_n$=64,200
70
30
60
40
350
400
°K
450
500

observed for pure or blended 16,900 $\bar{M}_n$ PPO (215°C). The Fox-Flory[53] parameters for PPO have been determined for seven PPO samples ranging in molecular weight from 2,280 $\bar{M}_n$ to 64,200 $\bar{M}_n$.[54] These give the dependence of PPO T_g upon molecular weight which can be expressed by the familiar Fox-Flory equation given for PPO from the results of this study as

$$T_g = 221 - \frac{1.48 \times 10^5}{M_n} \quad . \qquad (29)$$

There has been some suggestion[55] that PoClS and PPO form a compatible pair. As previously shown in this chapter (Figure 15), PPO and the high molecular weight PoClS ($\bar{M}_n$ = 235,000, $\bar{M}_v$ = 571,000, $\bar{M}_w$ = 658,000, $\bar{M}_w/\bar{M}_n$ = 2.81) sample used in these blends were clearly incompatible. The possibility the polymerization technique, monomer batch, or molecular weight may have an effect on the compatibility of PoClS/PPO blends was investigated by making 50/50 blends of two other PoClS samples with the PPO used through the previous blend studies ($\bar{M}_n$ = 16,900). One of these (PoClS-3) had a higher molecular weight ($\bar{M}_v$ = 1,213,000); it was polymerized to high conversion in bulk with 0.1 weight % benzoyl peroxide initiator from a different monomer batch. The other (PoClS-2) had a lower molecular weight ($\bar{M}_v$ = 224,000); it was polymerized in dulute toluene solution as described in Chapter III. Both PoClS blends were clearly incompatible; T_g's corresponding exactly to those of unblended PoClS (135°C) and PPO (217°C) were evident. This

means that both PpClS and PoClS are incompatible with PPO; however, a 50/50 blend of a copolymer of pClS and oClS containing about 27% pClS (Dow Chemicals) with PPO was found to exhibit a single although broad glass transition at about 159°C. Independently, Chatterjee[56] has found that copolymers of pClS and oClS with compositions between 35 and 65% pClS are compatible with PPO while those with greater than 65% pClS content are incompatible. Since PpClS and PoClS are both incompatible with PPO, then there must be a second compatibility-incompatibility transition for oClS-pClS copolymers with compositions between 0 and 35% pClS. Copolymers which are compatible with some homopolymer at intermediate copolymer compositions but are incompatible at extreme compositions are not altogether rare. Such behavior has been observed for PVC/poly(butadiene-co-acrylonitrile)[57] and PVC/poly(ehtylene-co-vinyl acetate)[58] for examples. For these reasons, further investigations of the system poly (pClS-co-oClS) are certainly warranted.

Blend Density Studies

The densities of all blends and blend polymers were measured in gradient columns of aqueous sodium nitrate as detailed in Chapter III. The densities of these materials are given in the Appendix for different samples of the same blend and as measured in columns of different gradients.

Determination of the standard deviation of the mean is also detailed in the Appendix.

The densities of the blends can be calculated from the sum of the weight fraction specific volumes (reciprocal density) of the pure components,[58,59] i.e.

$$\frac{1}{\rho} = \frac{W_1}{\rho_1} + \frac{W_2}{\rho_2} \qquad (30)$$

where W and ρ are weight fractions and densities, respectively. For these calculations, densities with the smallest standard deviations were selected. For the blend polymers, these were given in Table X. Figures 32 through 38 show the comparison of the calculated (solid curve) and measured blend densities. As for the blend polymers, blend densities with the smallest error bars were used in these plots; for equal standard deviations, the mean of the largest sample population was selected.

For the PS/PPO blends (Figure 32), measured blend densities are $\sim$0.01 gm cc^{-1} larger than the corresponding additivity values calculated from eq. (30) and indicated as a solid line below the density data points. Similarly, for all the copolymer/PPO blends, a slightly smaller but distinquishable density increase over additivity was observed. This increase in density appears smallest for the incompatible Copolymer F/PPO belnds, while the blend densities of the most incompatible blends of PpClS/PPO and PoClS/PPO in Figures 37

Figure 32. Plot of blend density versus weight fraction PPO (W_{PPO}) for PS/PPO and Copolymer B/PPO blends. Solid lines were drawn from densities calculated from additivity, eq. (30).

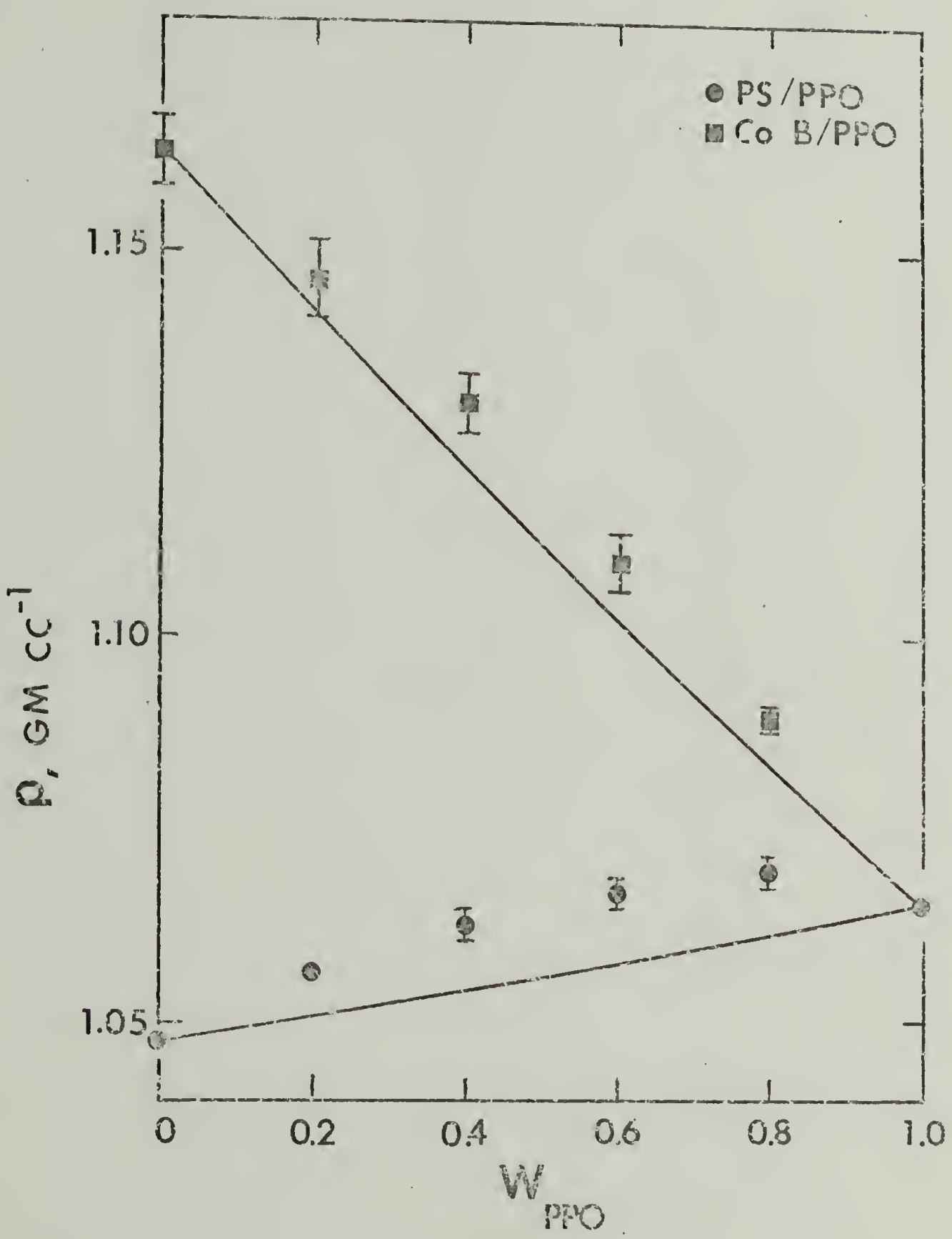
PS/PPO
Co B/PPO
1.15
1.10
1.05
Q, GM CC^{-1}
0
0.2
0.4
0.6
0.8
1.0
W_{PPO}

Figure 33. Plot of blend density versus weight fraction PPO (W_{PPO}) for Copolymer C/PPO blends. Solid line was drawn from densities calculated from additivity, eq. (30).

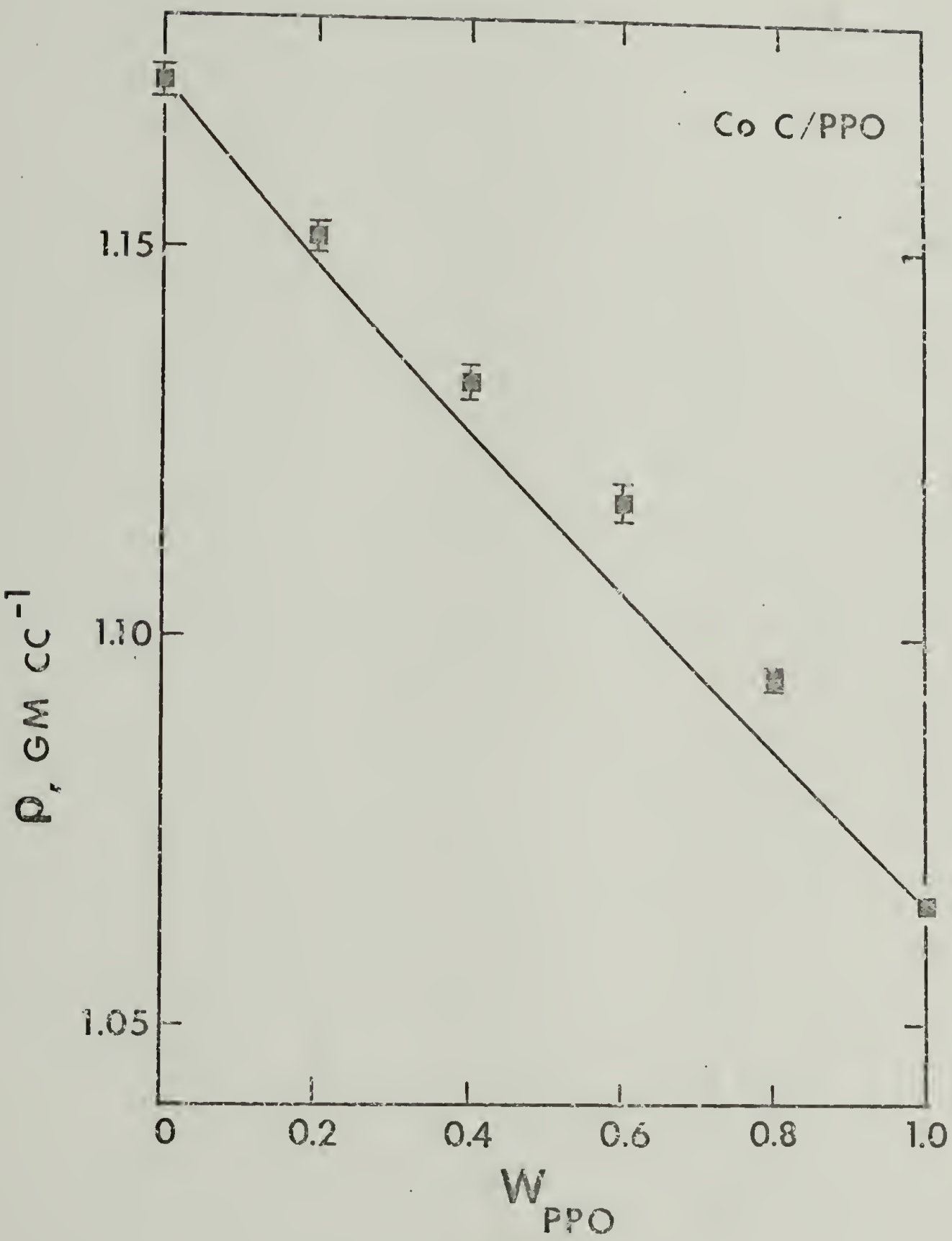
Co C/PPO
1.15
1.10
1.05
ρ, GM CC⁻¹
0
0.2
0.4
0.6
0.8
1.0
W PPO

Figure 34. Plot of blend density versus weight fraction PPO (W_{PPO}) for Copolymer D/PPO blends. Solid line was calculated from additivity, eq. (30).

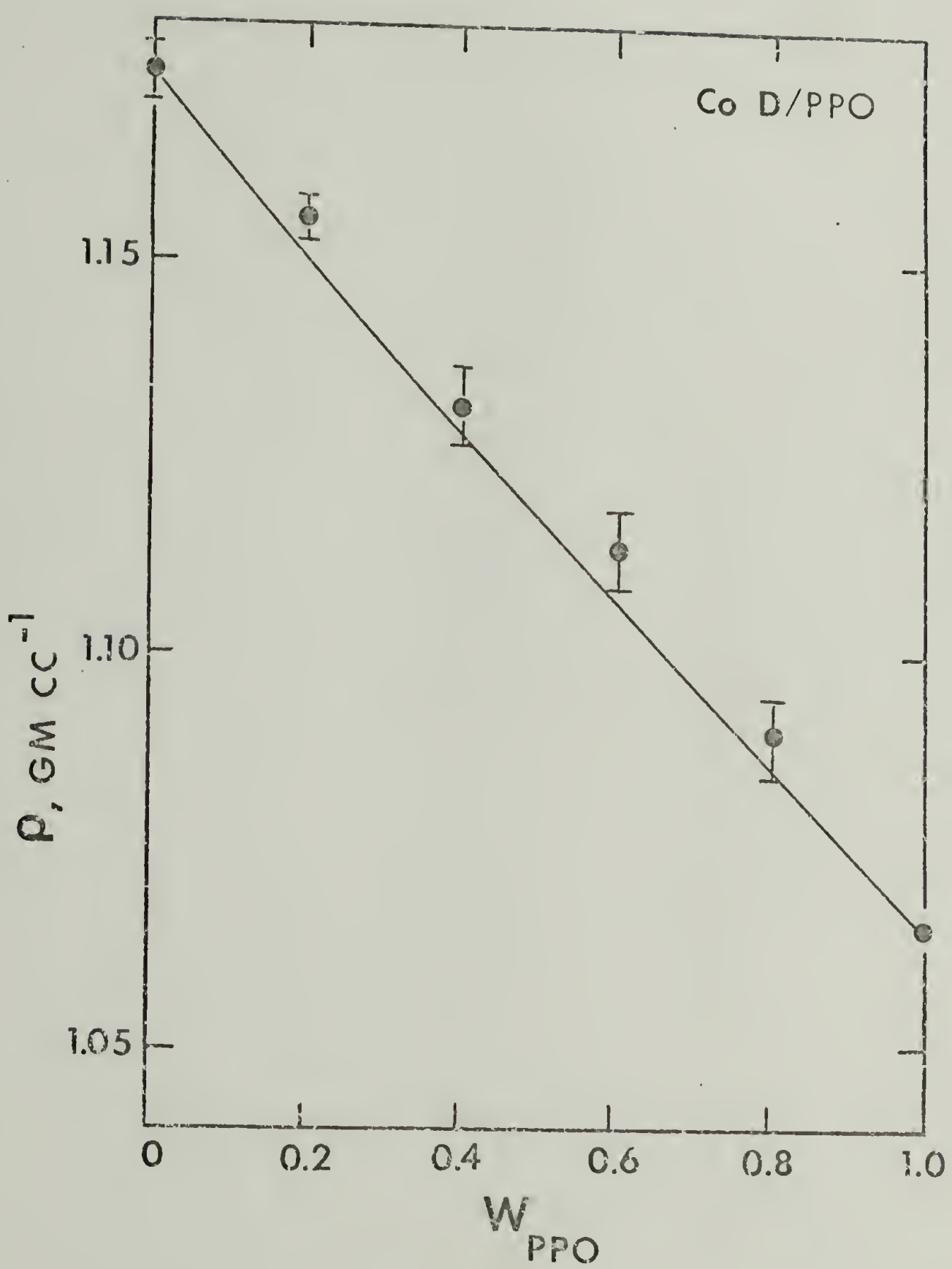
Co D/PPO
1.15
1.10
1.05
ρ, GM CC⁻¹
0
0.2
0.4
0.6
0.8
1.0
W PPO

Figure 35. Plot of blend density versus weight fraction PPO (W_{PPO}) for Copolymer E/PPO blends. Solid line was calculated from additivity, eq. (30).

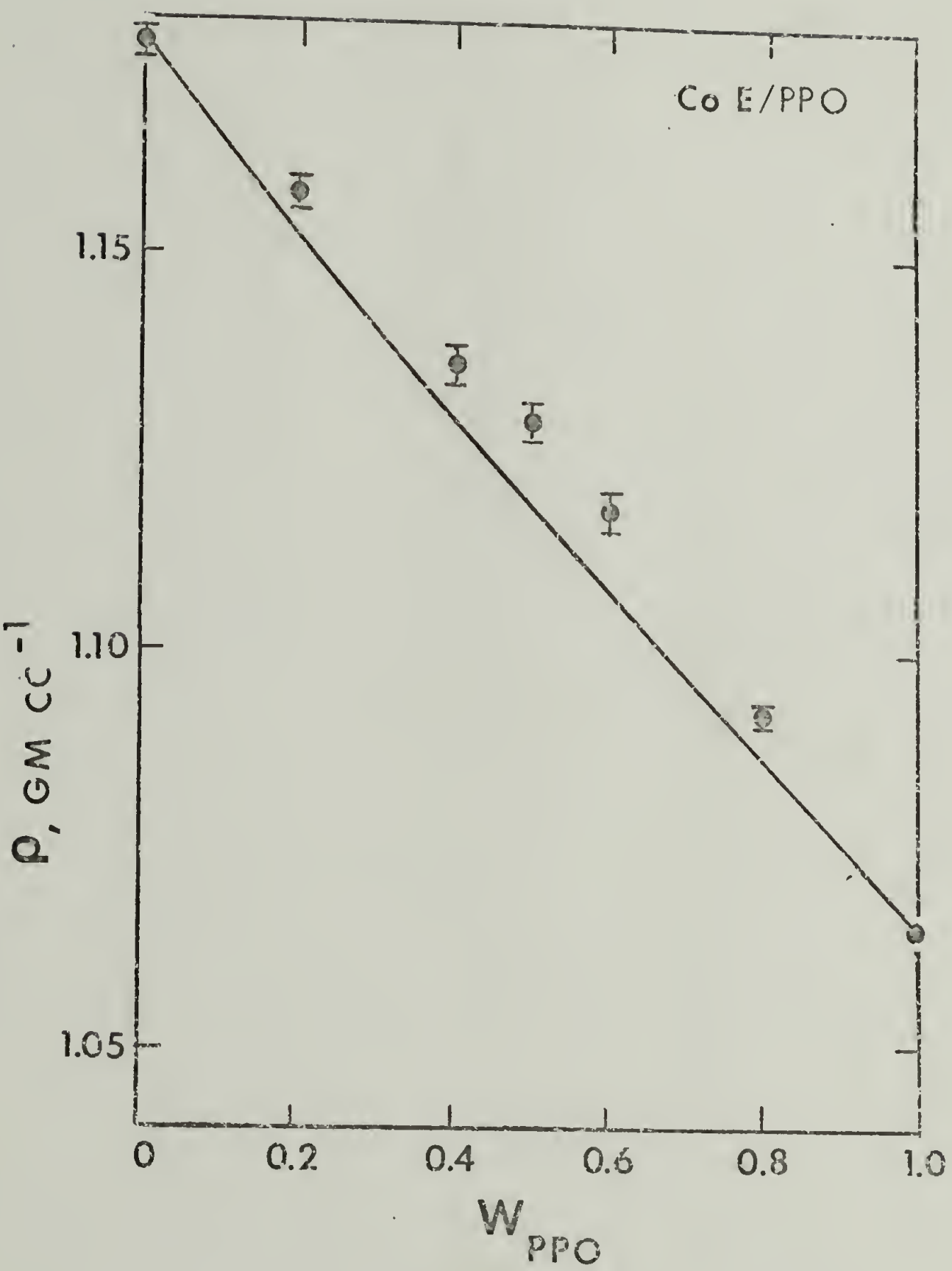
Co E/PPO
1.15
1.10
1.05
ρ, GM CC⁻¹
0
0.2
0.4
0.6
0.8
1.0
W PPO

Figure 36. Plot of blend density versus weight fraction PPO (W_{PPO}) for Copolymer F/PPO blends. Solid line was drawn from densities calculated from additivity, eq. (30).

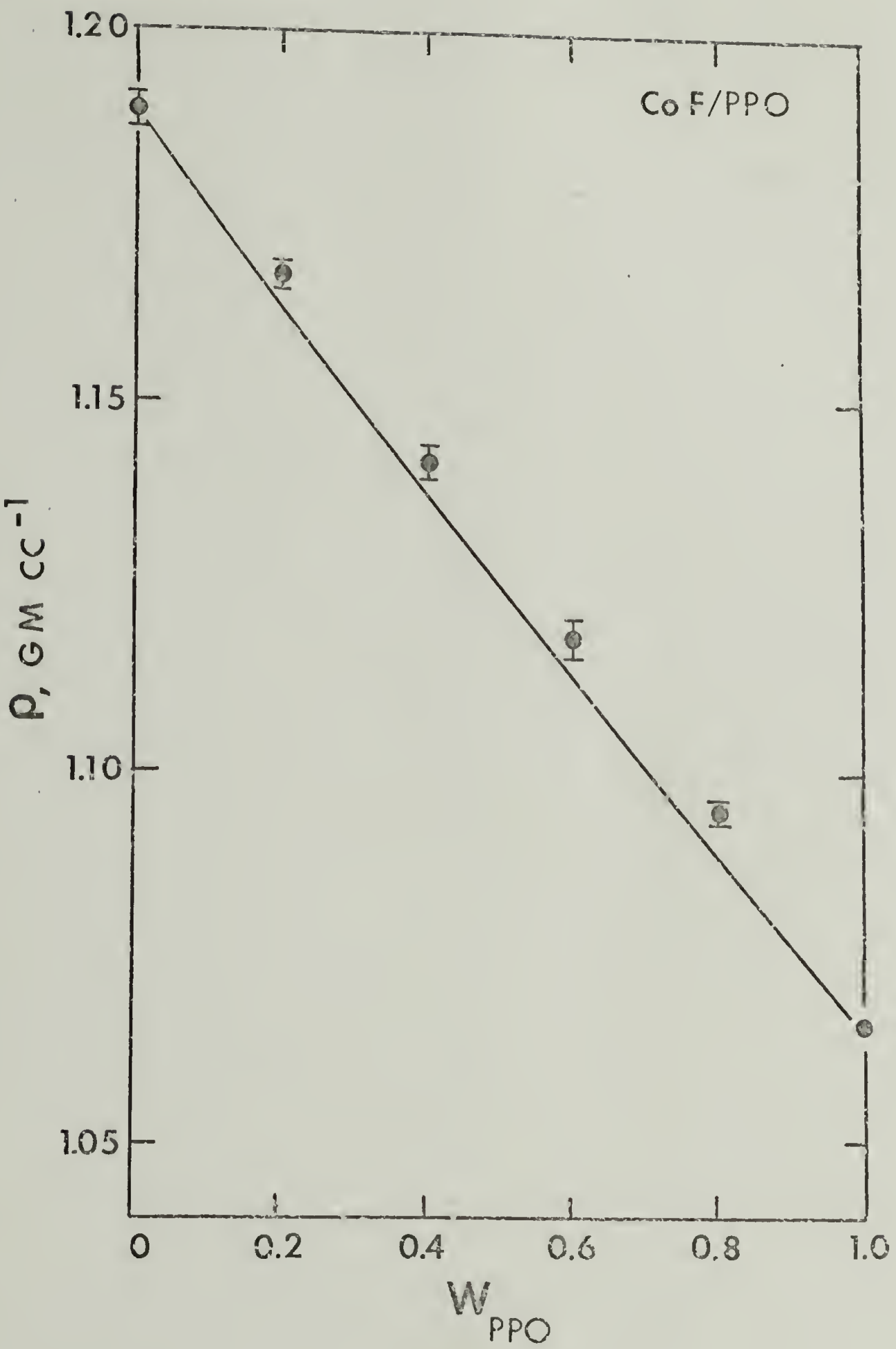
1.20
1.15
1.10
1.05
ρ, GM CC⁻¹
Co F/PPO
0
0.2
0.4
0.6
0.8
1.0
W PPO

Figure 37. Plot of blend density versus weight fraction PPO (W_{PPO}) for PpClS/PPO blends. Solid line was drawn from densities calculated from additivity, eq. (30).

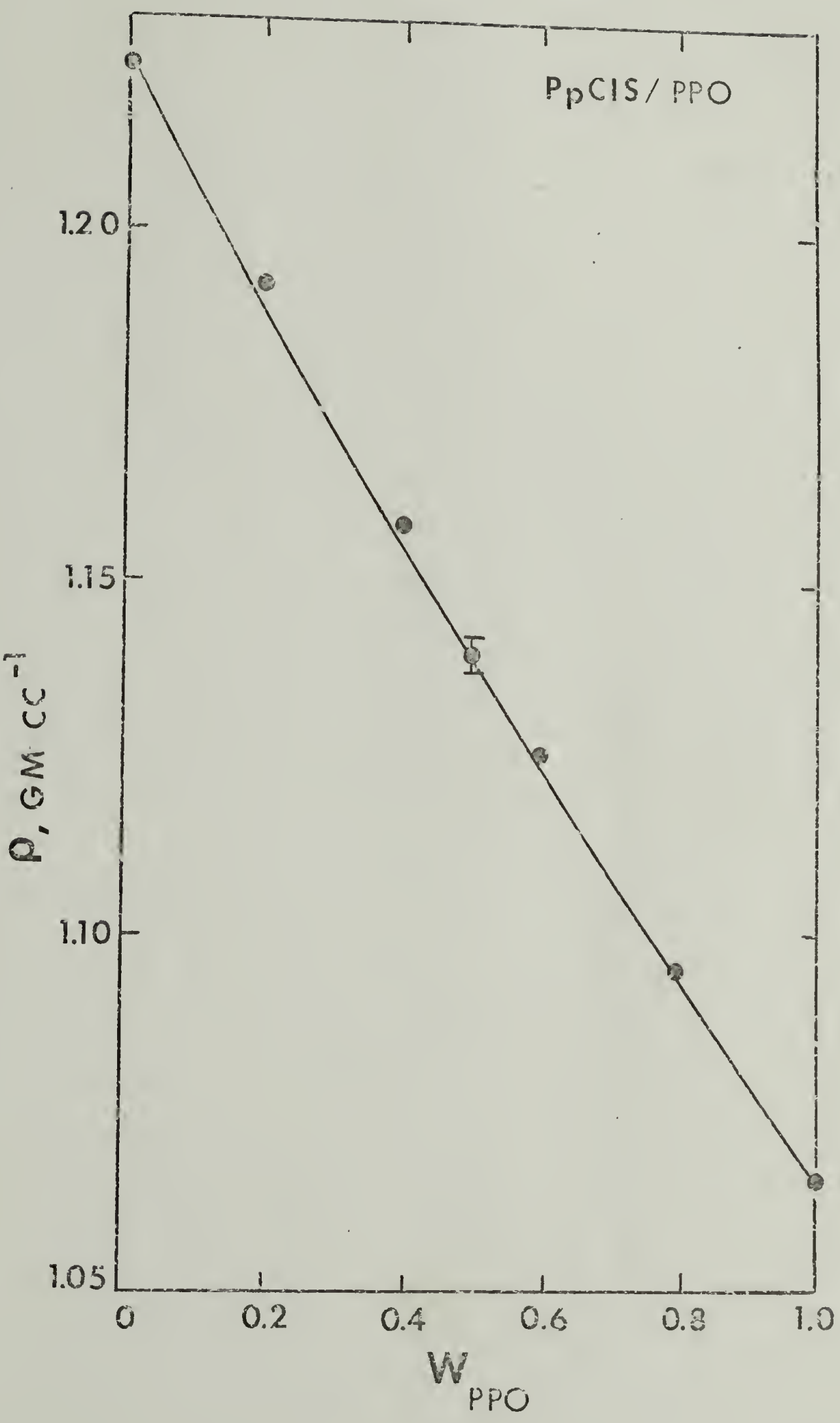
PpCIS/PPO
1.20
1.15
1.10
1.05
ρ, GM CC⁻¹
0
0.2
0.4
0.6
0.8
1.0
W PPO

Figure 38. Plot of blend density versus weight fraction PPO (W_{PPO}) for PoClS-1/PPO blends. Solid line was drawn from densities calculated from additivity, eq. (30).

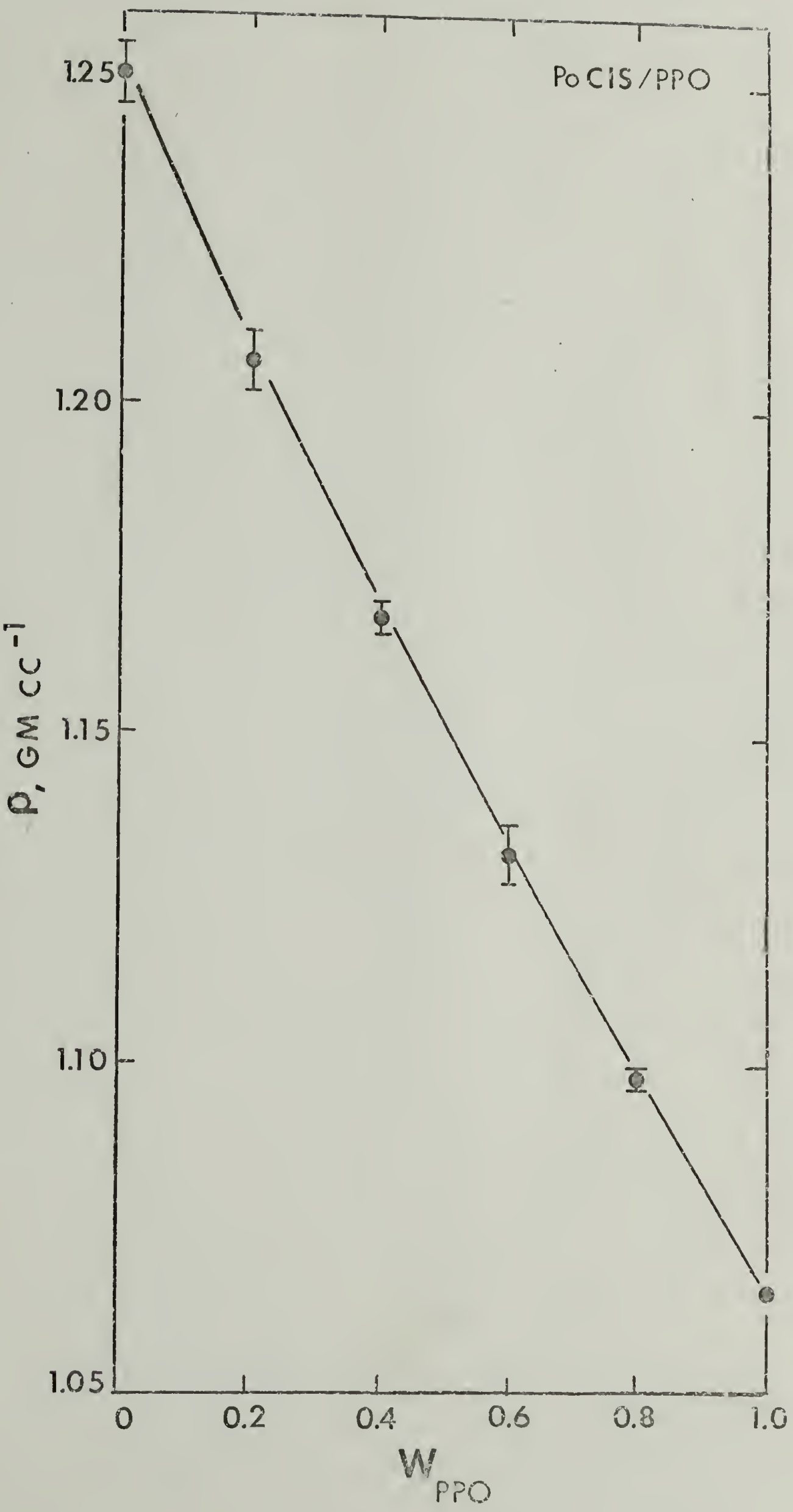
PoCIS/PPO
1.25
1.20
1.15
1.10
1.05
ρ, GM CC⁻¹
0
0.2
0.4
0.6
0.8
1.0
W PPO

and 38, respectively, agree with the additivity predictions within experimental error.

Increases in densities upon blending has also been observed in several other blend systems. For example, approximately the same magnitude of density increase, about 0.01 gm cc^{-1}, as found for PS/PPO has been reported for a compatible blend of PVC and a terpolymer of ethylene, vinyl acetate, and sulfur dioxide.[59] Somewhat larger density increases have been reported for three other compatible blends: PVC/poly (butadiene-co-acrylonitrile);[57,60,61] PVC/poly(ehtylene-co-vinyl acetate);[60] and PS/poly(vinyl methyl ether).[51] The largest density increase for any blend so far studied is that of 0.05 gm cc^{-1} or about 5% for PVC in a 50/50 blend with a copolymer of butadiene and acrylonitrile containing 41 wt % acrylonitrile reported by Rånby.[60,61] The densities and the magnitude of the density increase measured in this study for PS/PPO agree well with the results of Jacques and Hopfenberg[62] and Hopfenberg, Stannett, and Folk[63] as discussed in Chapter I.

The magnitude of the density increase, or alternately the decrease in mixing volume, in compatible polymer blends may be taken as a relative measure of compatibility. Alekseyenko[64] has defined a packing coefficient, K, for this purpose. This parameter, expressed as the ratio of actual to additive mixing volumes, is ≤ 1 for incompatible blends and >1 for compatible blends.

Hickman and Ikeda[59] and Zakrzewski[57] have suggested that the observed density increase or negative excess volume of mixing for compatible blends is a result of strong molecular interaction favoring better packing between molecules. This is reasonable because the largest density increases are observed for the more polar polymer pairs, e.g. PVC/poly (butadiene-co-acrylonitrile), for which intermolecular interactions are the strongest. By contrast, the nearly nonpolar pair of PS and PPO exhibited a much smaller density increase as a result of smaller intermolecular interactions. Evidence for such weak interactions, possible dipolar in nature, exists in the NMR results of Otocka[65] to which reference is made in Chapter I. As also discussed in Chapter I, these weak interactions account for a near zero value for the interaction parameter as determined by Shultz and McCullough[66] or calculated from solubility theory for PS/PPO. This means that the enthalpy of mixing for PS and PPO should be also nearly zero or slightly negative. As a result the free energy for mixing attains a favorable negative value (the thermodynamic requirement for compatibility).

The observed density increases for the Copolymer D/PPO and Copolymer E/PPO blends (Figures 34 and 35) are not surprising because as noted in the previous sections, these blends appear partially compatible. The more incompatible blend of Copolymer F/PPO would be expected to have a zero density increase but as Figure 36 shows there is a small but

finite increase in density from the calculated additivity values. As previously noted, the Copolymer F/PPO blends exhibit a small depression (perhaps 2-3%) in the T_g of the predominantly PPO phase and a small elevation in the T_g of the Copolymer F phase (Figure 22). In addition, there are indications from the quantitative measurements of the glass transition heights of these blends (Figure 26) that substantial quantities of Copolymer F and PPO molecules may be involved in interphase mixing. These results suggest that Copolymer F and PPO may be to a very small extent compatible. The reason for this can probably be attributed to the method of polymerization of Copolymer F. As indicated in Chapter III, Copolymer F was the only copolymer that was thermally polymerized (110^{o}C). As a result of the higher temperatures and the continuous nitrogen purge used during the polymerization, the monomer mixtures probably became richer in the higher boiling monomer of pClS. This means that the overall copolymer composition of 75.4 mole % pClS which is substantially higher than could be calculated for a feed composition of 60 mole % pClS probably was an average of a broader distribution of compositions than for the other copolymers that were polymerized by free radical initiation at lower temperature (60^{o}C) and in essentially closed tubes from which monomer escape in the effluent nitrogen purge was minimized. As a result of its probably compositional heterogeneity, Copolymer F may have some molecules whose compositions are in the

compatible range below 67.8 mole % pClS and therefore some miscibility with PPO was evident.

Solubility Parameter Theory and Compatibility-Incompatibility Transitions

As substantiated in the previous sections, blends of PPO and random copolymers of styrene and para-Chlorostyrene exhibited a compatibility-incompatibility transition at copolymer compositions between 67.1 and 67.8 mole % pClS. Below 67.1 mole % pClS, the copolymers were judged compatible with PPO by the presence of single, although broad glass transition and film clarity. Copolymers with compositions of 67.8 and 68.6 mole % pClS appeared only partially compatible with PPO as demonstrated by the appearance of two mixed-composition phases, one being copolymer-rich and the other PPO-rich. Compatibility in these transitional blends increased with increasing amounts of low molecular weight PPO. For example, at 80% PPO content, there was more PPO present in the copolymer-rich phase than for blends with lower PPO content. In addition, the high PPO content blends appeared clear while the low PPO content blends were somewhat hazy. These observations were explained by the increase in mixing entropy with decreasing overall molecular weight of the blend. Blends of PPO and copolymers with 75.4 mole % pClS compositions and higher chlorine contents were totally incompatible. The glass transitions of each of the two

phases corresponded exactly in temperature to those of the unblended components, there was a zero excess volume of mixing, and films molded from their blends were opaque.

As shown in Chapter I, solubility parameter theory appeared to adequately predict PS/PPO compatibility for solubility parameters calculated from the empirical parameters of Small.[67] It may be therefore expected that solubility parameter theory can predict the compatibility-incompatibility transition of the poly(S-co-pClS)/PPO system. The Small solubility parameters (δ) for PS and PPO used in Chapter I were 9.01 and 8.9, respectively. For PpClS and PoClS, these have been calculated as 9.25 and 9.46, respectively. Krause[49] has shown that for blends of polymers with molecular weights between 10,000 and 100,000, the critical difference between solubility parameters is between 0.35 and 0.11, above which phase separation or incompatibility is expected. For the above solubility parameters, $\Delta\delta$ is 0.11 for PS/PPO, 0.35 for PpClS/PPO, and 0.55 for PoClS/PPO. As evident, application of the Krause criteria would suggest that only PS and PPO can be compatible as experimental evidence confirms.

The solubility of the copolymers (δ_c) in this study can be calculated by the expression given by Krause[49]

$$\delta_c = V_s\delta_s + V_p\delta_p \qquad (31)$$

where V_s and V_p are the volume fractions of S and pClS in the copolymer, and δ_s and δ_p are the solubility parameters of PS (9.01) and PpClS (9.25), respectively. Volume fraction compositions are calculated from the mole fraction (N) compositions given in Table X by

$$V_s = \frac{N_s M_s/\delta_s}{N_s M_s/\delta_s + N_p M_p/\delta_p} \qquad (32)$$

where M_s and M_p are the molecular weights of S (104.2) and PpClS (138.6), and δ_s and δ_p ($V_s = 1-V_s$) are the densities of PS (1.0476 gm cc^{-1}) and PpClS (1.2230 gm cc^{-1}), respectively. The solubility parameters calculated from eq. (31) are given in Table XV.

TABLE XV. Solubility Parameters of Copolymers

Copolymer	N_s	V_s	w_s	δ_c (cal cc^{-1})$^{1/2}$
B	0.415	0.384	0.348	9.16
C	0.329	0.301	0.269	9.18
D	0.322	0.294	0.263	9.18
E	0.314	0.287	0.256	9.18
F	0.246	0.223	0.197	9.20

Krause proposed that two polymers will be incompatible if their interaction parameter (χ) is greater than a critical interaction parameter determined from the molecular weights of the two polymers by the equation given as

$$(\chi_{12})_{cr} = \frac{1}{2}\left[\frac{1}{x_1^{1/2}} + \frac{1}{x_2^{1/2}}\right] \qquad (33)$$

where x is the degree of polymerization of the polymer in terms of a reference volume, V_r. In eq. (33), the subscripts 1 and 2 refer to the copolymer and PPO, respectively. For the calculation of x, Krause suggested the approximation

$$x = \frac{M}{100} \qquad (34)$$

where M may be taken as the number-average molecular weight ($\bar{M}_n$). Finally, the interaction parameter of the copolymer/PPO pair can be approximated from the values of solubility parameters by the equation

$$\chi_{12} = \frac{(\delta_1 - \delta_2)^2}{6} \quad . \qquad (35)$$

For the molecular weights of Copolymer C and PPO, $(\chi_{12})_{cr}$ is calculated from eq. (33) as 0.0065. The limiting copolymer composition for phase separation, i.e. at the compatibility-incompatibility transition, can then be calculated from determination of δ_1 by setting the right side of eq. (35) equal to 0.0065. This value of δ_1 was calculated as 9.10, for which V_s was determined to be 0.633 from eq. (31) [noting the change in nomenclature for which δ_1 in eq. (35) is equivalent to δ_c in eq. (31)]. From eq. (32), the copolymer composition for the compatibility-incompatibility transition is calculated as 33.7 mole % pClS compared to 67.1 mole %

pClS as observed experimentally. Considering the severe limitations of solubility parameter theory outlined in Chapter I, this prediction is surprisingly good; however, any prediction of compatibility from solubility parameter theory is only as good as the values of the solubility parameters used for the two components. On the other hand, as a result of the high solubility parameters of both PpClS and PoClS, solubility parameter theory would predict that all copolymers of pClS and oClS should be incompatible with PPO. As noted earlier, there is some evidence that such copolymers with low pClS content, between 0 and 35 mole % pClS, may be compatible with PPO. This peculiar behavior of the poly(pClS-co-oClS)/PPO system should be investigated further.

REFERENCES

1. H. E. Bair, Polym. Eng. Sci., 10, 247 (1970).
2. W, M. Prest, Jr., and R. S. Porter, J. Polym. Sci., A-2, 10, 1639 (1972).
3. F. E. Karasz, H. E. Bair, and J. M. O'Reilly, J. Phys. Chem., 69, 2657 (1965).
4. S. de Petris, V. Frosini, E. Butta, and M. Baccaredda, Makromol. Chem., 109, 54 (1967).
5. A. S. Hay, Polym. Eng. Sci., 16, 1 (1976).
6. C. H. M. Jacques and H. B. Hopfenberg, Polym. Eng. Sci., 14, 441 (1974).
7. T. Lim, V. Frosini, V. Zaleckas, D. Morrow, and J. A. Sauer, Polym. Eng. Sci., 13, 51 (1973).
8. A. R. Shultz and B. M. Beach, Macromolecules, 7, 902 (1974).
9. F. M. Lewis, C. Walling, W. Cummings, E. R. Briggs, and R. F. Mayo, J. Amer. Chem. Soc., 70, 1519 (1948).
10. F. N. Kelley and F. Bueche, J. Polym. Sci., 50, 549 (1961).
11. F. Bueche, "Physical Properties of Polymers," John Wiley and Sons, New York, 1962, pp. 120-123.
12. J. J. Aklonis, W. J. MacKnight, and M. Shen, "Introduction to Polymer Viscoelasticity," Wiley-Interscience, New York, 1972, p. 66.
13. T. G. Fox and P. J. Flory, J. Appl. Phys., 21, 581 (1950).

REFERENCES (cont.)

14. M. Gordon and I. A. Macnab, Trans. Faraday Soc., 49, 31 (1953).

15. K. Ueberreiter and G. K. Kanig, J. Colloid Sci., 7, 569 (1952).

16. F. E. Karasz, private communication; data of N. Parker, General Electric Corporate Research and Development Center, Schenectady, New York.

17. S. C. Sharma, L. Mandelkern, and F. C. Stehling, J. Polym. Sci., B, 10, 345 (1972).

18. A. R. Shultz and C. R. McCullough, J. Polym.Sci., A-2, 10, 307 (1972).

19. D. J. Plazek, J. Phys. Chem., 69, 3480 (1965).

20. A. Eisenberg and B. Cayrol, J. Polym. Sci., C, 35, 129 (1971).

21. L. A. Wood, J. Polym. Sci., 28, 319 (1958).

22. M. Gordon and J. S. Taylor, J. Appl. Chem., 2, 493 (1952).

23. T. G. Fox, Bull. Amer. Phys. Soc., 1, 123 (1956).

24. E. A. Dimarzio and J. H. Gibbs, J. Polym. Sci., 40, 121 (1959).

25. S. Krause and N. Roman, J. Polym. Sci., A, 3, 1631 (1965).

26. G. Kanig, Kolloid Z., 190, 1 (1963).

REFERENCES (cont.)

27. H. Daimon, H. Okitsu, and J. Kumanotani, Polymer J., 7, 460 (1975).

28. A. R. Shultz and B. M. Gendron, J. Appl. Polym. Sci., 16, 461 (1972).

29. I. Uematsu and K. Honda, Rept. Progr. Polym. Phys. Japan, 8, 111 (1960).

30. N. W. Johnston, Macromolecules, 6, 453 (1973).

31. R. Koningsveld, Chem. Zvesti., 26, 263 (1972).

32. R. Koningsveld, L. A. Kelintjens, and H. M. Schoffeleers, Pure Appl. Chem., 1 (1974).

33. A. R. Shultz and B. M. Gendron, Polym. Prepr., 14, 571 (1973).

34. L. M. Robeson, M. Matzner, L. J. Fetters, and J. E. McGrath, in "Recent Advances in Polymer Blends, Grafts, and Blocks," edited by L. H. Sperling, Plenum Press, New York, 1973, p. 281.

35. E. M. Barrall, II, and J. F. Johnson, in "Thermal Characterization Techniques," edited by P. E. Slade, Jr., and L. T. Jenkins, Marcel Dekker, New York, 1970, p. 16.

36. J. H. Flynn, Thermo. Acta, 8, 69 (1974).

37. J. Letz, J. Polym. Sci., A-2, 7, 1987 (1969).

38. L. E. Nielsen, J. Amer. Chem. Soc., 75, 1435 (1953).

REFERENCES (cont.)

39. I. M. Ward, "Mechanical Properties of Solid Properties," Wiley-Interscience, New York, 1971, p. 176.

40. R. Buchdahl and L. E. Nielsen, J. Polym. Sci., 15, 1 (1955).

41. B. Wunderlich and D. M. Bodily, J. Polym. Sci., C, 6, 137 (1964).

42. H. Eyring, J. Chem. Phys., 4, 283 (1936).

43. J. Frenkel, "Kinetic Theory of Liquids," Clarendon, Oxford, 1946.

44. A. S. Marshall and S. E. B. Petrie, J. Appl. Phys., 46, 4223 (1975).

45. S. E. B. Petrie, in "Polymeric Materials: Relationships between Structure and Mechanical Behavior," edited by E. Baer and S. V. Radcliffe, American Society of Metals, Metals Park, Ohio, 1974.

46. V. R. Landi, Rubber Chem. Technol. 45, 222 (1972).

47. R. L. Scott, J. Polym. Sci., 9, 423 (1952).

48. R. Wetton, unpublished data.

49. S. Krause, J. Macromol. Sci.-Revs. Macromol. Chem., C7, 251 (1972).

50. R. H. Lacombe and I. C. Sanchez, J. Chem. Phys., submitted for publication.

51. T. K. Kwei, T. Nishi, and R. F. Roberts, Macromolecules, 7, 667 (1974).

REFERENCES (cont.)

52. R. J. Roe, S. K. Lo, and R. P. Chartoff, Polym. Prepr., 17(2), 167 (1976).

53. T. G. Fox and P. J. Flory, J. Appl. Phys., 21, 581 (1950).

54. J. R. Fried, unpublished results.

55. F. E. Karasz, W. J. MacKnight, and J. J. Tkacik, Polym. Prepr., 15(1), 415 (1974).

56. A. Chatterjee, unpublished results.

57. G. A. Zakrzewski, Polymer, 14, 347 (1973).

58. C. F. Hammer, Macromolecules, 4, 69 (1971).

59. J. J. Hickman and R. M. Ikeda, J. Polym.Sci.-Phys., 11, 1713 (1973).

60. B. G. Rånby, paper presented at the Herman Mark Symposium, New York, May, 1975.

61. Y. J. Shur and B. Rånby, J. Appl. Polym. Sci., 19, 2143 (1975).

62. C. H. M. Jacques and H. B. Hopfenberg, Polym. Eng. Sci., 14, 441 (1974).

63. H. B. Hopfenberg, V. T. Stannett, and G. M. Folk, Polym. Eng. Sci., 15, 261 (1975).

64. V. I. Alekseyenko, Vysokomol.Soedin, 2, 1449 (1960).

65. E. P. Otocka, Bell Telephone Laboratories memorandum for record (1968).

66. A. R. Shultz and C. R. McCullough, J. Polym. Sci., A-2, 10, 307 (1972).

REFERENCES (cont.)

67. P. A. Small, J. Appl. Chem., 3, 71 (1953).

C H A P T E R V

TENSILE PROPERTY STUDIES

Homopolymers and Copolymers Used in Blends

Young's modulus, stress at break (or yield), and strain at break (or yield) were determined for all blends and blend polymers by the techniques outlined in Chapter III and by the statistical treatment detailed in the Appendix. All modulus, stress, and strain values for the blends and blend polymers are tabulated in Table XVIII in the Appendix. For reference, the tensile properties of the blend polymers are summarized in Table XVI below.

TABLE XVI. Tensile Properties of Blend Polymers

Polymer	Young's Modulus $\times 10^{-10}$ dynes cm^{-2}	Stress at Break $\times 10^{-8}$ dynes cm^{-2}	Strain at Break, %
PS ($\bar{M}_n$=38,000)	2.69±.15	1.40±.14	0.50±.06
PS ($\bar{M}_n$=92,600)	3.09±.04	4.55±.05	1.76±.07
B	3.40±.04	4.19±.13	1.18±.03
C	3.37±.08	3.32±.15	0.83±.03
D	3.15±.07	4.49±.07	1.09±.04
E	3.04±.06	4.31±.22	1.11±.05
F	3.39±.03	7.14±.40	1.81±.12
PpClS	3.49±.09	4.58±.29	1.09±.06
PoClS-1	3.73±.08	7.09±.23	1.66±.08
PPO	2.66±.05*	7.07±.09*	2.73±.08

*values given are for stress and strain at yield.

The values of Young's modulus (E) given in Table XVI range from a low of 2.66×10^{-10} dynes cm^{-2} for PPO to a high of 3.73×10^{-10} dynes cm^{-2} for PoClS-1. Variation in stress at break (tensile strength) and strain or elongation at break among the polymers given in Table XVI is more pronounced. The smallest values of these properties were observed for the PS sample with the lower molecular weight ($\bar{M}_n$=38,000 and $\bar{M}_w$=81,800), while the largest values were for the highest molecular weight polymers, Copolymer F ($\bar{M}_n$= 216,000) and PoClS-1 ($\bar{M}_n$=235,000). The one exception here is PPC, which has high yield strength even at relatively low molecular weight ($\bar{M}_n$=16,900) due to its strong aromatic backbone. These observations may be explained by the well-known reciprocal dependence of stress at break (σ_B) to molecular wieght.[1] This relation may be given in the form of

$$\sigma_B = \sigma_B^o - \frac{K}{M} \qquad (36)$$

where σ_B^o is the limiting tensile strength at very high molecular weight, K is a constant, and M is molecular weight. For PS, σ_B has been reported to depend upon a molecular weight average somewhere between $\bar{M}_n$ and $\bar{M}_w$.[2] A similar relation to eq. (36) holds for ε_B.[1]

Mechanical property studies of PPO have been reviewed in Chapter I. The most distinguishing feature of the mechanical response of PPO under tensile deformation is that it yields and cold draws. This is in contrast to the behavior

of PS and the chlorostyrene derivatives given in Table XVI which exhibit a brittle mode of failure and craze extensively even at temperatures as low as -90°C.[3] Yield behavior has also been observed for bisphenol A polycarbonate and polyethylene terephthalate which like PPO have flexible oxygen linkages and phenyl groups in their main chain. The values of stress and strain at the maximum of the load-deformation curve, i.e. σ_Y and ε_Y, which are given for PPO in Table XVI, are equivalent to other values reported in the literature once allowance is made for differences in the tensile strain rate.[5,6,7] As mentioned in Chapter I, the yield strength of PPO has been shown to increase linearly with increasing strain rate.[5,6]

Compatible Polymer Blends

Typical stress-strain curves for PS, PPO and PS/PPO blends are given in Figure 39 for the low molecular weight PS sample ($\bar{M}_n$=38,000). Two features of these curves are particularly noteworthy. First, PS and two blends in which PS is the major component, i.e. PS-b40 and PS-b20, fail in the brittle mode, while PPO and the two blends with PPO as the major component, i.e. PS-b40 and PS-b20, yield and cold draw. Second, σ_B of the low molecular weight PS is increased by nearly 300% upon addition of only 20% PPO in the blend. With increasing PPO content of the blend, σ_B continues to increase but in a less dramatic fashion. At 80% PPO content,

Figure 39. Plot of tensile stress versus strain for low molecular weight PS ($\bar{M}_n$=38,000), for PPO, and for PS/PPO blends. Broken lines point to stress at break or to maximum stress at yield.

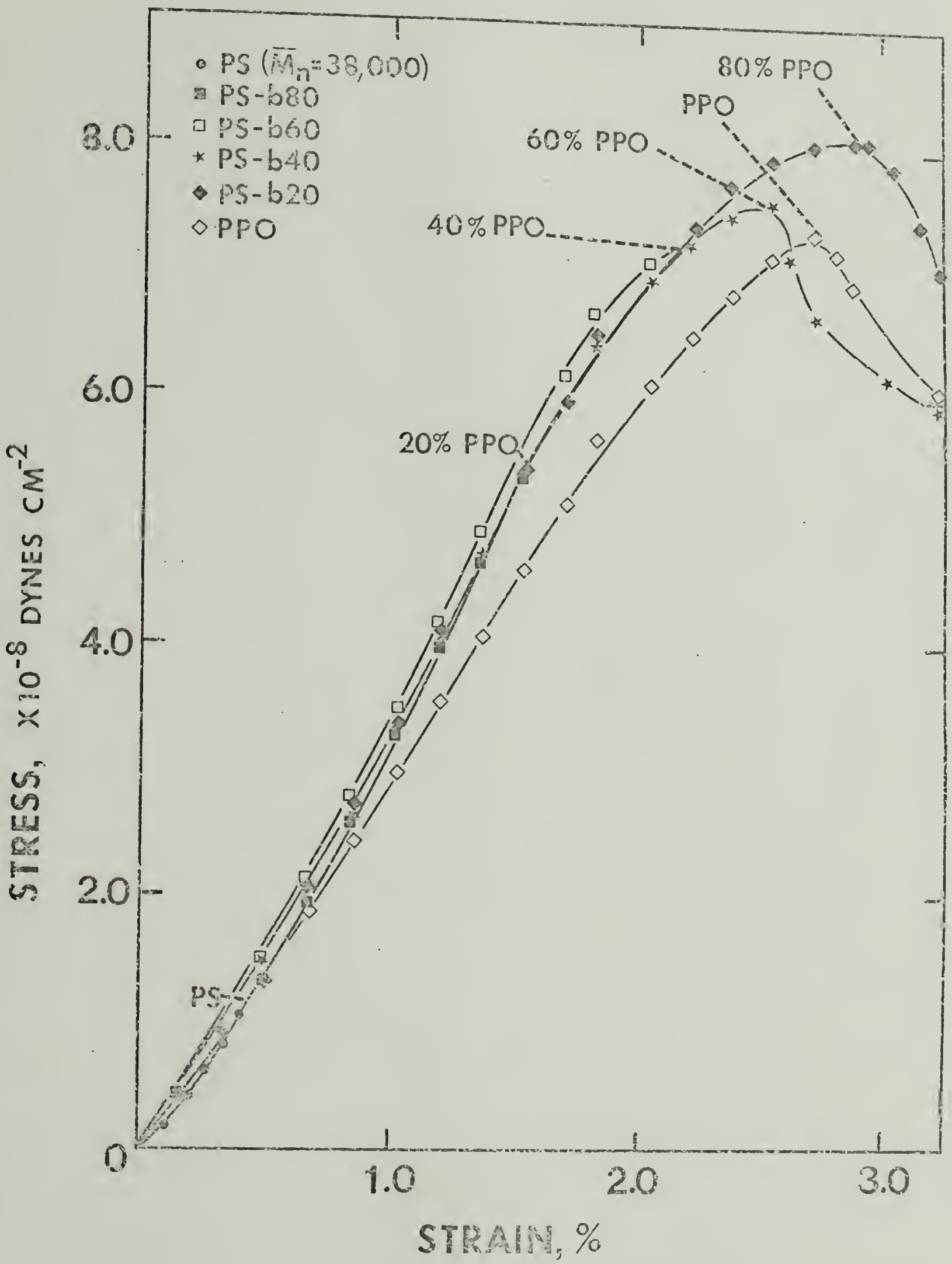
PS ($\bar{M}_n$=38,000)
PS-b80
PS-b60
PS-b40
PS-b20
PPO
80% PPO
PPO
60% PPO
40% PPO
20% PPO
PS
8.0
6.0
4.0
2.0
0
1.0
2.0
3.0
STRESS, X10^{-8} DYNES CM^{-2}
STRAIN, %

a maximum in σ_Y is reached at a level about 14% higher than that of unblended PPO. Similarly, at 60% PPO content, σ_Y of the PS/PPO blend is about 12% higher than that of PPO.

Young's modulus (E), stress at break (or yield), and elongation at break (or yield) are polotted versus volume fraction PPO (V_{PPO}) for the low molecular weight PS/PPO blends in Figure 40. As indicated from the stress-strain curves in Figure 39, tensile strength rapidly rises with increasing V_{PPO} and reaches a broad maximum at high V_{PPO}. The same trend is exhibited for the plot of ε versus V_{PPO}, while E is shown to be nearly independent of blend composition. For the particular molecular weight of the PS in these blends, E of the unblended PS component is nearly equal to that of PPO and blend modulus is not seen to exhibit any maximum or minimum within the error bounds of these measurements.

The same three tensile properties are plotted versus V_{PPO} for a higher molecular weight PS ($\bar{M}_n$=92,500) in Figure 41. Due to the higher molecular weight of the PS component, σ_B and ε_B of the blends are initially larger, but at high V_{PPO} they reach broad maxima which are only slightly higher in value than observed at identical blend compositions for the low molecular weight PS/PPO blends. These results suggest that at high V_{PPO}, the properties of the PS component contribute negligibly to those of the blends. Similar

Figure 40. Plots of Young's modulus (E), stress at break or yield (σ), and strain at break or yield (ε) versus volume fraction PPO (V_{PPO}) for the low molecular weights PS ($\bar{M}_n$=38,000)/PPO blends. Filled symbols indicate σ or ε at break, while unfilled symbols indicate those at yield.

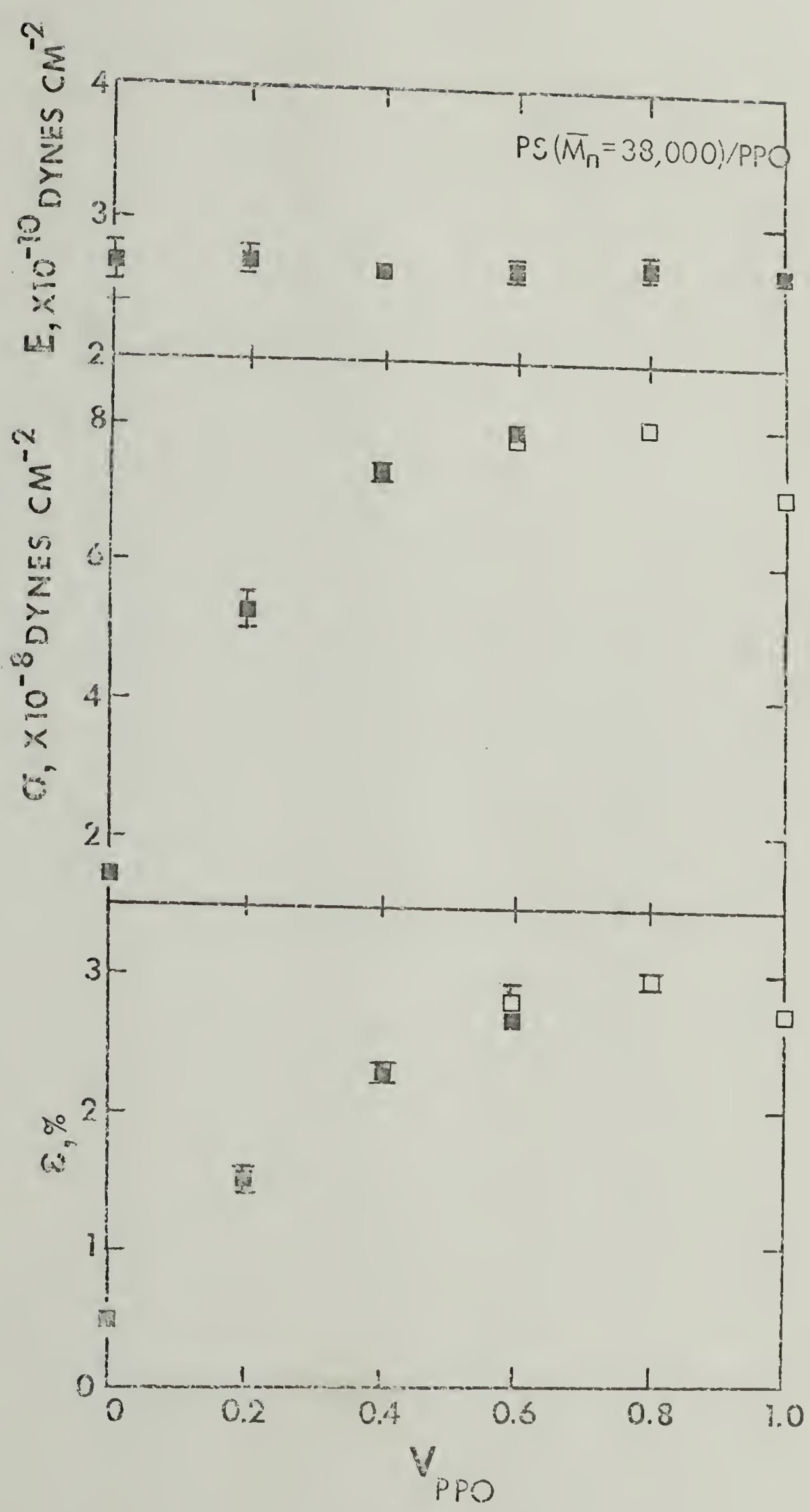
PS($\bar{M}_n$=38,000)/PPO
G, X10^{-8} DYNES CM^{-2}
E, X10^{-10} DYNES CM^{-2}
G, %
V_{PPO}
0
0.2
0.4
0.6
0.8
1.0
2
4
6
8
1
3

Figure 41. Plots of Young's modulus (E), stress at break or yield (σ), and strain at break or yield (ε) versus volume fraction PPO (V_{PPO}) for high molecular weight PS ($\bar{M}_n$=92,600)/PPO blends. Filled symbols indicate σ or ε at break, while unfilled symbols indicate those at yield.

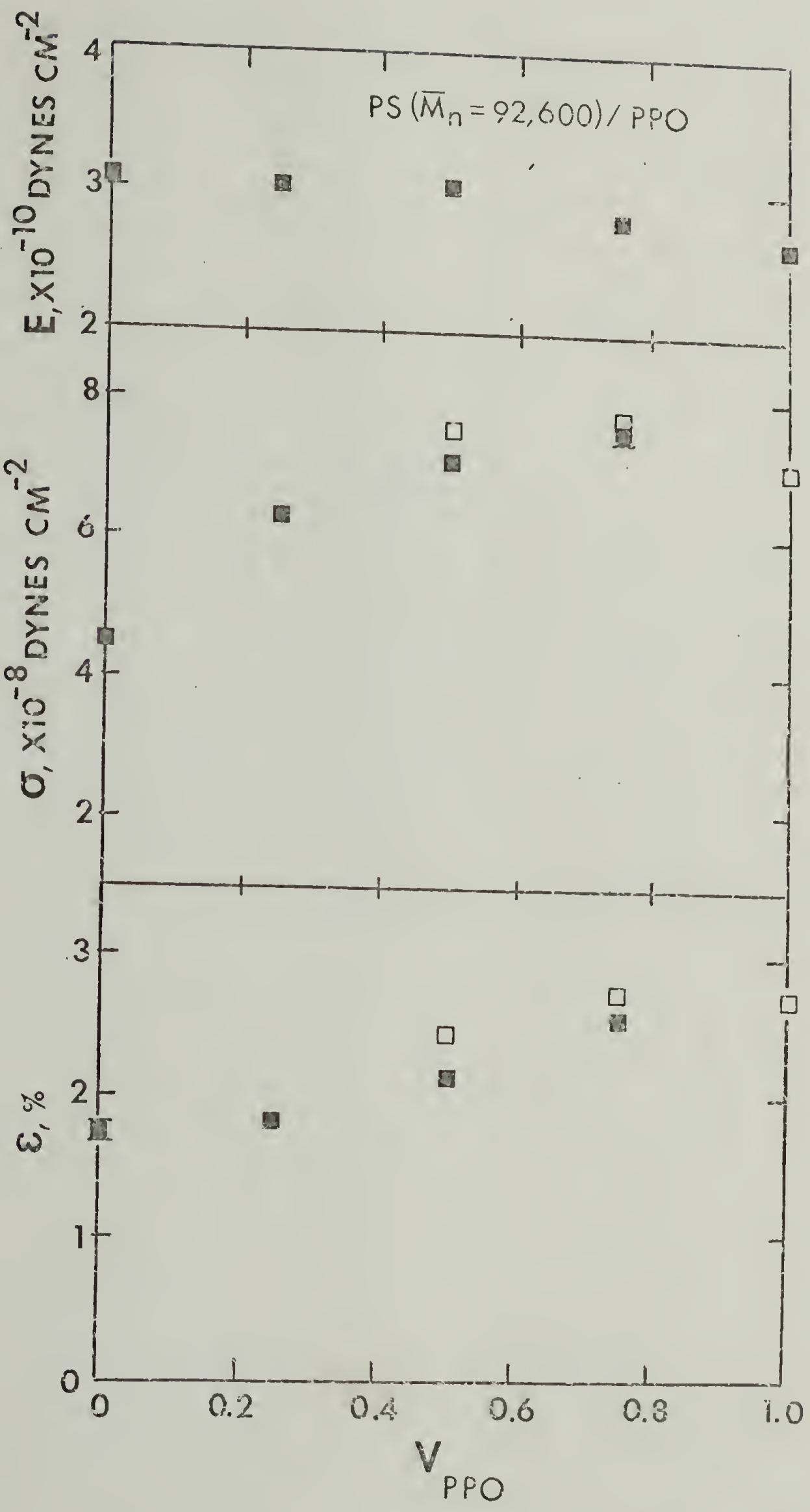
PS ($\bar{M}_n$ = 92,600) / PPO
E, X10^{-10} DYNES CM^{-2}
σ, X10^{-8} DYNES CM^{-2}
ε, %
V_{PPO}
0
0.2
0.4
0.6
0.8
1.0
1
2
3
4
6
8

observations have been made by Kleiner[8] for a wide range of PS molecular weights and molecular weight distributions.

Similar trends in tensile properties were observed for the two other compatible blends of Copolymer B/PPO (Figure 42) and Copolymer C/PPO (Figure 43). For both of these blends, σ increases with increasing V_{PPO} until a broad maximum is reached at high V_{PPO}. Young's modulus monotonically decreases with increasing V_{PPO}, while ε increases to a broad maximum or plateau at high V_{PPO}.

These results show that all the compatible blends exhibit similar tensile properties. They are characterized by high tensile strength or yield strength at all blend compositions. In fact, σ_Y of these compatible blends at high V^{PPO} is larger than that of PPO itself. It is attractive to assign this synergism in tensile strength to the observed increases in blend density cited in Chapter IV. Similar increases in density have been observed for unblended polymers upon annealing and result in an increase in tensile strength.[9,10,11] For example, PS and polycarbonate, show a 12-15% increase in tensile strength corresponding to a 0.2% increase in density upon annealing.[9] In the case of the blends, this increase in density results from attractive intermolecular interactions, while in the case of the unblended polymers, the density increase due to annealing results from a reduction in void volume and better liquid packing.

Figure 42. Plots of Young's modulus (E), stress at break or yield (σ), and strain at break or yield (ε) versus volume fraction PPO (V_{PPO}) for Copolymer B/PPO blends. Filled symbols indicate σ and ε at break, while unfilled symbols indicate those at yield.

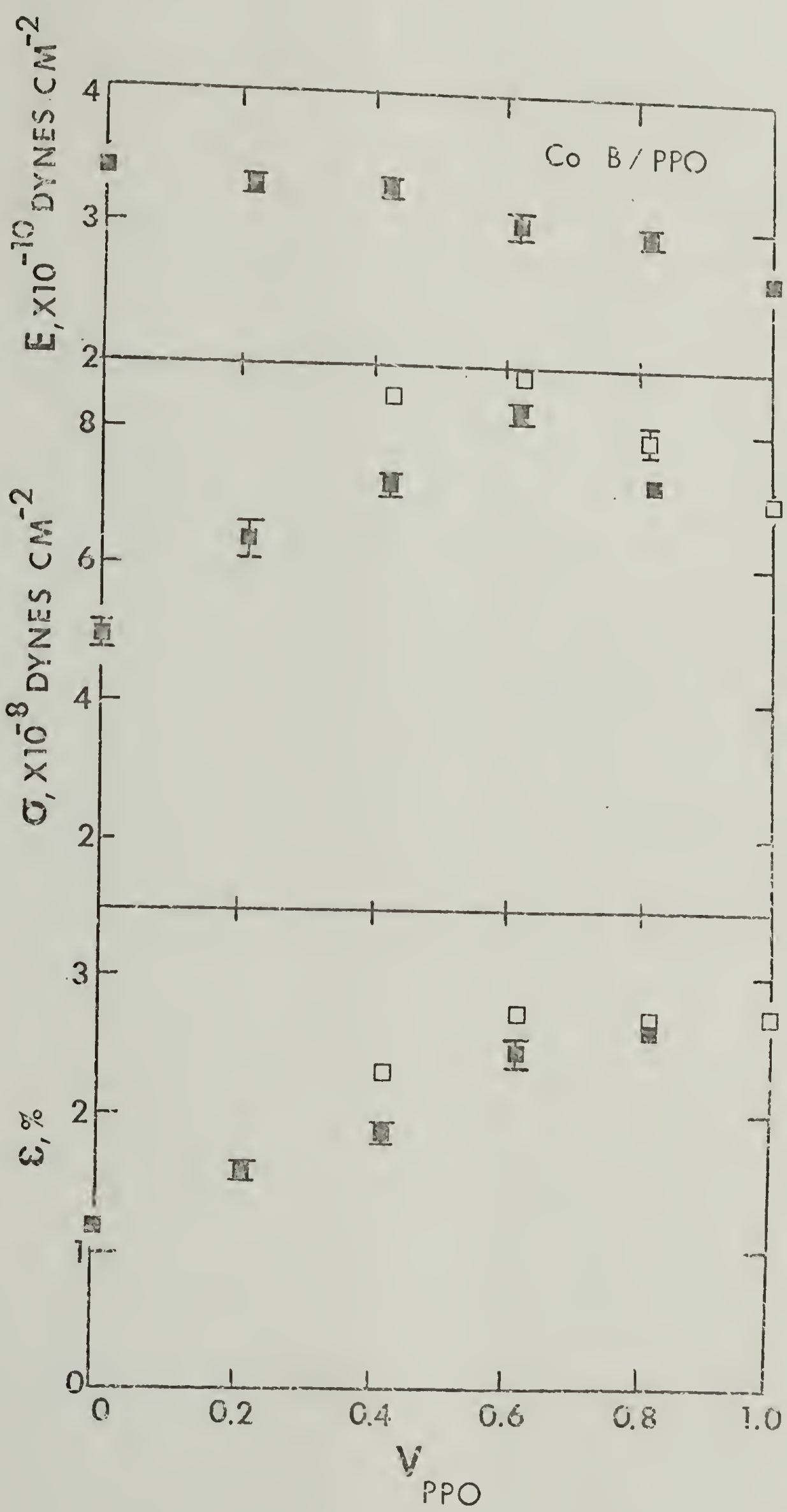
Co B / PPO
E, X10^-10 DYNES CM^-2
σ, X10^-8 DYNES CM^-2
ε, %
V PPO
0
0.2
0.4
0.6
0.8
1.0
1
2
3
4
6
8

Figure 43. Plots of Young's modulus (E), stress at break or yield (σ), and strain at break or yield (ε) versus volume fraction PPO (V_{PPO}) for Copolymer C/PPO blends. (●) represent values for annealed samples. Filled symbols indicate σ or ε at break, while unfilled symbols indicate those at yield.

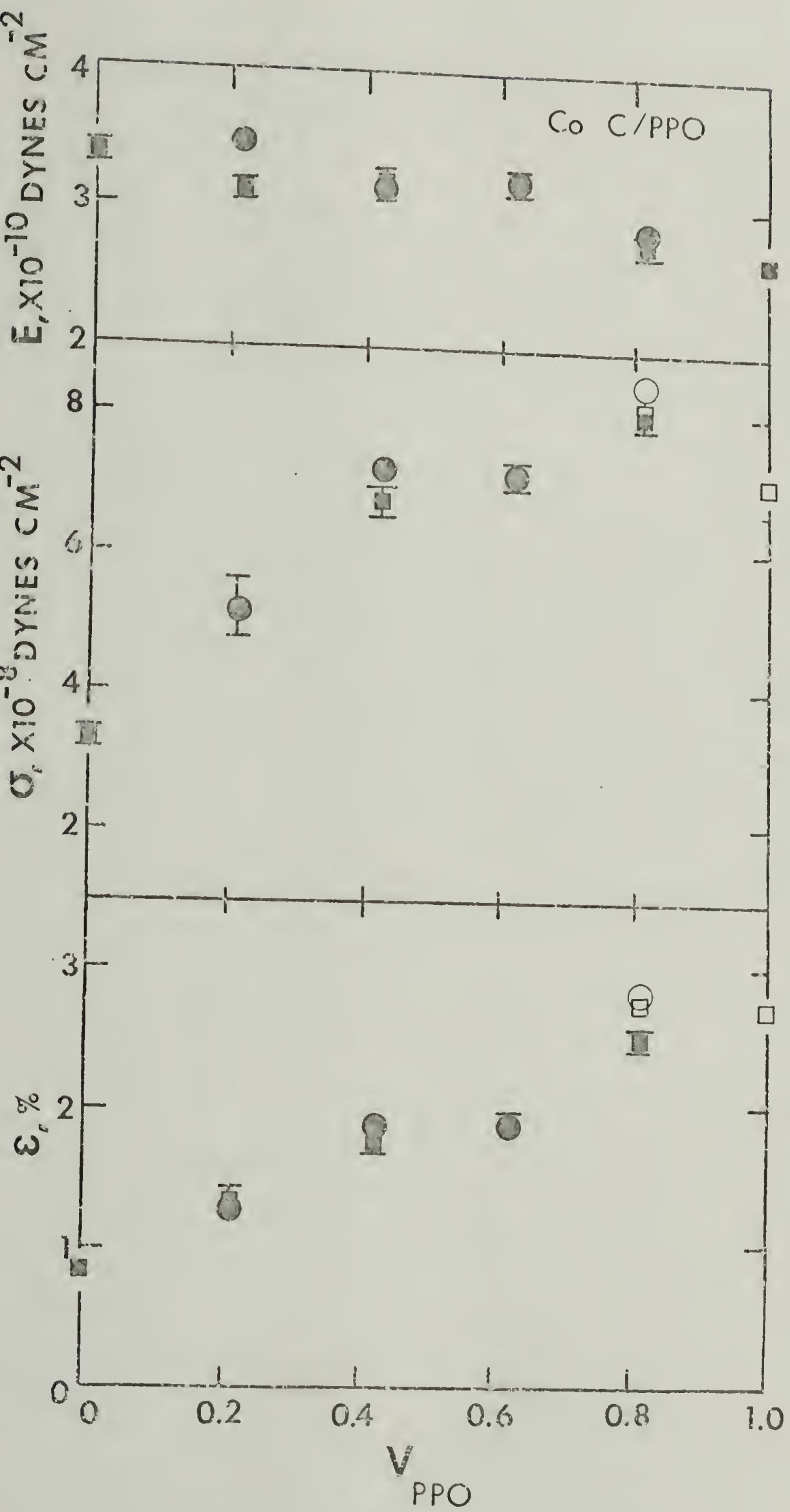
Co C/PPO
E, X10⁻¹⁰ DYNES CM⁻²
σr X10⁻⁸ DYNES CM⁻²
ωr %
4
3
2
8
6
4
2
3
2
1
0
0
0.2
0.4
0.6
0.8
1.0
V PPO

In addition, polymers such as polycarbonate and polyethylene terephthalate which ordinarily exhibit yield behavior, have been observed to undergo a ductile-to-brittle-transition in tensile and impact studies as a result of annealing.[10,11] This same ductile-to-brittle transition, or embrittlement, is exhibited by the compatible PS/PPO, Copolymer B/PPO, and Copolymer C/PPO blends. The annealing results suggest that ductility is associated, at least in part, with modes of motion that are enhanced by greater levels of excess thermodynamic properties, those of enthalphy and volume, trapped in the glass.[11] Yee[5] has shown that in PS/PPO blends embrittlement occurs at blend compositions at which a suppression of the β peak of PPO is observed. This indicates that brittle fracture ensues when the packing of molecules is sufficiently dense to restrict relaxational motions of portions of the polymer chain. For PPO, this secondary β peak has been attributed to hindered torsional oscillations of the phenylene units in the backbone around the C-O-C axis.[12,13]

As the data points (filed and unfilled symbols) in Figures 40 through 43 indicate, at high V_{PPO} some tensile specimens were observed to break by brittle fracture while some exhibited yielding behavior. The numbers of these specimens which failed by either mode are given in Table XVIII in the Appendix. Generally, the number of samples which exhibited yield behavior increased with increasing

V_{PPO}. These results may be explained on the basis of non-uniformity among different molded specimens. It may be that introduction of voids and other defects by the molding procedure can lead to premature failure for some samples. Nicholais and Dibenedetto[8] have shown that the criterion for brittle failure can be defined in terms of a critical defect size. When defects are larger than this critical size, brittle failure will occur before the stress-strain curve reaches a maximum, i.e. before yielding. For all blends, σ_Y was greater than σ_B as would be expected from the above arguments.

In Chapter III, mention was made to possible splitting of the broad glass transitions of Copolymer C/PPO blends upon annealing. If such observations are indicative of phase separation, it would be expected that annealed tensile specimens should exhibit lower tensile strength and elongation to break. This was not the case as indicated by the data points for annealed samples given in Figure 43. In each case, modulus, strength, and break strain values fell within the error bounds given for the unannealed samples. Transmission electron micrographs were taken of the cold fractured surfaces of both annealed and unannealed C-b60 blends prepared by the procedures given in Chapter III. These are given in Figure 44. Domains appear slightly larger and better defined in the annealed specimens but no evidence for macro-phase separation was evident.

Figure 44. Scanning electron micrographs of unannealed and annealed C-b60 blends. Top, surface of an injection molded dumbbell which had been fractured in the thin gauge length section after immersion in liquid nitrogen. Bottom, surface of dumbbell which had been annealed at 136°C for 17 hrs. in vacuum and which had been fractured in the identical manner to the unannealed sample.

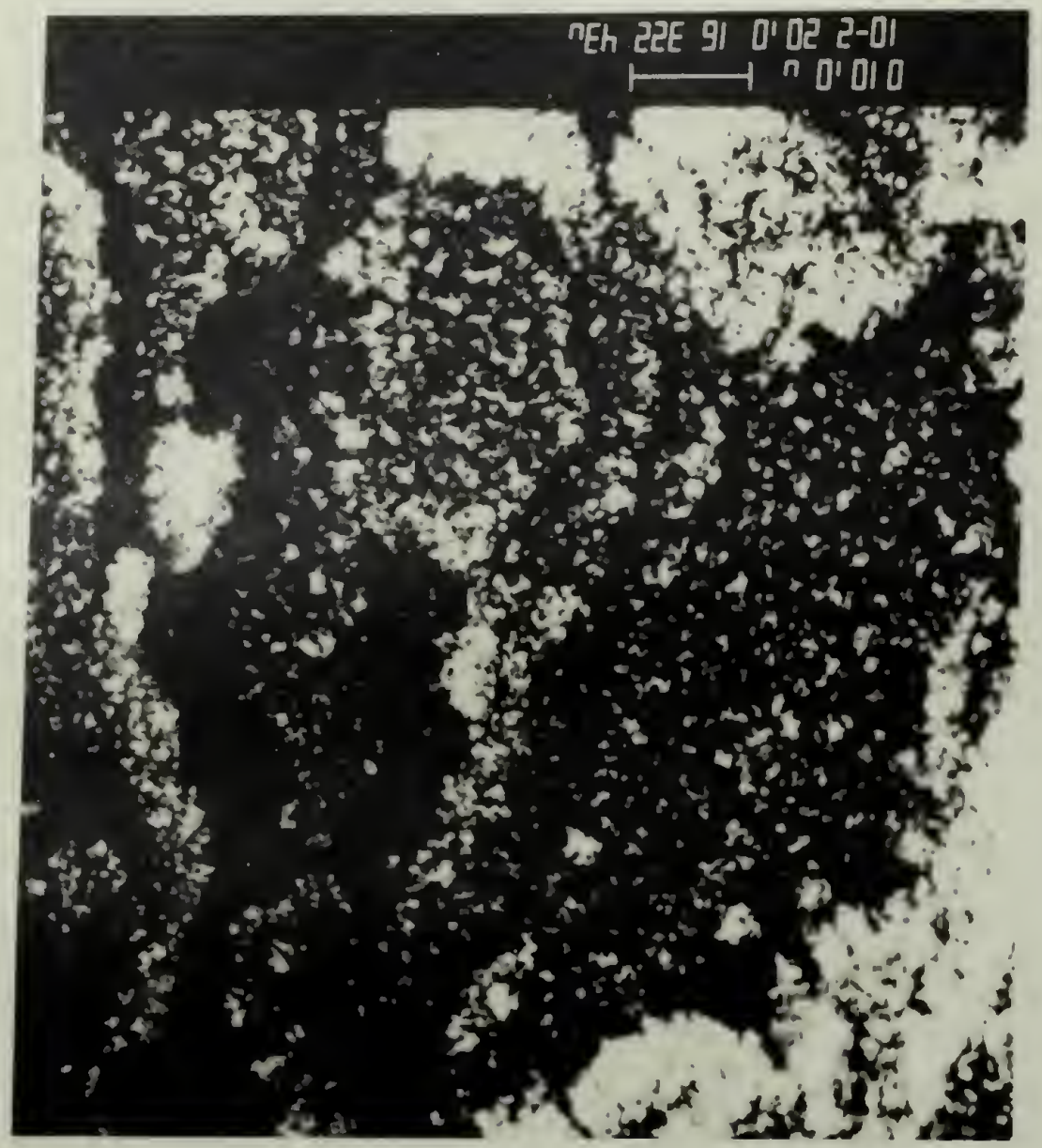
ηEh 22E 91 0'02 2-01
0'01.0 η

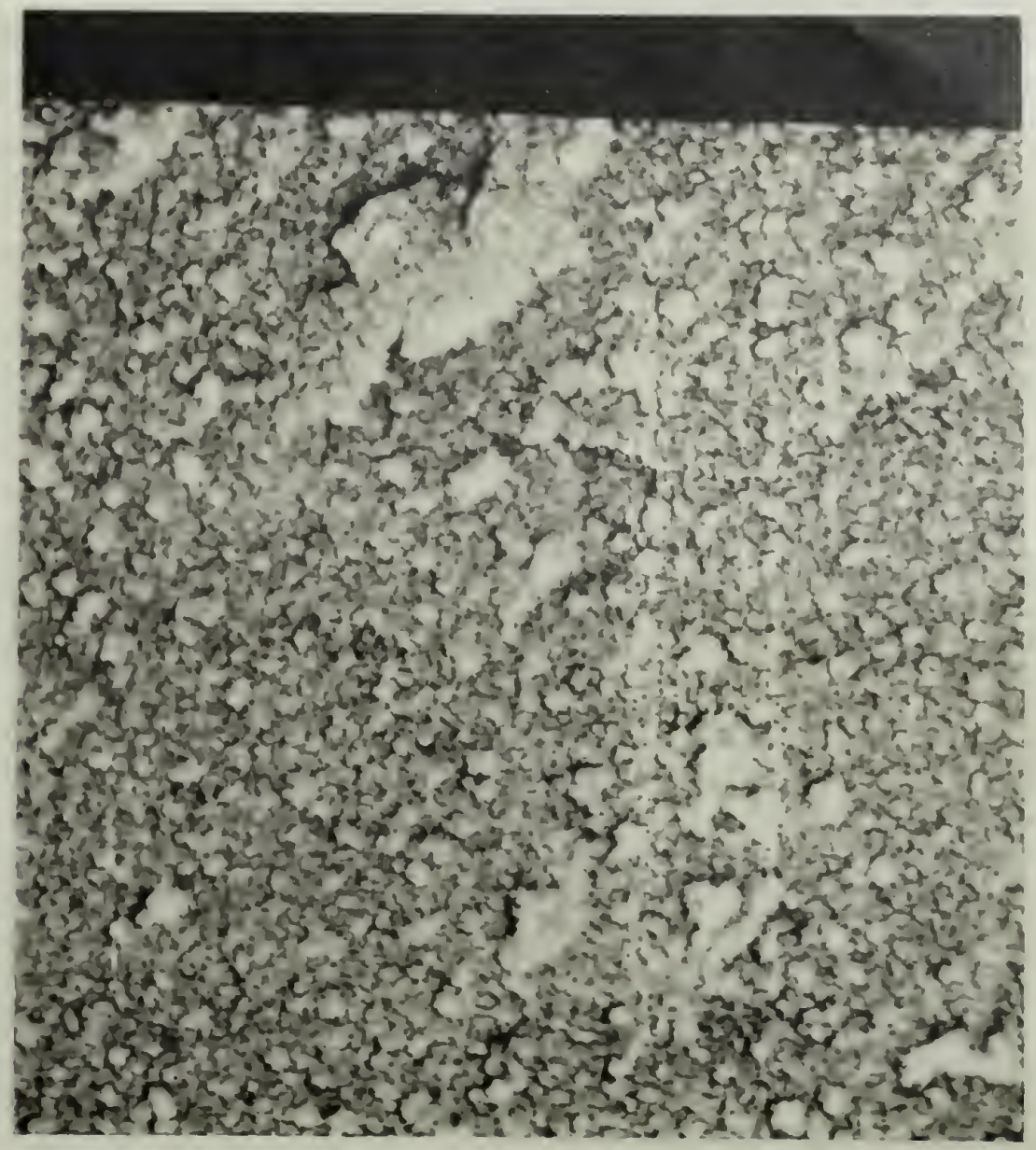

Incompatible and Transitional Blends

In Figures 45 and 46, Young's modulus, stress at break (yield), and elongation at break (yield) are plotted versus volume fraction PPO (V_{PPO}) for the two partially compatible blends of Copolymer D/PPO and Copolymer E/PPO. These two blends were shown in Chapter IV to exhibit two glass transitions at most blend compositions; however, there was an increase in the T_g of the low temperature transition above that of the unblended copolymer, and decrease in T_g of the high temperature transition below that of PPO. These observations and the very small, i.e. nonquantitative, heights of the glass transitions of the two phases indicated that some miscibility of the copolymer and PPO within the phases as well as between the phases was occuring. In addition, due to the overall decreasing molecular weight of the blend with increasing amount of PPO, increasing miscibility with increasing W_{PPO} was evident. This was observed as a larger elevation of the T_g of the copolymer-rich phase at high W_{PPO}. As Figures 45 and 46 indicate, these transitional blends exhibit a shallow minimum at low V_{PPO} for both stress and strain at break (or yield); but at high V_{PPO} the high values for stress and strain at break characteristic of the compatible blends are achieved. For the more incompatible blends, this minimum expands to higher V_{PPO} and the minimum becomes deeper. This is shown in Figures 47 to 49 for the incompatible blends of Copolymer F/PPO, PpClS/PPO, and PpClS/PPO.

Figure 45. Plots of Young's modulus (E), stress at break or yield (σ), and strain at break or yield (ε) versus volume fraction PPO (V_{PPO}) for Copolymer D/PPO blends. Filled symbols indicate σ or ε at break, while unfilled symbols indicate those at yield.

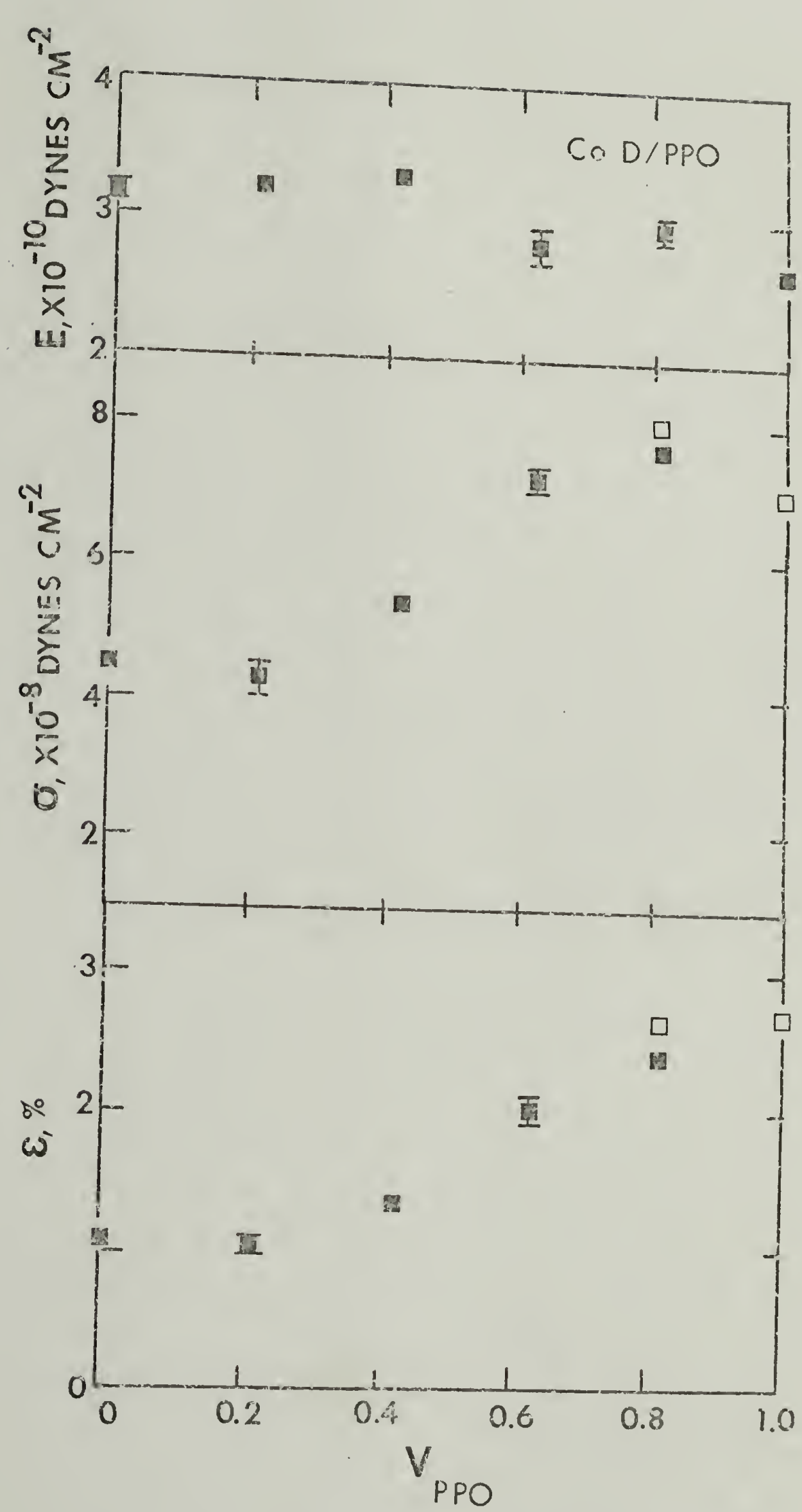
Co D/PPO
E, X10^-10 DYNES CM^-2
σ, X10^-8 DYNES CM^-2
ε, %
V PPO
0
0.2
0.4
0.6
0.8
1.0
2
3
4
6
8

Figure 46. Plots of Young's modulus (E), stress at break or yield (σ), and strain at break or yield (ε) versus volume fraction PPO (V_{PPO}) for Copolymer E/PPO blends. Filled symbols indicate σ or ε at break, while unfilled symbols indicate those at yield.

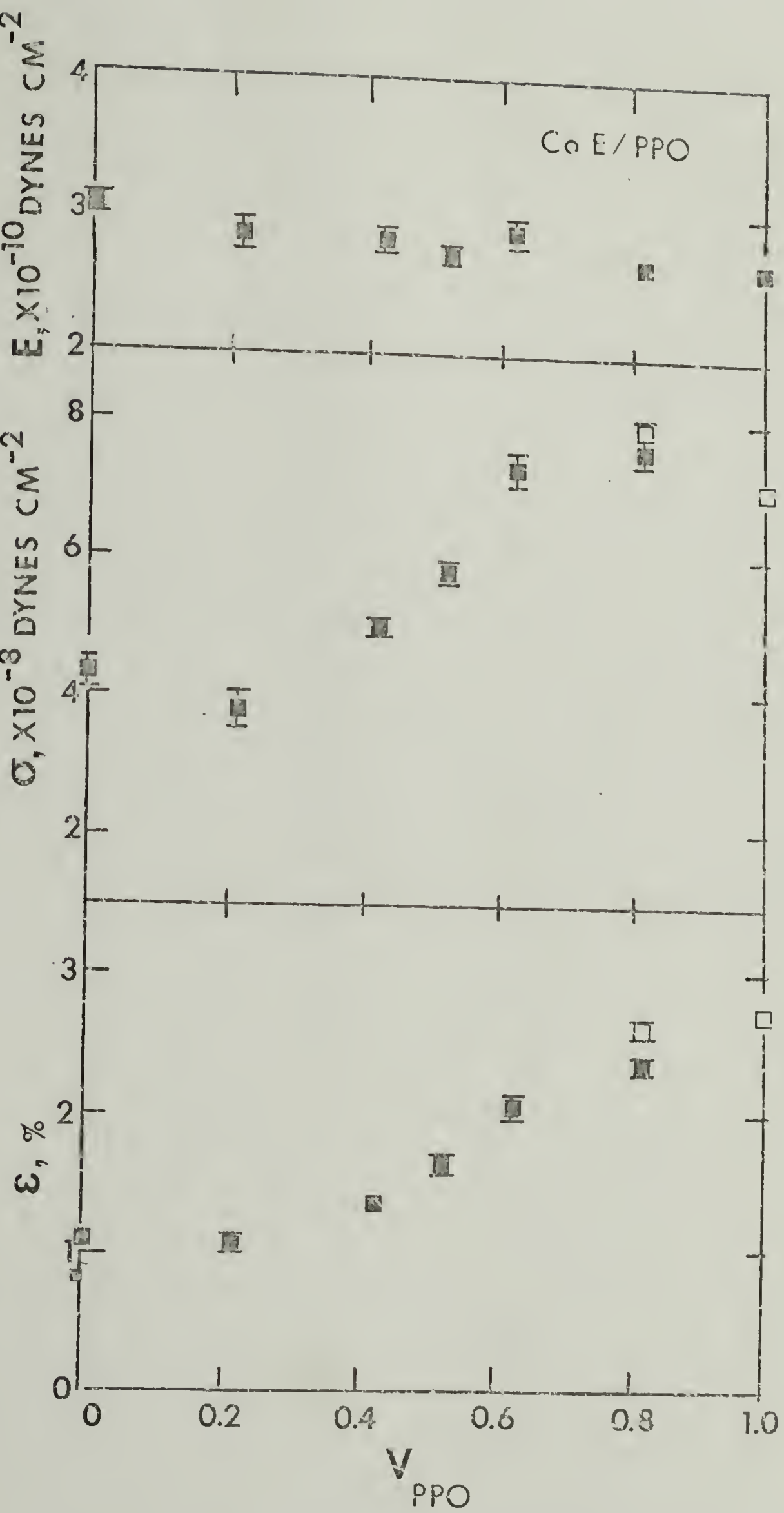
Co E/PPO
$E_s X10^{-10}$ DYNES CM^{-2}
$E_s X10^{-8}$ DYNES CM^{-2}
ε, %
V_{PPO}
0
0.2
0.4
0.6
0.8
1.0
1
2
3
4
6
8

Figure 47. Plots of Young's modulus (E), stress at break or yield (σ), and strain at break or yield (ε) versus volume fraction PPO (V_{PPO}) for Copolymer F/PPO blends. Filled symbols indicate σ or ε at break, while unfilled symbols indicate those at yield.

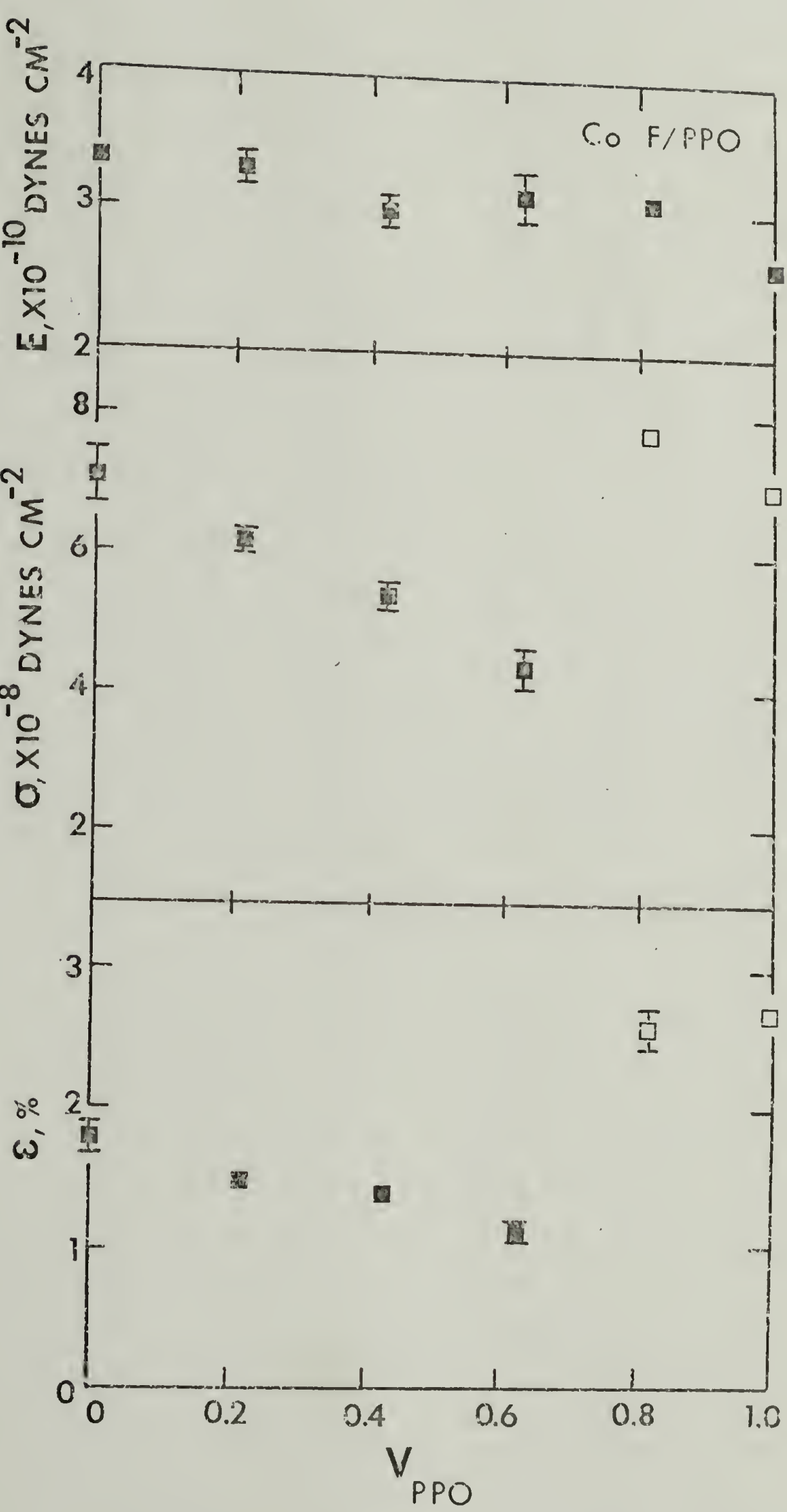
Co F/PPO
E, X10^-10 DYNES CM^-2
σ, X10^-8 DYNES CM^-2
ε, %
4
3
2
8
6
4
2
3
2
1
0
0
0.2
0.4
0.6
0.8
1.0
V PPO
HOH

Figure 48. Plots of Young's modulus (E), stress at break or yield (σ), and strain at break or yield (ε) versus volume fraction PPO (V_{PPO}) for PpClS/PPO blends. Filled symbols indicate σ or ε at break, while unfilled symbols indicate those at yield.

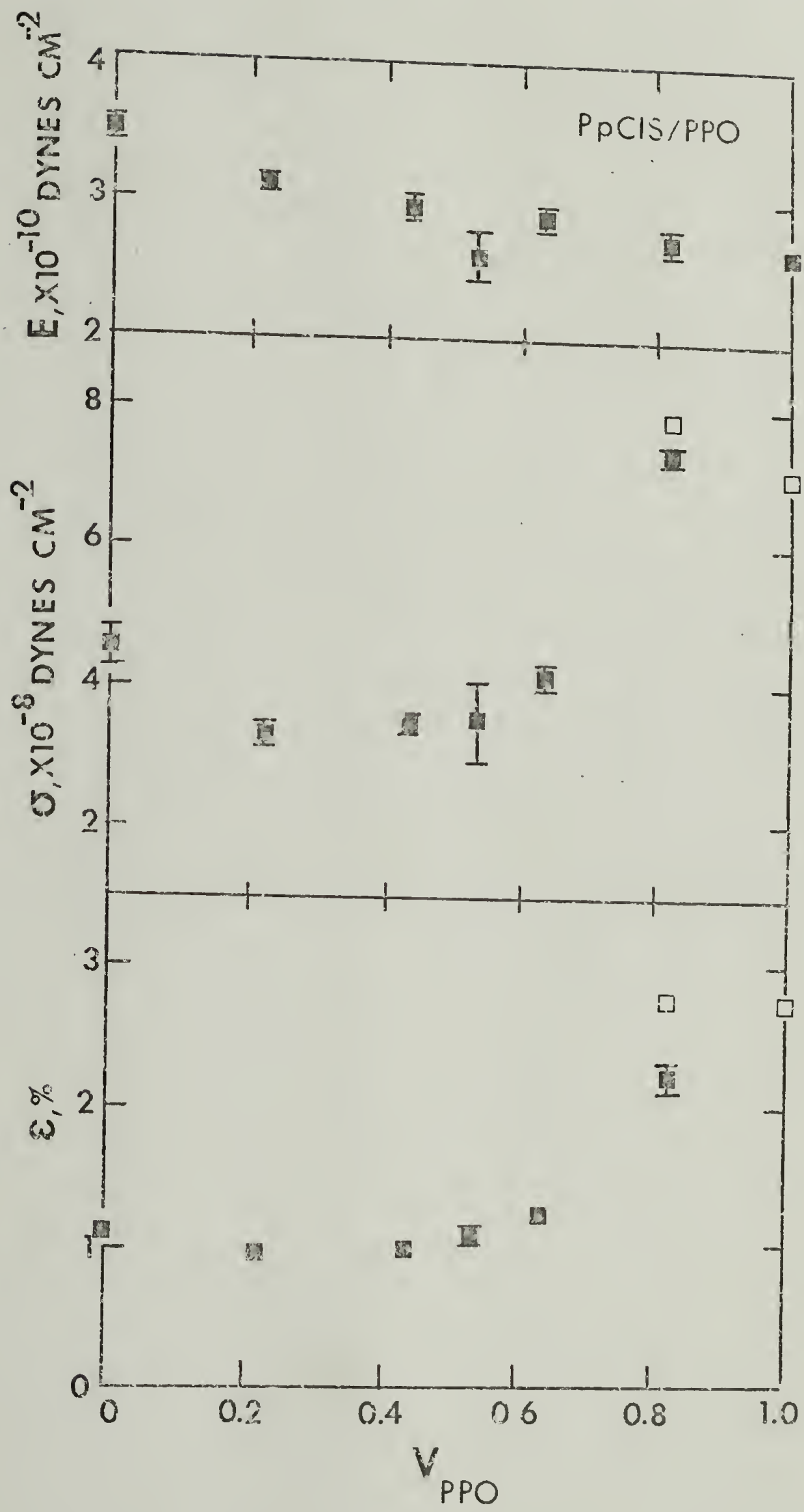
PpCIS/PPO
E, X10^-10 DYNES CM^-2
σ, X10^-8 DYNES CM^-2
ε, %
V PPO
0
0.2
0.4
0.6
0.8
1.0
2
3
4
6
8

Figure 49. Plots of Young's modulus (E), stress at break or yield (σ), and strain at break or yield (ε) versus volume fraction PPO (V_{PPO}) for PoClS/PPO blends. (■) represent blends containing PoClS-1 ($\bar{M}_v$=571,000), (◆) blends containing PoClS-2 ($\bar{M}_v$=224,000), and (●) blends containing PoClS-3 ($\bar{M}_v$=1,213,000). Filled symbols indicate σ or ε at break, while unfilled symbols indicate those at yield.

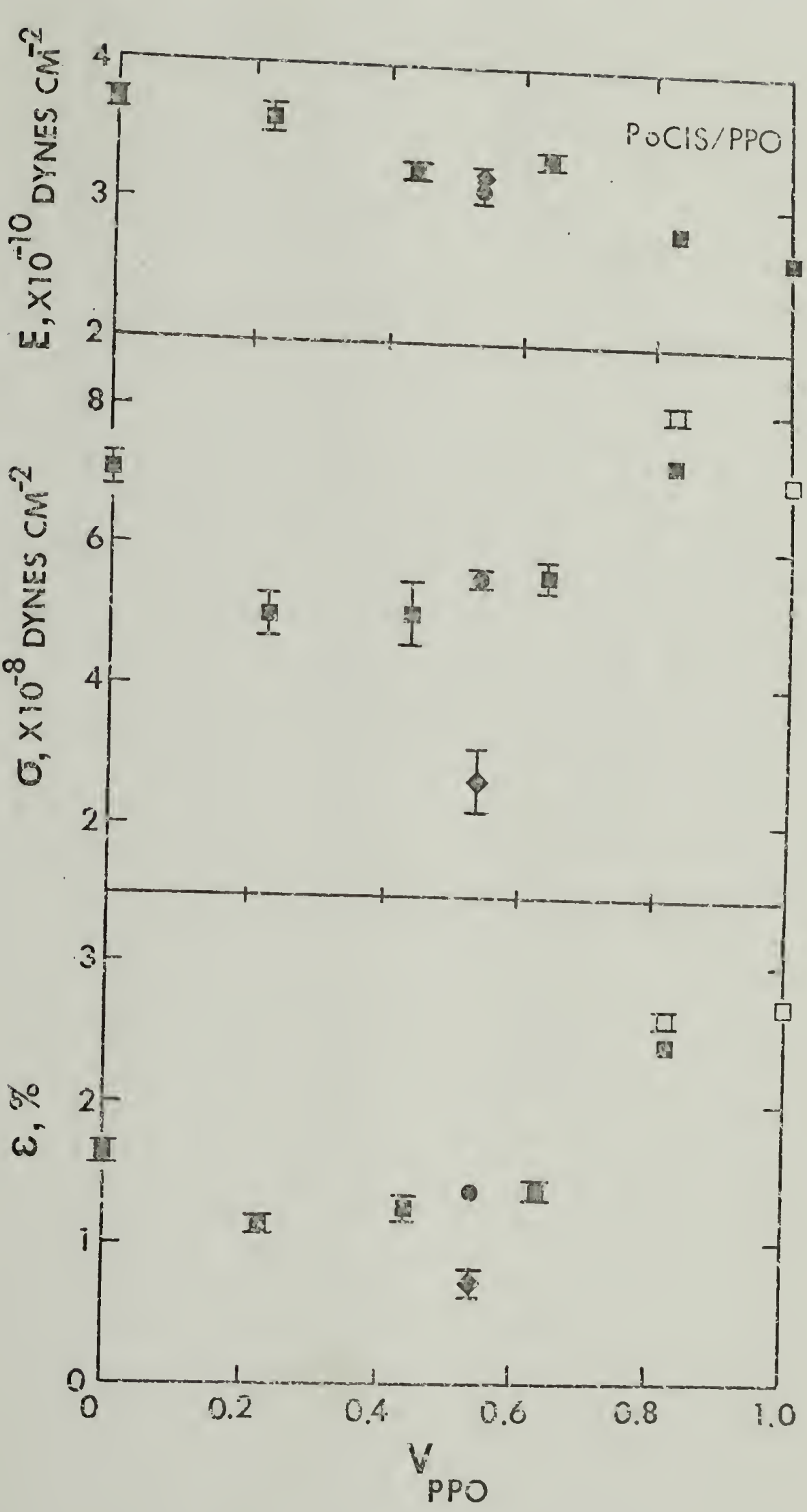
E, X10^-10 DYNES CM^-2
σ, X10^-8 DYNES CM^-2
ε, %
PoCIS/PPO
0
0.2
0.4
0.6
0.8
1.0
V_PPO

REFERENCES

1. L. E. Nielsen, "Mechanical Properties of Polymers and Composites," Marcel Dekker, New York, Vol. 2, pp. 271-275.
2. H. W. McCormick, F. M. Brower, and L. Kin, J. Polym. Sci., 39, 87 (1959).
3. B. Wellinghoff and E. Baer, Preprints, Org. Coatings and Plastics Chem., 36, 140 (1976).
4. J. R. Kastelic and E. Baer, J. Macromol. Sci.-Phys., B7(4), 679 (1973).
5. A. F. Yee, Polym. Prepr., 17(1), 145 (1976)
6. A. Wambach, K. Trachte, and A. Dibenedetto, J. Comp. Mater., 2, 266 (1968).
7. E. P. Cizek, U. S. Patent 3,383,435 (assigned to General Electric), August 11, 1967.
8. L. Kleiner, unpublished results.
9. P. B. Bowden, in "The Physics of Glassy Polymers," edited by R. N. Haward, Halsted Press, New York, 1973, p. 305.
10. R. M. Mininni, R. S. Moore, J. R. Flick, and S. E. B. Petrie, Macromol. Sci.-Phys, B8, 343 (1973).
11. S. E. B. Petrie, in "Polymeric Materials: Relationships Between Structure and Mechanical Behavior," edited by E. Baer and S. V. Radcliffe, American Society of Metals, Metals Park, Ohio, 1974.

REFERENCES (cont.)

12. S. de Petris, V. Frosini, E. Butta, and M. Baccaredda, Makromol. Chem., 109, 54 (1967).

13. A. Eisenberg and B. Cayrol, J. Polym. Sci., C, 35, 129 (1971).

14. L. Nicolais and A. T. Dibenedetto, J. Appl. Polym. Sci., 15, 1585 (1971).

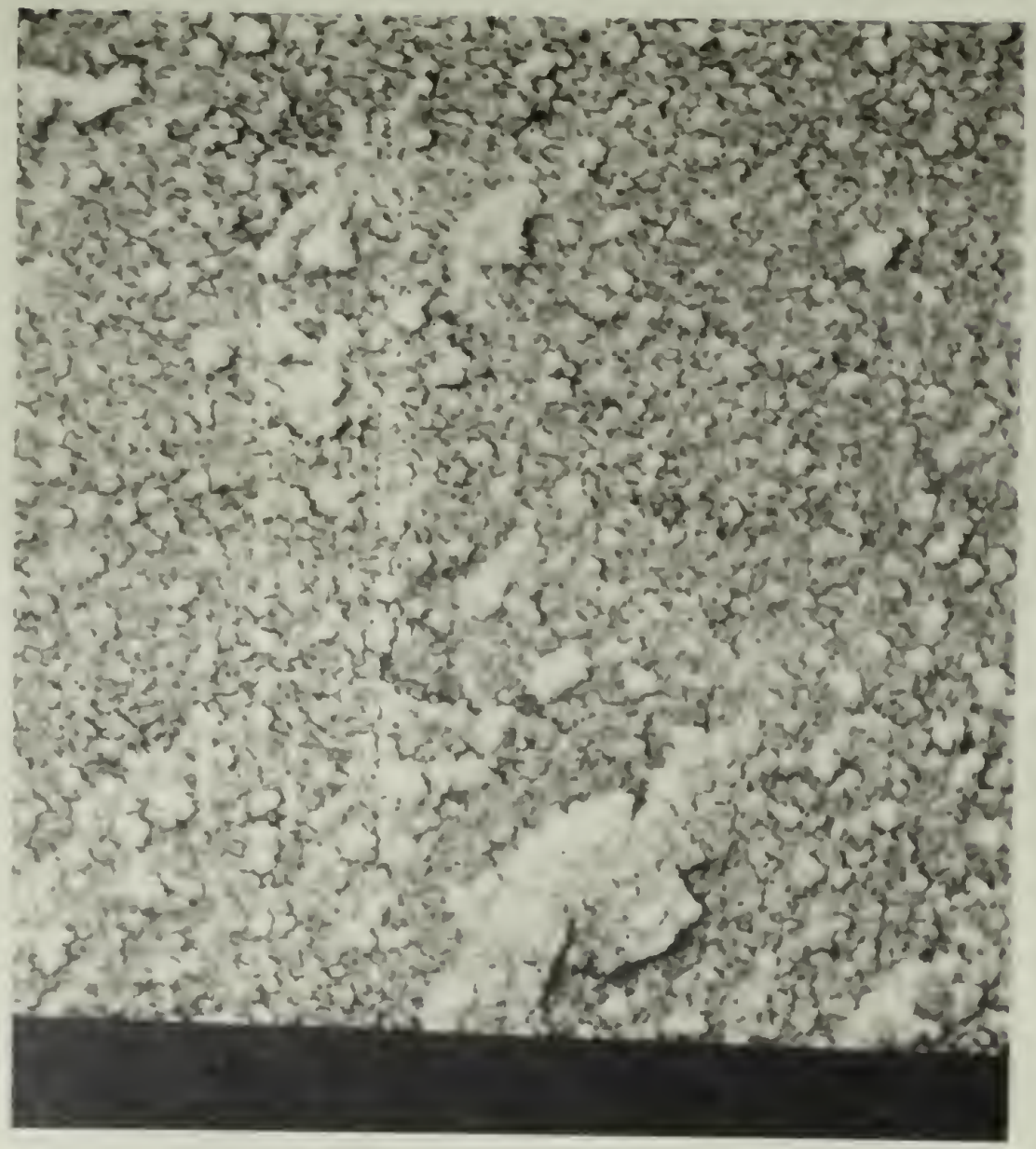

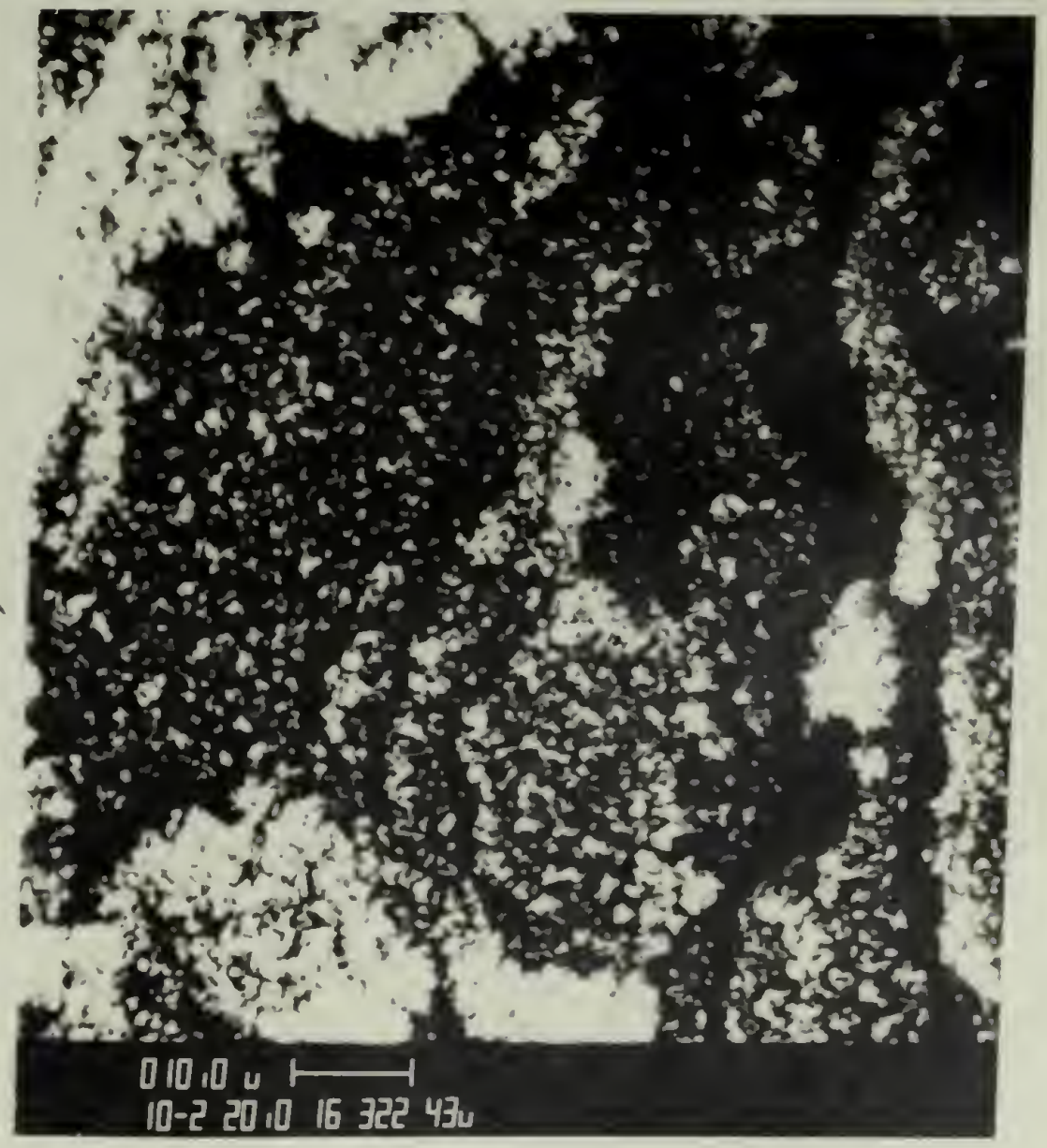
0 10 ,0 u
10-2 20 ,0 16 322 43u

C H A P T E R V I

APPENDIX: ERROR ANALYSIS AND DATA TABULATION

All measured and calculated blend densities are given in Table XVII at the end of this Appendix, while tensile properties of the blends and individual blend polymers are given in Table XVIII. Each value is expressed as

$$\bar{X} \pm S \tag{37}$$

where $\bar{X}$ is the sample mean and S is the standard deviation of the mean; S is related to the standard deviation (σ) of the sample population by the relation[1]

$$S = \sigma/\sqrt{N} \tag{38}$$

where N is the number of samples used to compute the mean. The standard deviation, σ, is defined by

$$\sigma = \sqrt{\frac{\Sigma (X_i - \bar{X})^2}{N-1}} \tag{39}$$

where i is the sample number index.

---

[1] H. D. Young, "Statistical Treatment of Experimental Data," McGraw-Hill, New York, 1962, p. 95.

Density Measurements

The best straight line determining the dependence of density upon vertical position in the liquid gradient columns was determined by the method of least squares. The standard deviation, S, of the measured density was then determined from a propagation of errors[2] by the procedure outlined below.

The equation relating density (ρ) to column position (x) is given by

$$\rho = f(m,x,b) = mx + b \tag{40}$$

where m is the slope of the line and b is the ordinate intercept. The variance (σ_ρ^2) is calculated from

$$\sigma_\rho^2 = \left(\frac{\partial \rho}{\partial m}\right)^2_{x,b} \sigma_m^2 + \left(\frac{\partial \rho}{\partial x}\right)^2_{m,b} \sigma_x^2 + \left(\frac{\partial \rho}{\partial b}\right)^2_{m,x} \sigma_b^2 \quad . \tag{41}$$

Taking the partial derivatives of eq. (40) as indicated in eq. (41) and substituting these into eq. (41) gives

$$\sigma_\rho^2 = x^2 \sigma_m^2 + m^2 \sigma_x^2 + \sigma_b^2 \quad . \tag{42}$$

The variances of the slope and the intercept are given by[3]

$$\sigma_m^2 = \frac{N\sigma^2}{\Delta} \tag{43}$$

---

[2] Ibid., pp. 96-101.

[3] Ibid., pp. 121-123.

and

$$\sigma_b^2 = \frac{\sigma^2 \Sigma x_i^2}{\Delta} \tag{44}$$

where

$$\Delta = N\Sigma x_i^2 - (\Sigma x_i)^2 \tag{45}$$

and

$$\sigma^2 = \frac{1}{N}\Sigma (mx_i + b - y_i)^2 \ . \tag{46}$$

The variance of the sample population in terms of the statistical distribution of disk positions in the column is given by

$$\sigma_x^2 = \frac{\Sigma (x_i - \bar{x})^2}{N} \tag{47}$$

Finally, the density of the blend is given by

$$\rho \pm \frac{\sqrt{\sigma_\rho^2}}{\sqrt{N}} \tag{48}$$

where σ_ρ^2 is determined by eq. (42) for the variances given in eqs. (43), (44), and (47).

For most blend components and blends, densities are given in Table XVII for different samples determined in different gradient columns for comparison. In all cases, values for the same blend or component agree within the error bounds indicated by eq. (48).

Tensile Measurements

The techniques used to determine the tensile properties of the blends have been outlined in Chapter III. For the particular chart speed (200 mm min^{-1}), crosshead speed (0.2 mm min^{-1}), load cell (20 kg), and specimen gauge length (8.9 mm) used in these measurements, tensile properties were determined by the following formulas which take into account clamp and instrumental corrections:

$$E = \frac{18.02}{h} \times 3.00 \times 10^{10} \text{ dynes cm}^{-2} \qquad (49)$$

$$T.S. = \frac{V}{119\ R} \times 1.007 \times 10^{9} \text{ dynes cm}^{-2} \qquad (50)$$

$$\varepsilon = \frac{H}{50} \times 1.7\ \% \qquad (51)$$

where

E, Young's modulus

h, horizontal displacement in cm along chart at 100% pen deflection at instrumental Range 1 (4 kg maximum displacement)

T.S., tensile strength or stress at break (yield)

V, vertical displacement of pen at break in mm

R, instrumental range factor (5.0 for Range 1, 2.5 for Range 2, and 1.0 for Range 5)

ε, strain or elongation at break (yield)

H, horizontal displacement in cm along chart at break (yield)

To calculate a representative mean for several samples from the same blend, those specimens whose modulus, tensile strength, or strain at break deviated significantly from the rest of the population were rejected according to Chauvenet's Criterion.[4] These were any values whose probability of occurrence was less than 1/2N, i.e. those that fall outside the range given by

$$\bar{X} \pm T\sigma \tag{52}$$

where T is the probability function defined by

$$P(T) = 1 - \frac{1}{2N} \quad . \tag{53}$$

When one sample value was rejected by the above criterion, the sample mean ($\bar{X}$) and σ were recalculated. Of 299 samples tested, or 897 tensile properties (modulus, stress, and strain), only 16 were rejected by the Chauvenet Criterion.

For the standard deviations of the mean given in Table XVIII, a particular confidence limit may be obtained by applying small sampling theory.[5] The error bounds are then given by

$$\pm t_c \frac{\sigma}{\sqrt{N-1}} \tag{54}$$

---

[4] Ibid., pp. 78-79.

[5] M. R. Spiegel, "Theory and Problems of Statistics," McGraw-Hill, New York, 1961, pp. 183-191.

where t_c is the critical value or confidence coefficient obtained from a "Student's" t distribution. For example, Young's modulus for six samples of Copolymer B was determined to be $(3.40\pm.04)\times10^{10}$ dynes cm^{-2}. For this population, no data points were rejected; therefore, for a 95% confidence level, t_c for six samples or five (N-1) degrees of freedom was used. From the appropriate table, t_c was found to be 2.57 which is substituted into eq. (54) to give error bounds of ±.11. Within a 95% certainty, the modulus of Copolymer B is therefore $(3.40\pm.11)\times10^{10}$ dynes cm^{-2}.

TABLE XVII. Density of Polymer Blends

Blend	No. Samples Tested	W_{PPO}	V_{PPO}	Measured Density gm cc^{-1}	Value Used*	Calculated Blend Density [by eq.(30)] gm cc^{-1}
PS	1	0	0	1.0476±.0008	X	-
	5			1.0478±.0012		-
PS-b80	1	0.200	0.197	1.0564±.0006	X	1.0512
	5			1.0583±.0013		-
PS-b60	1	0.400	0.396	1.0628±.0006	X	1.0547
	5			1.0622±.0012		-
PS-b40	1	0.600	0.596	1.0668±.0004	X	1.0583
	5			1.0681±.0012		-
PS-b20	1	0.800	0.797	1.0696±.0005	X	1.0620
	5			1.0712±.0012		-
(PPO)	1	1.0	1.0	1.0656±.0006	X	-
	6			1.0654±.0008		-
	12			1.0674±.0008		-
B	5	0	0	1.1630±.0043	X	-
B-b80	4	0.200	0.214	1.1464±.0051		1.1422
B-b60	5	0.400	0.421	1.1304±.0040		1.1220
B-b40	6	0.600	0.620	1.1100±.0038		1.1026
B-b20	5	0.800	0.813	1,0896±.0015		1.0838
C	1	0	0	1.1715±.0019	X	-
	1			1.1685±.0028		-
	5			1.1716±.0041		-
C-b80	4	0.200	0.215	1.1515±.0021	X	1.1487
				1.1578±.0052		-

*Densities selected on the basis of smallest error bounds for use in Figures 32 through 38 in Chapter IV.

TABLE XVII. (cont.)

Blend	No. Samples Tested	W_{PPO}	V_{PPO}	Measured Density gm cc^{-1}	Value Used	Calculated Blend Density [by eq. (30)] gm cc^{-1}
C-b60	1	0.400	0.423	1.1330±.0023	X	1.1267
	4			1.1327±.0050		-
C-b40	1	0.600	0.622	1.1175±.0025	X	1.1056
	5			1.1186±.0060		-
C-b20	1	0.800	0.814	1.0945±.0028		-
	5			1.0948±.0014	X	1.0852
D	6	0	0	1.1738±.0038	X	-
D-b80	5	0.200	0.216	1.1555±.0027	X	1.1503
D-b60	5	0.400	0.423	1.1318±.0050	X	1.1280
D-b40	4	0.600	0.623	1.1133±.0050	X	1.1064
	5	0.800	0.815	1.0895±.0050	X	1.0856
E	2	0	0	1.1762±.0019	X	-
	1			1.1735±.0027		-
	5			1.1757±.0041		-
E-b80	1	0.200	0.216	1.1575±.0020	X	1.1523
	5			1.1585±.0023		-
E-b60	1	0.400	0.423	1.1360±.0023	X	1.1293
	4			1.1350±.0048		-
E-b50	1	0.500	0.524	1.1287±.0024	X	1.1182
	5			1.1284±.0044		-
E-b40	1	0.600	0.623	1.1175±.0025	X	1.1072
	3			1.1152±.0056		-
E-b20	1	0.800	0.815	1.0893±.0029		-
	5			1.0919±.0014	X	1.0860

TABLE XVII. (cont.)

Blend	No. Samples Tested	W_{PPO}	V_{PPO}	Measured Density gm cc^{-1}	Value Used	Calculated Blend Density [by eq.(30)] gm cc^{-1}
F	2	0	0	1.1923±.0029		-
	1			1.1885±.0024	X	-
	5			1.1850±.0040		-
F-b80	1	0.200	0.217	1.1664±.0019	X	1.1619
	5			1.1655±.0045		-
F-b60	1	0.400	0.425	1.1420±.0022		-
	6			1.1411±.0022	X	1.1363
F-b40	1	0.600	0.625	1.1175±.0025	X	1.1117
	4			1.1181±.0051		-
F-b20	1	0.800	0.816	1.0930±.0029		-
	4			1.0941±.0017	X	1.0884
PpClS	2	0	0	1.2230±.0012	X	-
	4			1.2255±.0033		-
PpClS-b80	1	0.200	0.223	1.1918±.0007	X	1.1880
	1	0.400	0.436	1.1583±.0009	X	1.1548
	5			1.1613±.0046		-
PpClS-b50	6	0.500	0.534	1.1396±.0025	X	1.1389
PpClS-b40	1	0.600	0.633	1.1256±.0010	X	1.1236
	4			1.1272±.0047		-
PpClS-b20	1	0.800	0.821	1.0951±.0013	X	1.0939
	4			1.0957±.0017		-
PoClS-1	5	0	0	1.2506±.0049	X	-
PoClS-1-b80	5	0.200	0.227	1.2063±.0047	X	1.2082
PoClS-1-b60	5	0.400	0.439	1.1677±.0024	X	1.1694
PoClS-1-b40	5	0.600	0.637	1.1321±.0044	X	1.1327
PoClS-1-b20	5	0.800	0.824	1.0980±.0019	X	1.0983

TABLE XVIII. Tensile Properties of Polymer Blends

BLEND	NO. SAMPLES TESTED	W_{PPO}	V_{PPO}	YOUNG'S MODULUS $\times 10^{-10}$ dynes cm^{-2}	YOUNG'S MODULUS $\times 10^{-5}$ psi		STRESS AT BREAK** $\times 10^{-8}$ dynes cm^{-2}	STRESS AT BREAK** $\times 10^{-3}$ psi	STRAIN AT BREAK % **
PS*	4	0	0	2.69±.15	3.90±.22		1.40±.14	2.03±.20	0.50±.06
PS-b80	5	0.200	0.197	2.71±.10	3.93±.15		5.30±.28	7.69±.41	1.51±.09
PS-b60	5	0.400	0.396	2.65±.07	3.84±.10		7.32±.15	10.61±.22	2.28±.08
PS-b40	5	0.600	0.596	2.66±.09	3.86±.13		7.91±.06	11.47±.09	2.68±.03
						Y(3)	7.86±.13	11.40±.19	2.81±.13
PS-b20	6	0.800	0.797	2.69±.09	3.90±.13	Y(6)	8.03±.03	11.64±.04	2.95±.07
PPO	15	1.0	1.0	2.66±.05	3.86±.07	Y(15)	7.07±.09	10.25±.13	2.73±.03
B	6	0	0	3.40±.04	4.93±.06		4.91±.13	7.12±.19	1.18±.03
B-b80	5	0.200	0.214	3.29±.06	4.77±.09		6.38±.27	9.25±.39	1.60±.07
B-b60	5	0.400	0.421	3.28±.08	4.76±.12		7.21±.18	10.45±.26	1.88±.05
						Y(1)	8.50	12.33	2.30

* Polystyrene(PS) of $\overline{M_n}$ = 38,000, $\overline{M_w}$ = 82,000.

** Values preceded by Y are for stress and strain at Yield; parentheses indicate the number of samples tested which show yielding behavior.

TABLE XVIII. (cont.)

BLEND	NO. SAMPLES TESTED	W_{PPO}	V_{PPO}	YOUNG'S MODULUS $\times 10^{-10}$ dynes cm^{-2}	YOUNG'S MODULUS $\times 10^{-5}$ psi		STRESS AT BREAK $\times 10^{-8}$ dynes cm^{-2}	STRESS AT BREAK $\times 10^{-3}$ psi	STRAIN AT BREAK %
B-b40	5	0.600	0.620	3.03±.10	4.39±.15	Y(1)	8.30±.17 8.82	12.04±.25 12.79	2.46±.10 2.74
B-b20	6	0.800	0.813	2.97±.07	4.31±.10	Y(5)	7.28 7.91±.21	10.56 11.47±.30	2.61 2.68±.07
C	6	0	0	3.37±.08	4.89±.12		3.32±.15	4.81±.22	0.83±.03
C-b80	8 1A*	0.200	0.215	3.13±.09 3.45	4.54±.13 5.00		5.20±.41 5.14	7.54±.59 7.45	1.34±.10 1.27
C-b60	7 1A*	0.400	0.423	3.18±.11 3.13	4.61±.16 4.54		6.75±.21 7.19	9.79±.30 10.43	1.76±.07 1.86
C-b40	9 1A*	0.600	0.622	3.20±.09 3.19	4.64±.13 4.63		7.16±.19 7.11	10.38±.28 10.31	1.91±.07 1.88
C-b20	9	0.800	0.814	2.77±.08	4.02±.12		8.08±,22	11.72±.32	2.52±.08
	1A*			2.83	4.10	Y(6) Y(1)	8.10±.14 8.46	11.75±.20 12.27	2.76±.05 2.81

* Annealed (A) for 17 hrs. at ca. 20° below T_g.

TABLE XVIII. (cont.)

BLEND	NO. SAMPLES TESTED	W_{PPO}	V_{PPO}	YOUNG'S MODULUS $\times 10^{-10}$ dynes cm^{-2}	YOUNG'S MODULUS $\times 10^{-5}$ psi		STRESS AT BREAK $\times 10^{-8}$ dynes cm^{-2}	STRESS AT BREAK $\times 10^{-3}$ psi	STRAIN AT BREAK %
D	5	0	0	3.15±.07	4.57±.10		4.49±.07	6.51±.10	1.09±.04
D-b80	5	0.200	0.216	3.24±.03	4.70±.04		4.28±.24	6.21±.35	1.05±.06
D-b60	5	0.400	0.423	3.32±.04	4.81±.06		5.39±.10	7.82±.15	1.36±.01
D-b40	5	0.600	0.623	2.83±.13	4.10±.19		7.25±.16	10.51±.23	2.05±.10
D-b20	6	0.800	0.815	2.98±.10	4.32±.15		7.70	11.17	2.41
						Y(5)	8.09±.05	11.73±.07	2.68±.03
E	6	0	0	3.04±.06	4.41±.09		4.31±.22	6.25±.32	1.11±.05
E-b80	8	0.200	0.216	2.85±.11	4.13±.16		3.79±.28	5.50±.41	1.06±.05
E-b60	10	0.400	0.423	2.82±.09	4.09±.13		5.01±.14	7.26±.20	1.36±.05
E-b50	13	0.500	0.524	2.71±.06	3.93±.09		5.78±.17	8.38±.25	1.63±.06
E-b40	7	0.600	0.623	2.88±.10	4.18±.15		7.32±.24	10.61±.35	2.05±.09
E-b20	7	0.800	0.815	2.67±.05	3.87±.07		7.61±.22	11.03±.32	2.35±.07
						Y(5)	7.99±.08	11.59±.12	2.62±.07

TABLE XVIII. (cont.)

BLEND	NO. SAMPLES TESTED	W_{PPO}	V_{PPO}	YOUNG'S MODULUS $\times 10^{-10}$ dynes cm^{-2}	YOUNG'S MODULUS $\times 10^{-5}$ psi		STRESS AT BREAK $\times 10^{-8}$ dynes cm^{-2}	STRESS AT BREAK $\times 10^{-3}$ psi	STRAIN AT BREAK %
F	6	0	0	3.39±.03	4.92±.04		7.14±.40	10.35±.58	1.81±.12
F-b80	5	0.200	0.217	3.33±.11	4.83±.16		6.22±.19	9.02±.23	1.51±.06
F-b60	5	0.400	0.425	3.03±.12	4.39±.17		5.45±.22	7.90±.32	1.41±.04
F-b40	5	0.600	0.625	3.15±.18	4.57±.26		4.41±.30	6.39±.44	1.15±.08
F-b20	3	0.800	0.816	3.12±.05	4.52±.07	Y(3)	7.83±.03	11.35±.04	2.61±.15
PpClS	11	0	0	3.49±.09	5.06±.13		4.58±.29	6.64±.42	1.09±.06
PpClS-b80	15	0.200	0.223	3.13±.06	4.54±.09		3.32±.17	4.81±.25	0.94±.05
PpClS-b60	13	0.400	0.436	2.96±.10	4.29±.15		3.48±.13	5.05±.19	0.99±.04
PpClS-b50	3	0.500	0.534	2.62±.18	3.80±.26		3.51±.57	5.09±.83	1.08±.07
PpClS-b40	16	0.600	0.633	2.90±.09	4.21±.13		4.17±.18	6.05±.26	1.23±.05
PpClS-b20	12	0.800	0.821	2.72±.08	3.94±.12		7.39±.11	10.72±.16	2.21±.10
						Y(4)	7.88±.07	11.43±.10	2.78±.06

TABLE XVIII. (cont.)

BLEND	NO. SAMPLES TESTED	W_{PPO}	V_{PPO}	YOUNG'S MODULUS $\times 10^{-10}$ dynes cm^{-2}	YOUNG'S MODULUS $\times 10^{-5}$ psi	STRESS AT BREAK $\times 10^{-8}$ dynes cm^{-2}	STRESS AT BREAK $\times 10^{-3}$ psi	STRAIN AT BREAK %
PoClS-1	10	0	0	3.73±.08	5.41±.12	7.09±.23	10.28±.33	1.66±.08
PoClS-1-b80	5	0.200	0.227	3.62±.11	5.25±.16	5.05±.32	7.32±.46	1.15±.07
PoClS-1-b60	5	0.400	0.439	3.24±.06	4.70±.09	5.11±.44	7.41±.64	1.27±.09
PoClS-2-b50	2*	0.500	0.540	3.13±.06	4.54±.09	2.70±.45	3.92±.65	0.74±.09
PoClS-3-b50	3**	0.500	0.540	3.23±.07	4.68±.10	5.59±.16	8.11±.23	1.40±.04
PoClS-1-b40	5	0.600	0.637	3.35±.06	4.86±.09	5.64±.23	8.18±.33	1.41±.08
PoClS-1-b20	8	0.800	0.824	2.84±.05	4.12±.07	7.30	10.59	2.45
					Y(7)	8.05±.13	11.67±.19	2.64±.05

* PoClS-2 used was low molecular weight (solution polymerized); $\overline{M_v}$ = 224,000.

** PoClS-3 used was high molecular weight (bulk polymerized); $\overline{M_v}$ = 1,213,000.

TABLE XVIII. (cont.)

BLEND	NO. SAMPLES TESTED	W_{PPO}	V_{PPO}	YOUNG'S MODULUS $\times 10^{-10}$ dynes cm^{-2}	YOUNG'S MODULUS $\times 10^{-5}$ psi		STRESS AT BREAK $\times 10^{-8}$ dynes cm^{-2}	STRESS AT BREAK $\times 10^{-3}$ psi	STRAIN AT BREAK %
PS*		0	0	3.09±.04	4.48±.06		4.55±.05	6.60±.07	1.76±.07
PS-b75		0.250	0.247	3.05±.05	4.42±.07		6.39±.04	9.27±.06	1.84±.03
PS-b50		0.500	0.495	3.05±.03	4.42±.04		7.13±.08	10.34±.12	2.15±.05
						Y( )	7.59	11.01	2.46
PS-b25		0.750	0.747	2.82±.03	4.09±.04		7.58±.13	10.99±.19	2.57±.05
						Y( )	7.75±.05	11.24±.07	2.76±.04

*Polystyrene (PS) was Monsanto unlubricated HH101 of $\overline{M}_n$ = 92,600, $\overline{M}_w$ = 270,000. Values are the unpublished results of L. Kleiner.